SYNTHESIS AND CHARACTERIZATION OF INORGANIC COMPLEXES FOR THE MODIFICATION OF POLYMER PROPERTIES

BY

TIMOTHY J. FOLEY

A DISSERTATION PRESENTED TO THE GRADUATE SCHOOL
OF THE UNIVERSITY OF FLORIDA IN PARTIAL FULFILLMENT
OF THE REQUIREMENTS FOR THE DEGREE OF
DOCTOR OF PHILOSOPHY

UNIVERSITY OF FLORIDA

2002

This work is dedicated to all my friends and family.

ACKNOWLEDGMENTS

I would like to thank my advisor Jim for his guidance throughout my graduate career. I owe a debt of gratitude to two other people who were instrumental in my becoming who I am today as a chemist: my undergraduate research adviser Dr. Valerie S. Sheares and my high school chemistry teacher Ronald Henze. Additionally, I would like thank the many collaborators who have come together to help make this work possible, especially: Khalil Abboud, John Reynolds, Kirk Schanze, Paul Holloway, Ben Harrison, Mohammed Bougettaya, T.S. Kang, Lidia Matveeva, Dave Powell, Tom Cameron and Alison Knefley.

I would also like to thank my parents, my brothers, my grandparents and my friends for all of their support as I have continued my education. Finally I would like to thank my wife, Rebecca. Without her, I would not have been able to complete my studies.

TABLE OF CONTENTS

page

ACKNOWLEDGMENTS iii

LIST OF TABLES vii

LIST OF FIGURES ix

CHAPTER

1 INTRODUCTION 1

Inorganic Chemistry 4
Summary 8

2 ORGANOMETALLIC MONOMERS AND POLYMERS 9

Synthesis of Bis(2,3-dihydro-thieno[3,4-b][1,4]dioxine) 1,4-Divinyl-benzene (EVPVE) Monomer (EVPVE) (1) 12
Synthesis of Ru EVPVE (2) 14
Synthesis of Ru(η^5-C_5Me_5)([4-(diethoxy-phosphorylmethyl)-benzyl]-phosphonic acid diethyl ester) (3) 18
Alternate Synthesis of Compound 2 19
Electropolymerization of Compound 1 21
Electropolymerization of Compound 2 21
Spectroelectrochemistry of Poly 1 and 2 23
Attempted Synthesis of Bis-EDOT-VPV-Bis EDOT 24
Synthesis of Rhodium EVPVE (4) 26
Synthesis of Bisdodecyloxy EVPVE 30
Summary 33

3 SYNTHESIS, PHOTOLUMINESCENCE, AND ELECTROLUMINESCENCE OF LANTHANIDE TRIS- (β–DIKETONATE) COODINATION COMPLEXES 35

Synthesis of Lanthanide Tris(β diketonate) Complexes 36
Interactions of Ln Tris(β diketonate) Phenanthroline Complexes with Conjugated Polymers 37
Results From Solution Phase Experiments 37
Results From Thin Film Experiments 38
Polymeric Ligands 43

Conjugated Bipyridine Synthesis 43
Lanthanide Conjugated Bipyridine Complexes 44
Conjugated Diketone Synthesis 47
Synthesis of 1-(2,5-Dibromo-phenyl)-3-Phenyl-Propane-1,3-Dione (7) 48
Diketone Conjugated Polymer Synthesis 49
Diketonate Exchange Reaction 52
Summary and Conclusion 54

4 SYNTHESIS AND CHARACTERIZTION OF LANTHANIDE TETRAPHENYLPORPHYRIN COMPLEXS 56

Prior Investigations of LnTPP Complexes 57
Lanthanide Amides as Precursors to LnTPP Complexes 59
Synthesis, Isolation and Characterization of Bistetrahydrofuran Ln Tris(diphenylamide) ($Ln(NPh_2)_3$• 2 THF 61
Reaction of the LnTDPA Complexes with TPP 63
Lanthanide Tetraphenylporphyrin Chloride Synthesis 63
Mass Spectrometry of the Chloride Complexes 68
Synthesis and Crystal Structure of LnTPP(TP) Complexes 70
Synthesis of LnTPP(Klaui) Complexes 74
Proton NMR Analysis LnTPP(L) (L=TP or Klaui) 75
NMR Spectroscopy of YbTPP(TP) 76
NMR Spectrtoscopy of YbTPP(Klaui) 78
Synthesis of LnTPP(Diketonates) 81
Synthesis and Isolation of YbTPP(Cp*) (22) 82
Unexpected Reactions of the Chloride Complexes 87
Lithio N-benzyltetraphenylpoprphyrin (23) 87
Magnesium Tetraphenylporphyrin 88
LnTPP PL and EL 90
Nonconjugated Polymer Based Devices 94
Summary and conclusion 95

5 LANTHANIDE PHTHALOCYANINE COMPLEXES 96

Synthesis of LnPc(Cl) 97
Synthesis and Characterization of LnPc(Klaui) 98
Photoluminescence Experiments 105
Summary 108

6 EXPERIMENTAL PROCEDURES 110

General synthetic procedures 110
Photophysical Measurements 110
Nuclear magnetic resonance experimental 111
ESI Mass Spectroscopy 112

APPENDIX

CRYSTALLOGRAPHIC INFORMATION 134

LIST OF REFERENCES 166

BIOGRAPHICAL SKETCH 172

LIST OF TABLES

Table page

4-1. Photophysical Properties of LnTPPL measured in CH_2Cl_2. 91

A-1. Information for the crystal structure of **2** 135

A-2 Atomic coordinates) for **2**. 136

A-3. Crystal data and structure refinement for **8**. 138

A-4. Atomic coordinates for **8**. 139

A-5. Crystal data and structure refinement for **9** 141

A-6. Atomic coordinates for **9**. 142

A-7. Crystal data and structure refinement for **10** 144

A-8. Atomic coordinates **10**. 145

A-9. Crystal data and structure refinement for **13** 147

A-10. Atomic coordinates for **13**. 148

A-11. Crystal data and structure refinement for **16** 150

A-12. Atomic coordinates for **16**. 151

A-13. Crystal data and structure refinement for **17** 153

A-14. Atomic coordinates for **17**. 154

A-15. Crystal data and structure refinement for **22** 157

A-16. Atomic coordinates for **22**. 158

A-17. Crystal data and structure refinement for **24**. 160

A-18. Atomic coordinates for **24**. 161

A-19. Crystal data and structure refinement for **25** 163

A-20. Atomic coordinates for **25**.....164

LIST OF FIGURES

Figure page

1-1 Examples of conjugated polymers 1

1-2. Idealized mechanism for an electrochemical polymerization. 3

1-3. Transition metal catalyzed step polymerization 3

1-4. Lewis acid induced polymerization 4

1-5. Orbital interactions that compromise a π bond 5

1-6. Representative examples of organometallic polymers 6

2-1. Examples of complexes synthesized by Fagan (a) and Mann (b) 10

2-2. Examples of materials with architectures similar to those of the desired monomer 11

2-3. Synthetic scheme to used generate compound **1** 12

2-4. Proton NMR spectrum of compound **1** referenced to residual protons on $CDCl_3$ 13

2-5. Reaction yielding compound **2** 15

2-6. Proton NMR spectrum of compound **2** 16

2-7. ORTEP drawing of compound **2** 17

2-8. Synthesis of compound **3** 18

2-9. Proton NMR spectrum of **3**. 20

2-10. Electropolymerization of **1**. 21

2-11. Electropolymerization of **2**. 22

2-12. Proposed unit in Poly **2** responsible for observed electrochemistry 23

2-13. Comparative CVs of Poly **1** and **2**. 23

2-14. Spectroelectrochemistry of Poly **1**.....24

2-15. Spectroelectrochemistry of Poly **2**.....25

2-16. Proposed synthetic route to Bis-EDOT aldehyde.....26

2-17. Proton NMR spectrum of the product of the reaction to intended to yield Bis-EDOT aldehyde 27

2-18. Attempted routes to iron containing monomers 28

2-19. Synthetic scheme utilized to generate compound **4**.....29

2-20. One dimensional proton NMR of **4** 31

2-21. Synthetic scheme utilized to generate **5**. 32

2-22. Proton NMR spectrum of **5**. 34

3-1. Synthetic scheme detailing the diketonate complexes generated. 37

3-2. Near infrared PL of some of the Ln tris (β-diketonates) in benzene 39

3-3. EL spectrum of 10 mol% $Yb(DNM)_3Phen$ + PPP-OR11.....40

3-4. Device architecture for PLED used in this work. 41

3-5. Performance of a device constructed from 10 mol% $Yb(DNM)_3Phen$ + PPP-OR11.....42

3-6. Synthetic scheme followed to produce the bipyridine based conjugate polymer. 45

3-7. Synthetic procedure used to generate the conjugated bipyridine/ $Nd(TTFA)_3$ complex. 46

3-8. UV-visible absorption spectra and visible fluorescence from the bipyridine monomer and the monomer neodymium complex 47

3-9. Two of the considered structures for a diketone based conjugated polymer.48

3-10. Synthetic route to 1-(2,5-dibromo-phenyl)-3-phenyl-propane-1,3-dione 49

3-11. The two possible tautomers for β-diketones.....49

3-12. Proton NMR spectra of 1-(2,5-Dibromo-phenyl)-3-phenyl-propane-1,3-dione. 51

3-13. Synthesis of Diketone containing polymer.....52

3-14. Example of the proposed exchange reaction that could be used to attach a lanthanide complex to the conjugated diketone polymer. 53

3-15. Further exchange reaction leading to possible crosslinking in polymer/lanthanide complexes. 54

4-1. Commonly used synthetic pathway to LnTPP(acac)complexes 58

4-2. Recently developed alternate synthetic path to a LnTPP complex 59

4-3. Thermal ellipsoid plots of **8** and **9**. 63

4-4. Synthesis of anhydrous LnTPP complex 65

4-5. Thermal ellipsoid plots of **10** and **13**. 67

4-6. Results of electrospray ionization mass spectroscopy of **13** 69

4-7. Proposed mechanism accounting for the observation of acetamide in the mass spectra 71

4-8. Synthesis of LnTPP(TP) complexes 72

4-9. Thermal ellipsoid plots of **16** and **17** 73

4-10. Numbering and synthesis of the LnTPP(Klaui) compounds 75

4-11. One-dimensional proton NMR spectrum of **16** 79

4-12. COSY spectrum of **16** 80

4-13. Expansion of Figure 4-12 from 7 to 16 ppm 80

4-16. COSY spectrum of **21** 84

4-17. Expansion of Figure 4-15 from 2 to 11 ppm 84

4-18. Thermal ellipsoid plot of **22**. 86

4-19. Proposed reaction accounting for the observation of **22** 89

4-20. Thermal ellipsoid plot of **23**. 90

4-21. Reaction generating the MgTPP complex. 90

4-22. Performance of the various Yb complexes 92

4-23. Performance of a device utilizing YbTPP(TP)/ PPP/OR11 in the active layer 93

5-1. Examples of common mono-ring LnPc complexes....97

5-2. Synthesis of LnPc(Cl)DME....98

5-3. Synthetic scheme to generate LnPc(Klaui) complex....99

5-4. Thermal ellipsoid plots of **25** and **24**....100

5-5. One-dimensional proton NMR of **24**....103

5-7. Expansion of Figure 5-6 from 2 to 9.5 ppm....104

5-8. One dimensional proton spectrum of **25** at 292 K....106

5-9. One-dimensional proton NMR spectrum of **25** at 332 K....107

5-10. Absorption spectrum of YbPc(Klaui) in methylene chloride....108

5-11. Photoluminescence spectra of selected Er containing coordination complexes....109

ABSTRACT THE OF DISSERTATION PRESENTED TO THE GRADUATE SCHOOL
of the University of Florida in Partial Fulfillment of the
Requirements for the Degree of Doctor of Philosophy

SYNTHESIS AND CHARACTERIZATION OF INORGANIC COMPLEXES FOR THE MODIFICATION OF POLYMER PROPERTIES

By

TIMOTHY J. FOLEY

August, 2002

Chair: James M Boncella
Department: Chemistry

Research detailed in this work examines the effect of combining inorganic compounds with polymeric materials. The first chapter introduces the reader to terms and ideas not in common knowledge. Chapter 2 relates the influence of an organometallic moiety on a conjugated polymer's electrochemical and spectroelectrochemical properties. The remaining chapters deal with the synthesis, isolation, and characterization of lanthanide coordination complexes, whose ultimate use will be the production of near infrared light. The first complexes examined for this purpose, were the lanthanide tris β diketonates. Following that discussion is a discourse on the properties of lanthanide tetraphenylporphyrin and phthalocyanine complexes. These complexes have been shown, by work performed in our labs, to be superior to the diketonate complexes for the production of near infrared light. Specific details are provided on how these complexes

were generated and characterized. Additionally, the performance of these complexes in electroluminescent devices is reported and the influence of the macrocycles on the production of near infrared light is demonstrated. Finally, details are provided on attempts to generate near infrared luminescent polymers with lanthanide complexes directly incorporated into or onto the polymer backbone.

CHAPTER 1
INTRODUCTION

Traditionally materials chemistry has focused on either inorganic or organic systems almost to the exclusion of the other.[1] Recently researchers have been exploring the possibility of combining organic and inorganic systems to generate materials with properties intermediate between the two or with entirely new properties.[2] One area of research that has seen exceptional growth is the interactions of conjugated polymers with organometallic and inorganic coordination complexes. Ideally, new properties can be gained by the through-bond or the through-space interaction of conjugated polymers with inorganic complexes.

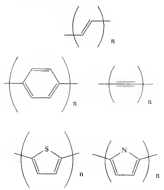

Figure 1-1 Examples of conjugated polymers

A polymer is defined as a large molecule or macromolecule whose structure is composed of small molecules that have been chemically joined. The arrangement of the small molecules or monomers in macromolecules has usually been performed so that polymer has an orderly, repeating structure on the molecular level. Polymer scientists have devised several classifications for these polymers based on monomer structure and

the consequence of the structure on the material properties of the polymer. Of the many classes available, the research in this work will be primarily concerned with the type known as conjugated polymers.

Conjugated polymers are defined as polymers that have a rigid backbone composed primarily of sp^2 or sp carbon atoms (Figure1-1).[3] The extended π system of the polymer leads to orbitals that are very close in energy, which allows extensive orbital mixing. In contrast, most organic compounds have discreet orbitals producing materials that are primarily insulators. It has been shown that conjugated polymers can be p or n doped leading to materials that are organic semiconductors. Doping levels for these materials (~20%) are substantially higher than for traditional inorganic semiconductors (~1%).[4] Accompanying the increase in conduction upon doping are dramatic changes in the optical properties of the conjugated polymer. The optical changes, usually red shifted absorptions, occur as a result of the introduction of the new lower lying energy states[5].

Because of the interest in these compounds, several different avenues are available for their production. The three routes used to synthesize conjugated polymers in this work are: electrochemical synthesis, transition metal catalyzed step polymerization, and Lewis acid induced polymerization.

Electrochemical synthesis relies on the use of cathodically or anodically generated radical ions of the monomer. Radical ions couple to one another or to the neutral monomer to produce dimers (Figure 1-2). Oxidation or reduction of the dimer then occurs again and the process repeats itself until the growing polymer is no longer soluble in the reaction medium.[6]

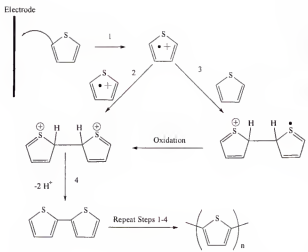

Figure 1-2. Idealized mechanism for an electrochemical polymerization.

Transition metal catalyzed step growth polymerization requires that the monomers have two reactive functionalities that play an integral role in the polymerization reaction. Typically, one of the monomers contains either a halide or psuedo-halide and the other monomer posses an electropositive functionality such as a boronic acid or a metal (Figure 1-3.)[7] The two monomers are then coupled using a late transition metal catalyst and an oxidative addition reductive elimination cycle. Examples of this chemistry would include, but are not limited to, the Suzuki and Stille couplings.

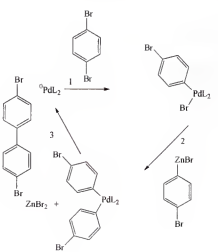

Figure 1-3. Transition metal catalyzed step polymerization

Lewis acid induced polymerization reactions are similar in nature to electrochemical methods; this method uses chemical reagents to oxidize the monomer to the radical ion which then undergoes the coupling. One major difference between these two mechanisms is that the polymer generated by this method is already p doped. In order to generate the neutral polymer this material must be reduced, as opposed to electrochemical methods that generate the neutral polymer (Figure 1-4).[8] This polymerization is complicated by the possibility of the monomer and polymer undergoing deleterious reactions due to the harsh nature of the conditions and as such is used less frequently than the two previously discussed methods.

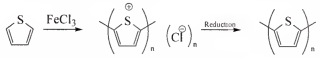

Figure1-4. Lewis acid induced polymerization

Inorganic Chemistry

The field of inorganic chemistry is concerned with all of the elements of the periodic table and the reactions they can undergo.[9] Due to the large amount of information encompassed by this definition, subdivisions are commonly used to differentiate areas of broad interest.[10] Two fields of inorganic chemistry that will be discussed in this work are organometallic and coordination chemistry.

Organometallic complexes are defined as molecules that have a direct bond between a carbon atom and a metal atom.[11] From this simple definition arises a great multitude of complexes; these complexes are often categorized by the mode in which the carbon atom is bound to the metal. Carbon can be bound to metals through a σ bond, a π bond, a combination of the two, or a dative bond. The type of organometallic bonding

that will be most relevant to the discussion is the π type. A π bound ligand requires the π electrons of an organic fragment to donate to an empty d_σ orbital on a metal, the metal then back donates to the organic fragment from a filled d_π orbital to the π^* orbital on the organic fragment (Figure 1-5).

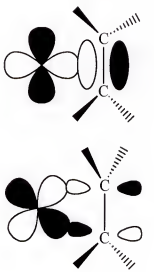

Figure1-5. Orbital interactions that compromise a π bond, 1 demonstrates the donation from the organic fragment to the metal, and 2 demonstrates the back donation from the metal to the ligand.

Complexes with π bound ligands are generally synthesized by ligand substitution or an oxidation state change of a metal in the presence of π coordinating ligand. In a substitution reaction, a labile ligand is replaced by a π coordinating ligand and the metal retains its initial oxidation state. Substitution reactions can be reversible or irreversible depending on the strength of the metal ligand interaction. Metals also can bind π ligands when they experience a change in oxidation state. The facility of this reaction depends on the conditions of the reaction, the metal center, and the nature of the intended ligand.

Using the π coordinating properties of transition metals, it is possible to generate a polymer with a metal attached to the backbone. As might be expected, these

organometallic polymers have properties that are significantly different from the purely organic counterpart.[12]

There are two main types of organometallic polymers found in the literature: those in which the metal is directly bound to the backbone and those in which the metal is bound to a substituent of the polymer (Figure 1-6). Special attention has been paid to the way in which the optical properties of these hybrid materials differ from their solely organic counterpart. Nonlinear optoelectronic effects reported in these papers are often attributed to metal to ligand and ligand to metal charge transfer interactions.

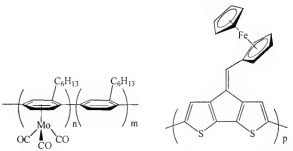

Figure 1-6. Representative examples of organometallic polymers

An application of these polymers would be in the area of electrochromic materials. As previously discussed, conjugated polymers can experience dramatic color change when charge is injected into their band structure. Attaching an organometallic fragment to a conjugated polymer may affect its band structure producing unexpected properties unique to this type of system.

As stated, this work will also detail the use of coordination complexes in polymeric systems. The area of lanthanide coordination chemistry will be the main form of coordination chemistry discussed. In complexes of this nature, the geometry of the ligands around the metal is determined by electrostatic attractions and steric repulsions. Due to low orbital interactions, the stability of a complex is based on the denticity of the

ligand, with ligands having high coordination numbers generally forming the more stable complexes.[11] This chemistry stands in stark contrast to transition metal coordination chemistry, where orbital interactions between the metal and ligand determine the bonding and geometry of the complex.

Novel material properties for inorganic/organic polymeric systems do not necessarily require that the inorganic material be attached to the polymer. Interesting properties can be achieved by combining a coordination complex with a conjugated polymer. Coordination compounds can be blended with conjugated polymer and the two can experience non-bonded through-space interactions.[13]

A potential use for these materials would be as the emitting layer in a light-emitting device (LED). Devices for this purpose can be as simple as a slide of ITO glass, an active layer, and a low work function metal. In a device of this type holes or positive charges are injected from the indium tin oxide (ITO) glass (the anode) and electrons or negative charges are injected from the metal (the cathode). The two charges then migrate towards each other through the active layer until they recombine and the energy that is generated can be released as either heat or light. When the energy is released in the form of light, it is considered electroluminescence. Examples exist of several different types of inorganic compounds being utilized for this purpose.[14]

Lanthanides have been shown to be particularly useful in this application for several reasons. The ions of the lanthanides have transitions with relatively narrow emission bands, having a full width at half height of 100 nm or less. This is attributed to the low radial extent of the *f* orbitals, leading to a limited interaction with the coordinating ligands. Limited interaction of the *f* orbitals also allows the transitions to

occur at approximately the same wavelength without regard to the nature of the ligand. These spectra differ substantially from the spectra observed for transition metals complexes, which are typified by broad emission bands whose maxima are directly related to the identity of the ligand attached to the metal.[15]

Summary

Dramatic changes in material properties have been observed in purely organic polymers by simply making minor changes to the structure of the monomer. In the next chapter, the effect of attaching an organometallic substituent to a conjugated polymer will be discussed. In later chapters, the synthesis and isolation of discrete lanthanide containing complexes will be detailed. Once the syntheses have been detailed, the effect of blending those complexes with polymers will be examined, with particular attention being paid to the production of near infrared light.

CHAPTER 2
ORGANOMETALLIC MONOMERS AND POLYMERS

Work reviewed in the introductory chapter cited general examples of organometallic polymeric systems. These materials have the possibility to be used in several different applications.[16] In this chapter, the discussion will pertain to the direct interaction between transition metals and conjugated polymers.[17] Details of the synthesis of these materials and the effects of the combinations will be related.

The organometallic portion of this project was inspired by the work of Fagan and Mann. Fagan published several examples of tris(acetonitrile)ruthenium pentamethylcyclopentadienide cations $[RuCp^*(CH_3CN)_3]^+$ reacting with aromatic groups generating $[\eta^6\text{-arene RuCp}^*]^+$ (Figure 2-1).[18] Mann has been able to build on this work constructing thiophene-based materials with appended ruthenium cations (Figure 2-1).[19]

The electrochemical polymerization of Mann's complexes has been reported to proceed with moderate success.[20] One of the obstacles to the polymerization of these materials was that the attachment of the metal to the terminal rings appeared to hinder the oxidation of the monomer. Since the oxidation of the monomer is crucial to the polymerization reaction, we proposed that placing the metal in the center of the monomer would minimize its influence on the terminus of the monomer.

Our first task was to generate a conjugated molecule that would have an arene ring at its center to which two ethylenedioxythiophenes (EDOT) rings could be attached. This architecture was chosen because Mann had shown that $[RuCp^*]^+$ preferentially

binds to phenyl rings over thiophenes. EDOT was selected, in lieu of thiophene, as the terminal ring in the molecule for two reasons. First, EDOT has a lower oxidation potential than thiophene allowing the electropolymerization of EDOT to occur more readily. Second, the ether linkages in the β positions of the ring prevent coupling in these positions during polymerization, making a polymer with a well defined, unambiguous structure.

a

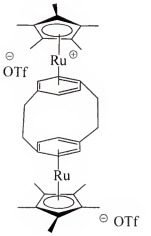

b

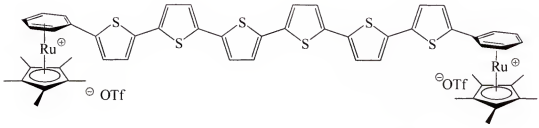

Figure 2-1. Examples of complexes synthesized by Fagan (a) and Mann (b)

The basic idea for the monomer was a modification of work performed by VanderLooy.[21] Wherein, a dialdehyde was allowed to react with an aryl phosphonium salt in a Wittig reaction, yielding molecules whose structures are similar to the complex shown Figure 2-2a. The low isolated yields for the reaction, in addition to the variety of possible side products made this synthetic methodology unappealing. In similar work by

Kubo, multiple Wittig reactions were used to generate the polymer shown in Figure 2-2b.[22] Low yields for this reaction lead to a polymer whose molecular weight was not well defined.

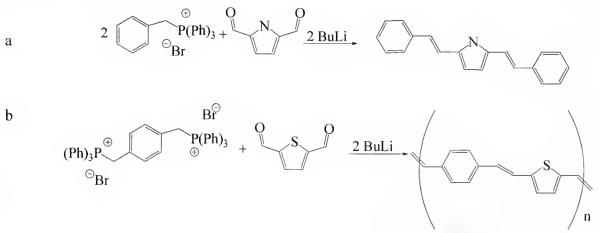

Figure 2-2. Examples of materials with architectures similar to those of the desired monomer

The Wittig reaction, discussed in the previous examples was capable of producing the desired complexes but in low yields. Because the monomer would be the starting material for various organometallic complexes, it would need to be relatively pure in large quantities. Soltzing and Roncali utilized Horner-Wadsworth-Emmons (HWE) reactions in preference to Wittig reactions, to generate various vinylene linked EDOT monomers, which could then be electropolymerized.[23] The compounds produced by these reactions were easily purified and could be produced on the gram scale. Therefore, by using an HWE reaction to link an EDOT to a phenyl ring *via* a vinylene spacer, a monomer with the desired architecture would be obtained in the highest yield.[24]

Synthesis of Bis(2,3-dihydro-thieno[3,4-b][1,4]dioxine) 1,4-Divinyl-benzene (EVPVE) Monomer (EVPVE) (1)

The synthesis of the bis(2,3-dihydro-thieno[3,4-b][1,4]dioxine) 1,4-divinyl-benzene uses the Horner-Wadsworth-Emmons reaction between two equivalents of 2,3-dihydro-thieno[3,4-b][1,4]dioxine-5-carbaldehyde and the [4-(diethoxy-phosphorylmethyl)-benzyl]-phosphonic acid diethyl ester (Figure 2-3). Neither the diphosphonate, nor the aldehyde are commercially available and must be synthesized. Fortunately, a host of possible synthetic routes are available in the literature to these two compounds.[25]

The aldehyde and the diphosphonate are dissolved in dimethoxyethane (DME) and then cannulated into a slurry of sodium hydride in DME at room temperature. Care must be taken in the synthesis of the monomer as it sensitive to the order of addition of the reactants and to the reaction solvent. Adding the aldehyde or the diphosphonate sequentially, in either order, to the hydride does not give a tractable product. For reasons not known at this time, it is critical that the addition of the two reactants be simultaneous.

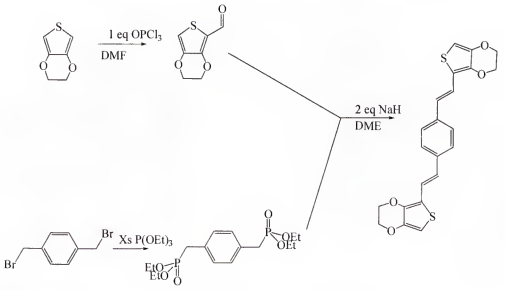

Figure 2-3. Synthetic scheme to used generate compound **1**

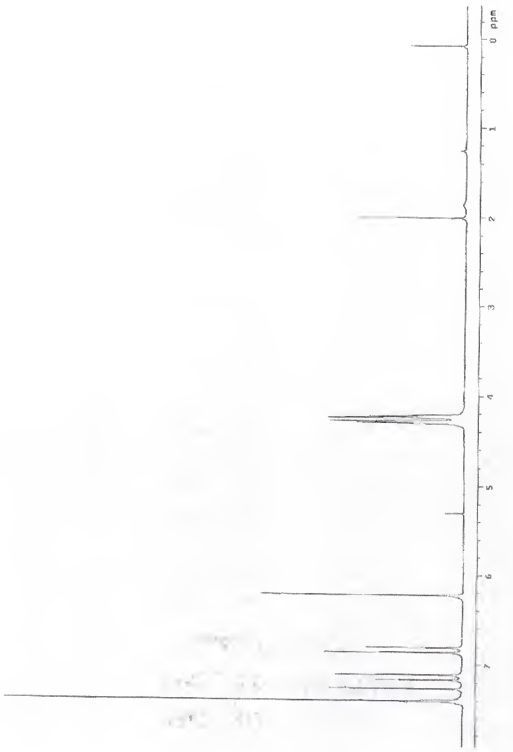

Figure 2-4. Proton NMR spectrum of compound **1** referenced to residual protons on $CDCl_3$.

Use of the hydride is preferred over other bases such as LDA or butyl lithium due to the ease of its handling. Immediately following the addition of the aldehyde and diphosphonate, the solution darkened and hydrogen gas began to evolve from the reaction. The reaction was brought to reflux under an atmosphere of nitrogen and was maintained at that temperature for 12 hr. Water was then used to quench the reaction and the product, a yellow amorphous mass, was isolated by filtration.

The proton NMR spectrum of the material, shown in Figure 2-4, is consistent with the expected structure. A sharp singlet was observed at 7.39 ppm and is assigned to the 4 protons on the phenyl ring. Peaks corresponding to the 4 vinylic hydrogen atoms are observed at 7.13, and 6.83 ppm as two sets of doublets. These peaks have a coupling constant of 16.1 Hz, as is expected for *trans* protons. A singlet at 6.22 ppm (2 H) is assigned to the proton on the EDOT α to the sulfur. The multiplet of multiplets centered at 4.28 (2 H) and 4.24 (2 H) ppm are assigned to the ethylene protons on the EDOT.

Synthesis of Ru EVPVE (2)

The organometallic monomer was prepared by the reaction of $[Ru(\eta^5\text{-}C_5Me_5)(CH_3CN)_3]^+$ with **1** in refluxing tetrahydrofuran (THF) under an atmosphere of nitrogen. A precipitate formed during the reaction that was separated from the solution by filtration. The THF solution contained **2** and **1** in a 40:60 ratio as determined by NMR. Isolation of the product was achieved by layering a methylene chloride solution of the crude product with diethyl ether. Golden yellow crystals of **2** formed on the walls of the flask, which were separated by filtration from the mother liquor.

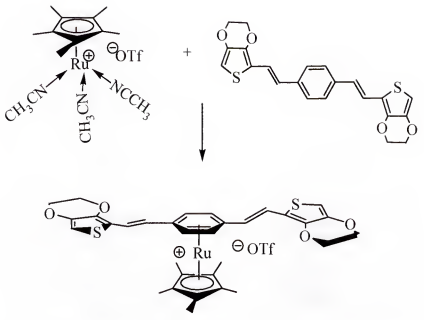

Figure 2-5. Reaction yielding compound **2**

Proton NMR spectroscopy confirmed the identity of **2.** [20](Figure 2-6) A pair of doublets, corresponding to the vinyl protons appears at 7.05 (2 H) and 6.27 ppm (2H) ($^3J_{H-H}$=16 Hz). A sharp singlet corresponding to the α proton on the thiophene is observed at 6.30 ppm, almost overlapping with the lower frequency vinlyene doublet. As expected, the arene protons experience a dramatic shift up field to 6.00 ppm (4 H) upon complexation of the arene to the ruthenium ion. The resonance frequencies of the EDOT ethylene protons are essentially unaffected by the reaction, so the peaks appear relatively close to those of the purely organic material. The protons on the methyl of the pentamethylcyclopentandienide group appear at 1.79 ppm (15 H).

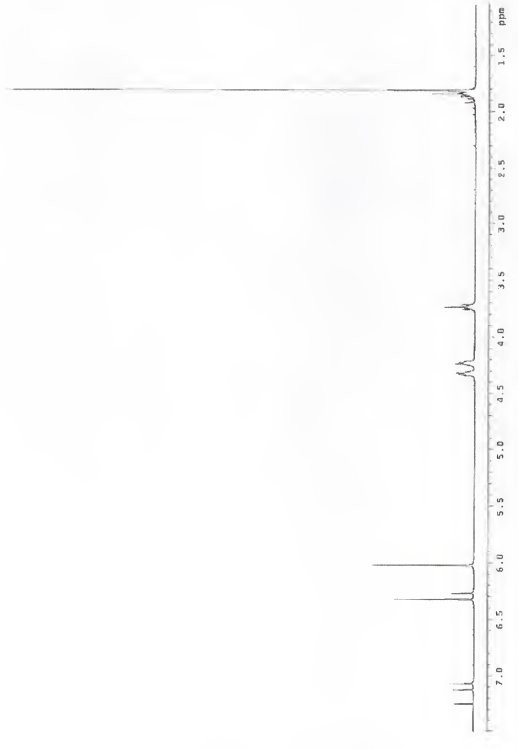

Figure 2-6. Proton NMR spectrum of compound **2**.

The structure of the monomer was also confirmed by X-ray crystallography, with the thermal ellipsoid plot shown in Figure 2-7. The average ruthenium aromatic carbon distance is 2.231(2) Å, with a Ru centroid distance of 1.714(1) Å. The average distance from the Ru to the carbon atoms of the Cp* is 2.182(6) Å, with a metal to Cp* centroid distance of 1.808(2) Å. An angle of 0.5 ° exists between the phenyl ring and the Cp* making them essentially parallel to each other. Measuring from the α carbon on one EDOT to the α carbon on the other EDOT, the molecule is 16.821(4) Å long. All other interatomic measurements are within expected values.

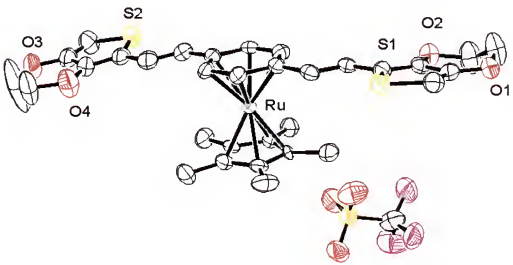

Figure 2-7. ORTEP drawing of compound **2** with thermal ellipsoids at the 50% probability level

Identification of the insoluble side product formed during the reaction was stymied by a complex NMR spectrum for the material. In the spectrum, there were several different Cp* resonance peaks and multiple peaks in the aromatic region which could correspond to hydrogen atoms on the phenyl portion of the EVPVE. It would appear from the spectrum that the reaction conditions lead to several side products. It is possible that the sulfur can coordinate to the ruthenium in a η-1 fashion and then undergo

a nucleophilic attack at the carbon α to the sulfur to generate a thiolate complex. Loss of ruthenium by this reaction would provide a decomposition pathway for the otherwise robust complex.

Synthesis of Ru(η^5-C_5Me_5)([4-(diethoxy-phosphorylmethyl)-benzyl]-phosphonic acid diethyl ester) (3)

In an attempt to increase the yield of the monomer, a different route to **2** was investigated. The [4-(diethoxy-phosphorylmethyl)-benzyl]-phosphonic acid diethyl ester was treated with $[Ru(\eta^5\text{-}C5Me5)(CH3CN)_3]^+$ in refluxing THF. The progress of the reaction was monitored by NMR, with the reaction coming to completion after ~5 hr. Concentrating the reaction mixture followed by layering with pentane gave **3**, as a tan crystalline material (Figure 2-8).

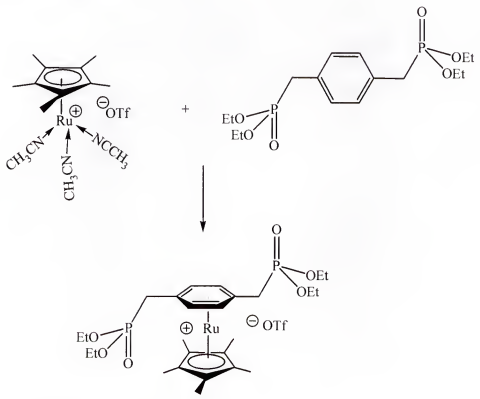

Figure 2-8. Synthesis of compound **3**

Proton NMR spectroscopy confirmed the identity of **3**. As shown in Figure 2-9, the spectrum of **3** contains 2 singlets (5.92 ppm (4 H), 1.92 ppm (15 H)) corresponding to the phenyl ring protons and to the protons on the (η^5-C_5Me_5). The phenyl ring protons, as expected, are shifted upfield by 1.26 ppm verifying the coordination of the metal to the diphosphonate. Additionally, the peaks appearing at 4.15 ppm (8 H) and 1.36 ppm (12 H) are assigned to the methylene and methyl of the ethoxy, respectively. A doublet is observed at 2.70 ppm (4 H, $J_{H\text{-}P}$ 29.9 Hz), which has been assigned as the methylene between the phenyl ring and the phosphorous.

Alternate Synthesis of Compound 2

A solution of **3** was combined with 2 equivalents of the EDOT aldehyde in DME and then added to a DME / potassium hydride slurry. Observations for this reaction are similar to that which was observed for the synthesis of **1**. The reaction was completed in *ca.* 6 Hr, without the formation of an insoluble side product. The yield of the product went from approximately 40% to almost 75%. The identity of the compound was confirmed by proton NMR. Clearly, the reversal of the reaction order eliminated decomposition pathways that had previously limited the yield of **2**.[26] It is also expected that the coordination of the metal to the ring prior to the deprotonation increases the stability of the intermediate anion in the Horner-Wadsworth-Emmons reaction.

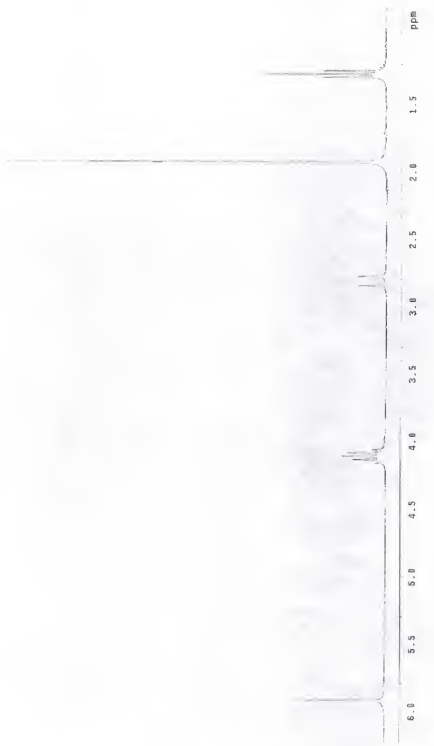

Figure 2-9. Proton NMR spectrum of **3**.

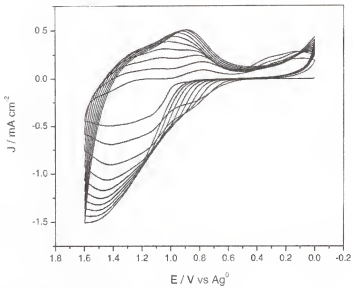

Figure 2-10. Electropolymerization of **1**.

Electropolymerization of Compound 1

A 0.5 mM dichloromethane solution of compound **1** was electropolymerized onto an electrode of ITO glass in a 0.1 M solution of tetrabutylammonium tetrafluoroborate. The 10-cycle polymerization was run at a 100 Mv/s scan rate with the scans shown in Figure 2-10. Onset of the polymerization begins with the first cycle at 1.1 V and as the polymerization continues the potential for subsequent couplings decreases to ~0.7 V. In addition, the resistance to further oxidations increases with the increasing polymer film thickness, as expected.

Electropolymerization of Compound 2

The electropolymerization of **2** was run under the same conditions as **1**, with the traces for the polymerization cycles shown in Figure 2-11. Initially, an oxidation is observed at ~1.3 V, corresponding to the coupling of monomers. Subsequent scans showed a much lower oxidation potential and have been tentatively assigned to the oxidation of the vinylene EDOT- EDOT –vinylene (VEEV) unit expected in the

oligomeric material. In polymeric systems made entirely of VEEV a similar redox cycle has been observed. We propose that the ruthenium metal breaks the communication between the VEEV units making them behave as if they were small molecules.[25] (Figure 2-12) This supposition is further confirmed by a comparison of the cyclic voltamagrams of poly **1** and poly **2** (Figure 2-13). In this experiment, the two electrodes that had been coated with polymer film by electropolymerization were removed from the reaction mixture, washed with the electrolyte, and placed into an electrochemical cell containing only the electrolyte. The film of poly **1** had a very wide profile similar to an ill-defined polymer with an $E_{1/2}$ of 0.73 V, similar to the polymer reported by Kubo that had an $E_{1/2}$ of 0.72.[23] In contrast, the cyclic voltamagram of the poly **2** film had a shape similar to a small molecule and an $E_{1/2}$ of 0.931 V.

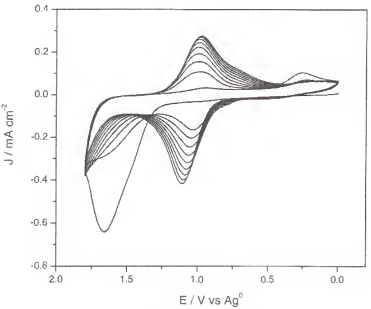

Figure 2-11. Electropolymerization of **2**.

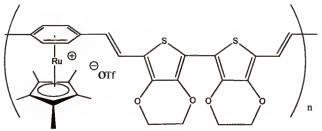

Figure 2-12. Proposed unit in Poly **2** responsible for observed electrochemistry.

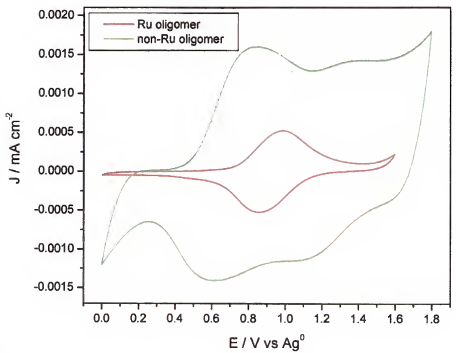

Figure 2-13. Comparative CVs of Poly **1** and **2**.

Spectroelectrochemistry of Poly 1 and 2

Spectroelectrochemical experiments were performed on the two films; this entailed applying a voltage to the film as the UV-visible absorption of the material was measured (Figure 2-14 and 2-15). For the poly **1** film it was observed that on going from 0.0 V to 1.2 V an absorption grew in at ~1.75 eV or 709 nm. An increase of the material's absorption in the red region of the visible spectrum causes the film to change

from a golden yellow to a bluish green. This behavior was reversible and the color of the film could be switched back and forth repeatedly with no degradation in the intensity of the color.

The poly **2** film shows little electro-optic activity as the applied voltage increases from 0 to 1.50 V, but experiences a dramatic increase in its absorbance at 2.0 eV or 620 nm on going from 1.5 to 1.8 V. The color change is not reversible and occurs at approximately the same potential as the electrochemical oxidation of $[RuCp^*(C_6H_6)]^+$.[27] This may account for the dramatic color change in the poly **2** film, but it has not been confirmed at this time.

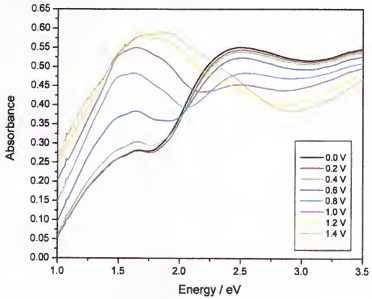

Figure 2-14. Spectroelectrochemistry of Poly **1**.

Attempted Synthesis of Bis-EDOT-VPV-Bis EDOT

To further explore this family of polymers, an attempt was made at extending the length of the polymer chain by 2 EDOT rings (Figure 2-16). The first step in the synthesis was the dimerization of EDOT, for which there are several synthetic routes available.[28] To access this material, the route as shown was chosen due to the ease of

isolation of the product from the inorganic side products, a problem that is not easily resolved in other systems. Following the coupling reaction, one of the rings must be functionalized with an aldehyde. Several different routes were used in an attempt to prepare this material, but none were successful. The method that generated the cleanest material was the Vilsmeier oxidation, with the NMR spectrum of the product shown in Figure 2-17.

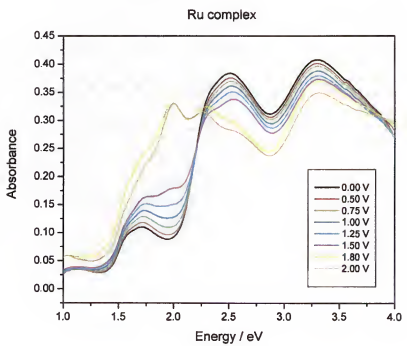

Figure 2-15. Spectroelectrochemistry of Poly **2**.

The aldehyde is expected to have 4 peaks in its NMR spectrum, the proton on the aldehyde at ~10 ppm, the α proton on the thiophene at ~6 ppm, and the 2 multiplets which are assigned to the ethylene protons at ~4 ppm. Instead 5 peaks are observed. The identity of the fifth peak is unknown but it is intimately related to the material as several recrystallizations do not change the relative integration for the peaks. Additionally the

material generated by the reaction does not successfully undergo a HWE reaction. Further efforts will be required to properly determine the identity of this material.

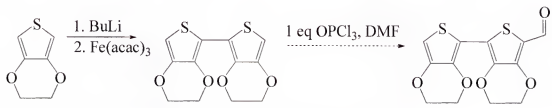

Figure 2-16. Proposed synthetic route to Bis-EDOT aldehyde.

Synthesis of Rhodium EVPVE (4)

Following the successful synthesis of compound **2**, we endeavored to generate another organometallic monomer. In the literature there are few examples of other arene metal Cp* complexes, and these are limited to iron, ruthenium, cobalt, rhodium, and iridium.[29,30,31] Attempts to make the iron based congeners of compounds **2** or **3** by light promoted arene exchange reactions were meet with failure.[32] When the synthesis of iron based **2** was attempted the monomer photopolymerized and no iron arene complex was found that would undergo an exchange reaction with the diphosphonate to make the iron containing version of **3**.(Figure 2-18)

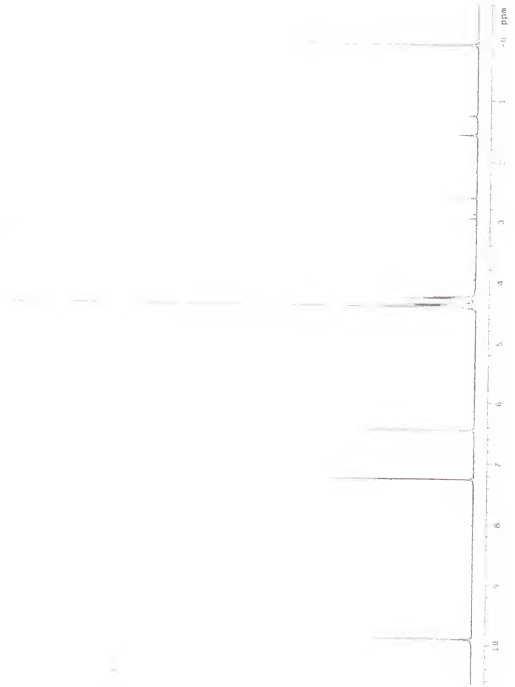

Figure 2-17. Proton NMR spectrum of the product of the reaction to intended to yield Bis-EDOT aldehyde

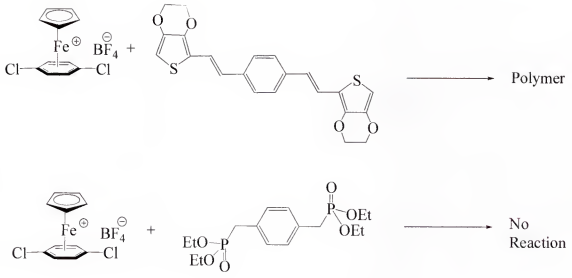

Figure 2-18. Attempted routes to iron containing monomers

Focus then shifted to the synthesis of a rhodium containing EVPVE monomer. Rhodium coordination chemistry is slightly different from the analogous ruthenium examples. In the case of ruthenium, the acetonitriles on the $[Ru(\eta^5\text{-}C_5Me_5)(CH_3CN)_3]^+$ complex are labile and are easily substituted, but in $[Rh(\eta^5\text{-}C_5Me_5)(CH_3CN)_3]^{2+}$ the acetonitriles are inert to substitution.[33] To circumvent this complication, a weakly coordinating ligand must be chosen in preference to acetonitrile when attempting to generate Rh arene complexes(Figure 2-19).[34] Literature examples have focused mainly on the use of methanol, acetone, and dichloromethane (DCM). Preliminary attempts to generate the Rh EVPVE, in these solvents following the standard literature procedures, were not successful. In a final attempt, the $[Rh(\eta^5\text{-}C_5Me_5)(acetone)_3]^{2+}$ complex was generated and was concentrated to a viscous oil. The complex cannot be isolated due to intramolecular and intermolecular decomposition reactions therefore, the oil was dissolved in DCM and the EVPVE was added generating a green–orange slurry. The

solution was then stirred for two days at room temperature and the complex was isolated as a yellow-orange powder. Attempts to accelerate the reaction, by heating the mixture, resulted in the formation of an intractable material. In addition, attempts to generate compound **4** by the action of silver nitrate on the rhodium dimer in the presence of EVPVE were unsuccessful. In that experiment, the EVPVE was oxidized and metallic silver plated out as a film on the sides of the reaction vessel.

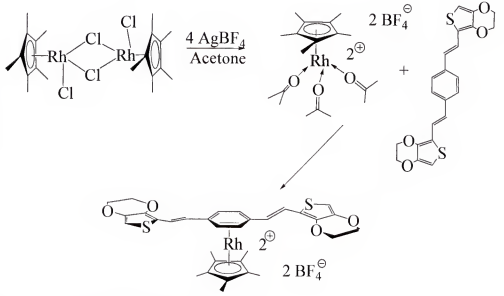

Figure 2-19. Synthetic scheme utilized to generate compound **4.**

Compound **4** was identified by the effect of the rhodium on the peak positions of the EVPVE in the proton NMR spectrum.[35] An examination of the aromatic region of the spectrum reveals that the alkene protons have shifted to 7.90 ppm (2 H) and 6.90 ppm (2 H) (J_{H-H} 16 Hz) (Figure 2-20). The peak assigned to the phenyl ring has shifted downfield to 7.88 ppm (4 H). This is in contrast to the upfield shift of the phenyl protons in **2**, and is attributed to the greater positive charge on the rhodium. The remaining peaks in the NMR spectrum of **4** are relatively unaffected in their position relative to the spectrum of **2**.

Due to the small amount of monomer generated in these experiments, it was not possible to perform electropolymerization experiments on this material. Future work with this complex will focus on generating it in a sufficient quantity to allow a full exploration of its electrochemistry.

Synthesis of Bisdodecyloxy EVPVE

It has been well demonstrated that conjugated polymers are typically insoluble in most organic solvents. To circumvent this problem, long alkyl side chains have been attached to conjugated polymers to increase the solubility of the material. In our system, we attempted to increase the solubility of our polymer by attaching dodecyloxy side chains to the phenyl ring of the monomer. The bisdodecyloxydiphosphonate required for this experiment is not commercially available and therefore had to be synthesized. The synthesis began with 2,5-dihydroxy-terephthalic acid diethyl ester, utilizing dodecylbromide in a Williamson ether synthesis to yield 2,5-bis-dodecyloxy-terephthalic acid diethyl ester. The ester was then reduced with $LiAlH_4$ to (2,5-bis-dodecyloxy-4-hydroxymethyl-phenyl)-methanol. Conversion of the diol to the dibromide was achieved using the triphenylphosphonium dibromide. Care must be taken at this point in the synthesis as benzyl bromides are a potent lachrymators and allergens. Reaction of the dibromide with phosphorous acid triethyl ester yielded the bisdodecyloxydiphosphonate. This was then reacted with the 2,3-dihydro-thieno[3,4-b][1,4]dioxine-5-carbaldehyde to yield **5** (Figure 2-21). The overall yield of the reaction based on the starting amount of terephthalic acid ester is 12%, but the yield based on the final reaction is approximately 45%.

Figure 2-20. One dimensional proton NMR of **4** (Note peak center at 2.05 ppm is due to residual protons on d_6 acetone.)

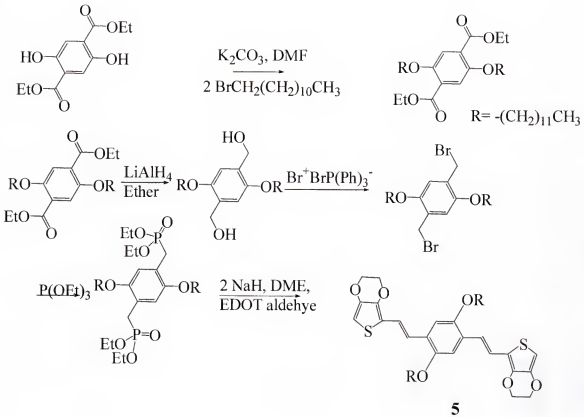

Figure 2-21. Synthetic scheme utilized to generate **5**.

The identity of compound **5** was confirmed by proton NMR, with the spectrum shown in Figure 2-22. The two peaks for the vinylic hydrogen atoms appear at 7.33 (2 H) and 7.00 (2H) ppm. Additional confirmation for the success of the HWE reaction is provided by the appearance of the thiophene peak at 6.20 ppm (2 H). The two protons for the phenyl ring are shifted upfield, relative **1,** to 7.26 ppm due to the electronic contributions of the alkoxides. The hydrogen atoms on the ethoxy portion of the EDOT ring appear at 4.27 and 4.23 ppm (8 H), respectively. The peaks for the protons on the methylenes α to the dodecyloxy oxygen atoms are at 4.11 ppm. The remaining 46 protons associated with the dodecyloxy side chains, appear from 2 to 1 ppm. Attempts to attach the $[Ru(\eta^5\text{-}C_5Me_5)]^+$ to the backbone have been made, but the isolation of the

metallated monomer from the nonmetalleted monomer has proven to be difficult. Future synthetic efforts may focus on a route similar to the alternate route to compound 2.

Summary

In this chapter, the results of several synthetic approaches to generating organic and organometallic electropolymerizable monomers have been presented. It was shown that **2** can be synthesized in a higher yield by first generating **3** and then performing a Horner-Wadsworth-Emmons reaction, as opposed to the direct action of $[Ru(\eta^5\text{-}C_5Me_5)CH_3CN)_3]^+$ on **1**. The polymerization of **2** is presented and is compared to the results observed for **1**. It was found that films of both polymers could be formed and that the metal had a direct effect the electro-optic properties of poly **2**. Compound **4** has been successfully synthesized and isolated with further investigations of its properties being planned. Variants on the EVPVE structure have been investigated and a more soluble version of the monomer, compound **5,** is now available for investigation.

Figure 2-22. Proton NMR spectrum of **5**.

CHAPTER 3
SYNTHESIS, PHOTOLUMINESCENCE, AND ELECTROLUMINESCENCE OF LANTHANIDE TRIS- (β–DIKETONATE) COODINATION COMPLEXES

The central theme of the work in this chapter is to demonstrate the ability of lanthanide tris(β diketonate) complexes to act as competent sources of near infrared electroluminescence and photoluminescence. A second topic to be discussed is the feasibility of generating a lanthanide containing conjugated polymer in an attempt to remedy the problems caused by phase separation in the polymeric thin films responsible for NIR electroluminescence.

Photoluminescence (PL) and electroluminescence (EL) for lanthanides was first reported in cases where the ions were sequestered in inorganic semiconductors. [36] Following those reports, visible PL spectra were recorded for lanthanide coordination complexes, where the ligands on the metal were organic chromophores whose triplet states were higher in energy than the *f-f* orbital transition responsible for fluorescence.[37] The organic chromophores were required because *f-f* orbital transitions are forbidden by selection rules. Due to this, the molar absorptivity of the ions is low, and it is difficult to directly excite the lanthanides.[38] Excited states can be produced on the organic ligands, and this energy can then be directly transferred to the metal to produce an excited state. This energy transfer process is colloquially called the "antennae effect".[39] More recently, the antennae effect has been shown to be equally valuable for producing electroluminescence from lanthanide coordination complexes.[40]

In some reports on visible EL, lanthanide tris(β diketonate) phenanthroline complexes were placed between two electrodes in devices of varying architectures. When a potential is applied to the device current flows, and the device lumineses.[41] One of the more effective architectures involves blending the Ln complexes with conjugated polymers in the active layer of the device.[42(b)] The working premise for this setup is that the conjugated polymer readily conducts charge from the electrodes to the Ln complex whereupon the charges recombine on the complex producing an excited state similar to that observed for the antennae effect. Energy transfer to the metal occurs and fluorescence follows. It has been demonstrated that this device architecture can improve the operating efficiency of visible polymeric light emitting devices (PLED) and therefore we wished to explore this effect for the production of near infrared light.

Synthesis of Lanthanide Tris(β diketonate) Complexes

The synthesis of the lanthanide tris(β diketonate) complexes was effected following the literature procedure.[42] Complexes were synthesized using five different β diketonates ligands: pentane-2,4-dione (acac), 2,2,6,6-tetramethyl-heptane-3,5-dione (TMHD), 1,3-diphenyl-propane-1,3-dione (DBM), 1,3-di-naphthalen-2-yl-propane-1,3-dione (DNM), and 4,4,4-trifluoro-1-thiophen-2-yl-butane-1,3-dione (TTFA) (Figure 3-1). In addition to varying the β diketonates on the complexes, the Lewis bases that occupied the seventh and eighth coordination sites on the complexes were also varied. Bases examined include bipyridine, phenanthroline, bathophenanthroline, and water. Lanthanides investigated were chosen because of their demonstrated near infrared luminescence in inorganic host matrices.

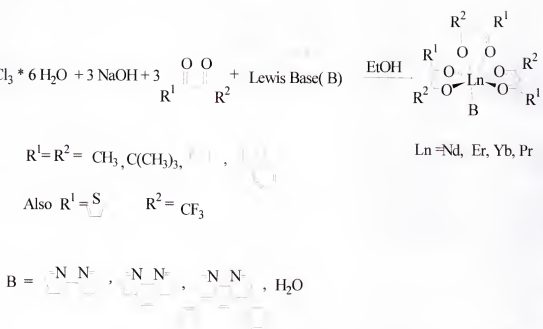

Figure 3-1. Synthetic scheme detailing the diketonate complexes generated.

Interactions of Ln Tris(β diketonate) Phenanthroline Complexes with Conjugated Polymers

The influence of the diketonates on the fluorescence of several of the polymer/ lanthanide blends was explored in solution and in thin films by Ben Harrison. It was generally found that the complexes quenched both the EL and the PL of the conjugated polymers effectively, but the NIR fluorescence efficiency varied with the nature of the R group on the diketone. In the first section, the data collected from the PL solution experiments will be discussed, followed by an outline of results from thin film EL experiments.

Results From Solution Phase Experiments

The NIR photo luminescence from some of the complexes generated are presented in Figure 3-2. Intensities for the spectra are all on the same relative scale, but quantum yields for the transition have not been determined. Fluorescence from the Yb $^2F_{5/2} \rightarrow {}^2F_{7/2}$ transition is the most intense of the near infrared emitting ions studied.

Neodymium has three observed transitions, $^4F_{13/2} \rightarrow {}^4I_{13/2}$, $^4F_{13/2} \rightarrow {}^4I_{11/2}$, and $^4F_{13/2} \rightarrow {}^4I_{9/2}$ producing light at 1350, 1060, and 930 nm, respectively. One transition was recorded for Erbium, $^4I_{15/2} \rightarrow {}^4I_{13/2}$ that is responsible for the 1537 nm light. The weakest fluorescence observed was from the Pr^{3+} ion, whose $^1D_2 \rightarrow {}^3F_4$ transition produces the 1040 nm band. We attribute the differences in the observed intensities to the efficieny of the energy transfer from the ligand to the metal and to the ability of the lanthanide excited state to relax by nonradative pathways. In general, TTFA proved to be the most successful ligand for PL and TMHD to be the least. We believe that theses two observation are related. It has been shown that in certain circumstances C-H bonds can quench NIR luminescence.[43] Thus, by reducing the number of C-H bonds that are close to the metal, the PL should increase. The observed qualitative PL results agree with this expectation.

Results From Thin Film Experiments

In the thin films, it was observed that the complex /polymer combination with the best luminescent properties were the DNM ligand complexes blended with PPP-OR11. Of the lanthanides investigated, ytterbium had the strongest NIR emission and so discussion in this section will focus on its properties. The emission wavelength of the various compounds is invariant with the ligand identity and the complexes exhibit a similar trend in their electroluminescence intensity as a function of the ligand. The EL and PL for a 10 mol% mixture of the lanthanide in the polymer are both shown in Figure 3-3, with the PL spectrum being recorded on the device prior to operation.

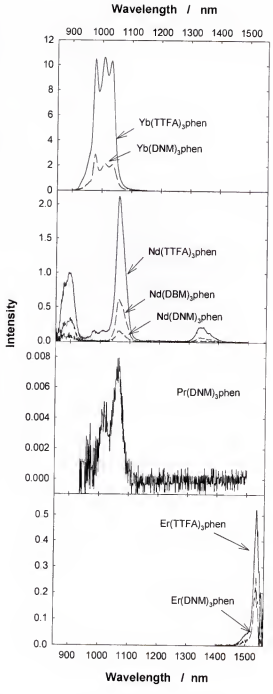

Figure 3-2. Near infrared PL of some of the Ln tris (β-diketonates) in benzene. Excitation wavelength varied with the absorption maxima of the ligand

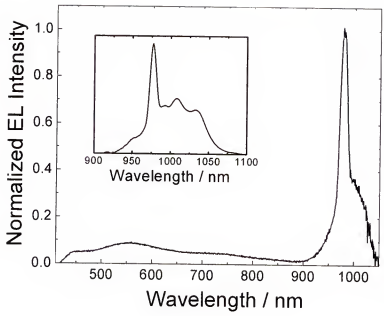

Figure 3-3. EL spectrum of 10 mol% $Yb(DNM)_3Phen$ + PPP-OR11 device obtained at 0.6 mA/mm^2. The inset shows PL spectrum from the same film (λ_{ex} = 370 nm).

Near-IR electroluminescent devices were constructed from ITO glass coated with PEDOT-PSS. The $Yb(DNM)_3Phen$ and PPP-OR11 blend was cast from a solution in which the concentration of the lanthanide complex was varied relative to the number of polymer repeat units. Calcium (50 Å) and Al (2000 Å) layers were deposited by thermal evaporation under a high vacuum. When the device is functioning, electrons are injected from the calcium and are removed at the ITO electrode. Positive and negative charges migrate towards one another and when the charges recombine, the excited state energy generated is responsible for light production. The architecture for the device is shown in Figure 3-4.

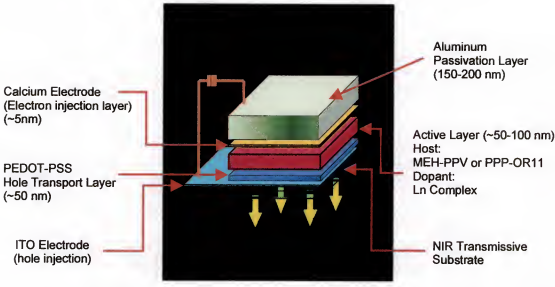

Figure 3-4. Device architecture for PLED used in this work.

Differences in the observed peak shapes in the spectra are attributed to the different responses of the detectors at longer wavelengths. In the EL spectrum, the detector's sensitivity drops off markedly at 1000 nm, cutting off the wavelengths longer than ~1000 nm. In the visible, fluorescence from the conjugated polymer is quenched up to 95%. The remaining 5% is responsible for the broad emission centered at 550 nm. The $Yb(DNM)_3Phen$ device features EL NIR emission that turns on at ~ 4.5 V, and the intensity of the emission increases as the applied voltage is increased. The plot in Figure 3-5 demonstrates that there is a direct correlation between the current density and the intensity of the light emitted from the device. As may be expected, when more charge is injected, the probability of having a radiative event increases. At ~ 10 V the device short circuits and the NIR radiance goes to zero.

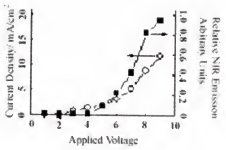

Figure 3-5. Performance of a device constructed from 10 mol% $Yb(DNM)_3Phen$ + PPP-OR11. Open circle, current densities; closed square, near IR irradiances.

The relationship between the relative NIR irradiance and the current density was also studied at various compositions of [Yb] (from 1 mol% to 20 mol%). At [Yb] < 10 mol%, a significant amount of visible EL is observed. For devices with [Yb] <10 mol% a lower resistivity was observed; therefore, a higher current density at a lower applied voltage. However, even for high current densities (10 mA/mm^2), little NIR output was recorded. Concentrations of 10 mol% quench most visible EL and for [Yb] ≥ 10 mol %, a significant NIR output was observed even at low current densities (1 mA/mm^2). In terms of quantum efficiency, 20 mol% loading in the device operates more efficiently than 10 mol %. This data suggests that at higher concentrations of $Yb(DNM)_3Phen$ the complexes act more efficiently as traps for charge carriers, resulting in high EL efficiencies at lower current densities.

It might be assumed that the most efficient devices would be constructed with the highest loading of the lanthanide complex. Loading the device higher than 20% does not result in an increase in operating efficiency; in fact, it begins to decrease. At the higher loading levels, self-aggregation of the complexes may become prevalent and self-

quenching events more probable. It is likely that the solubility of the diketone in the polymer is a critical factor in self-aggregation, and thus, the functioning of the PLED. A possible route to eliminate solubility issues for the complexes would be to incorporate them into a processible conjugated polymer.

Polymeric Ligands

In an attempt to increase device efficiency and reduce aggregation effects among the Ln complexes, efforts were made to generate monomers that would be able to incorporate the metal onto the backbone of conjugated polymers. Direct communication between the metal and the conjugated polymer would obviate the need for an energy transfer from the polymer to the ligands on the metal, because the polymer itself would become a ligand. Additionally, it has been shown by work in our lab that the Ln complexes have a tendency to separate from the conjugated polymers in which they are blended, presumably decreasing the efficiencies of the devices through self-quenching. The direct attachment of the Ln to the polymer should inhibit phase separation, thereby decreasing the probability of self-quenching.

Conjugated Bipyridine Synthesis

Initially, we investigated the attachment of a conjugated bipyridine to a Ln complex. Our system was intended to be similar to that reported by Yu.[44] Starting with the dimethylbipyridine, we generated the α,α' dibromomethylbipyridine by refluxing with NBS in carbon tetrachloride. The halogenated bipyridine was then converted to the diphosphonate by refluxing in phosphoric acid triethyl ester. In parallel with this procedure, 1,4 dibromo 2,5 bishexyloxybenzene was synthesized by means of a Williams ether synthesis from 1 bromohexane and 1,4 dibromo 2,5 bisphenol. The alkoxybenzene was then transformed to 4 bromo 2,5 bishexyloxybenzaldehyde by a halo lithium

exchange followed by quenching with dimethylformamide (DMF). Utilizing a Horner-Wadsworth-Emmons reaction, the phosphonate and the aldehyde were combined to generate Compound **6** (Figure 3-6). Compound **6** is an orange solid that when illuminated with a UV hand lamp fluoresces aquamarine. The intended use for **6** was to polymerize it in a Suzuki style polymerization and then attach to lanthanide complex to it

Lanthanide Conjugated Bipyridine Complexes

Attachment of the lanthanide complex to the polymer would follow a procedure in which a bis aquo Ln tris(β diketonate) would be refluxed in an anhydrous noncoordinating solvent such as benzene with a Lewis base (Figure 3-7).[45] The reaction would be driven by azeotropic removal of water from the reaction by means of a Dean Stark apparatus leaving only the Lewis base to coordinate to the complex. The progress of the reaction could be conveniently followed by observing the change in the intensity of the fluorescence of the bipyridine. Assuming there is no spectral overlap between the β diketonate on the lanthanide and the Lewis base, which for this system there was not, the visible PL intensity of the conjugated system should decrease as the reaction progresses. In conjunction with the aforementioned change, the absorption spectra of the monomer should blue shift as electron density from the bipyridine is shared with the lanthanide.

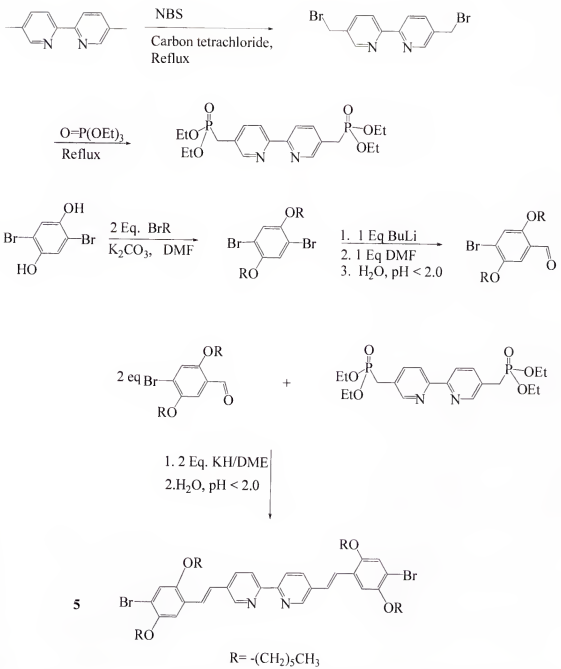

Figure 3-6. Synthetic scheme followed to produce the bipyridine based conjugate polymer.

Before time and effort were spent on investigating the polymerization of the monomer, it was decided to determine if the monomer paired with a lanthanide complex would luminesce in the NIR. In our initial attempt to generate a complex, we chose to coordinate $Nd(TTFA)_3 \cdot 2\ H_2O$ to compound **6**. When the two reactants were combined,

the solution strongly fluoresced in the visible, but after refluxing for ~4 hours, there was a 64% drop in PL QY in the visible and a 75 nm blue shift in the absorption spectrum. The quenching of the monomer fluorescence indicated that the Nd had coordinated to the monomer (Figure 3-8). Additionally, the blue shift in the absorption of the monomer can be interpreted as a decrease in conjugation due to the coordination of the electron withdrawing effects of the neodymium complex. This material was examined and found to have no observable NIR PL in solution regardless of the excitation wavelength.

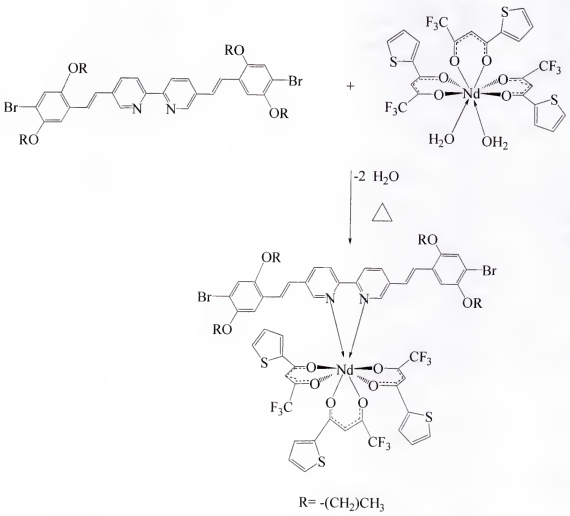

R= -$(CH_2)CH_3$

Figure 3-7. Synthetic procedure used to generate the conjugated bipyridine/ $Nd(TTFA)_3$ complex.

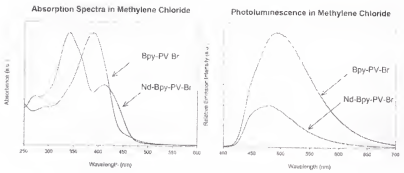

Figure 3-8. UV-visible absorption spectra and visible fluorescence from the bipyridine monomer and the monomer neodymium complex

These results are somewhat surprising as a limited amount of fluorescence would be expected from the diketonate complex, even if the bipyridine were not transferring energy to the Nd. The use of this ligand for NIR emission has yet to be fully explored, and it maybe appropriate for use with other lanthanide ions. Further experiments are required to determine if other complexes will luminesce with this ligand.

Conjugated Diketone Synthesis

Another polymer that was envisaged as being of utility to our investigation was a β–diketone containing polymer. Two modes of incorporating a diketone into a polymer can be imagined: one in which the diketone is a constituent of the polymer backbone and one in which the diketone is pendant to the polymer backbone (Figure3-9). In our studies, we chose to investigate a system where the diketone would be appended on to the polymer. In the literature, there had been no interest in using diketones as substituents on conjugated polymers. Before we could investigate generating a diketone containing conjugated polymer-lanthanide complex, a diketone containing conjugated polymer would need to be generated. The first step in this process was the successful synthesis of a diketone containing monomer.

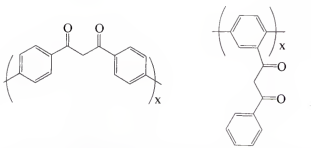

Figure 3-9. Two of the considered structures for a diketone based conjugated polymer.

Synthesis of 1-(2,5-Dibromo-phenyl)-3-Phenyl-Propane-1,3-Dione (7)

Compound **7** was generated by the reaction of 2,5-dibromo-benzoyl chloride with the anion of acetophenone (Figure 3-10). The 2,5-dibromo-benzoyl chloride was generated according to literature procedure, and the anion was generated by the action of potassium hydride on acetophenone.[46] The reaction was allowed to proceed for 5 hours, and quenched in water having a pH less than 2. The product precipitated from the solution as an amorphous, orange-yellow solid and was isolated by gravity filtration and purified by recrystallization from an ethanol and water mixed solvent system.

Diketones have two tautomers designated as the keto or enol form, for complexes with strongly electron withdrawing substituents, the enol is preferred (Figure 3-11).[47] The enol isomer is readily identified by the resonance in the proton NMR spectrum at or above 15 ppm. Deshielding of the proton located between the oxygens is responsible for the peak position and provides a convenient means of identifying these compounds. The NMR spectrum of the product displays a peak at 16.24 ppm (1H) and a peak at 6.73 ppm (1 H) that corresponds to the proton located on the carbon that is α to both ketones. Peaks in the aromatic region of the spectrum appear as a superposition of the NMR spectra of the starting materials.

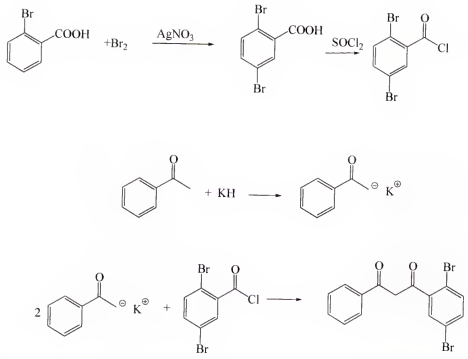

Figure 3-10. Synthetic route to 1-(2,5-Dibromo-phenyl)-3-phenyl-propane-1,3-dione

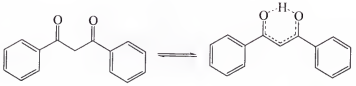

Figure 3-11. The two possible tautomers for β-diketones, the preferred tautomer for **7** is shown on the right.

Diketone Conjugated Polymer Synthesis

The polymer synthesis involved a Suzuki style coupling reaction where 0.2 equivalents of the dibromo diketone and 0.8 equivalents of 2,5 bishexyloxy 1,4 dibromo benzene were reacted with one equivalent of a 1,4 diboratobenzene.[48] The 1,4 dibromo 2,4 bishexyloxybenzene was added to increase the solubility of the incipient polymer and the spatial separation of the diketones. The reaction was catalyzed by a

diphenylphosphino ferrocene ligated palladium complex in the presence of excess base (Figure 3-13).

Polymer generated by this reaction was identified by proton NMR spectroscopy and by GPC. Because the polymer would have a random structure, the amount of diketone incorporated could not necessarily be predicted, but had to be determined experimentally. By using the relative integration of the enol proton at 15 ppm to the methylene peak of the alkoxy side chain at ~3.5 ppm, the ratio of the diketone to alkoxy side chains was established at ~ 6 alkoxy side chains to one diketone. The M_n of the material was 2556 g/mol giving the average polymer chain a length of 10 repeat units. Attempts to increase the chain length and the quantity of the polymer produced in this reaction have not been successful. Currently, we believe that the diketone maybe impeding the progress of the reaction by interacting with the palladium. Studies utilizing other catalysts may be required to optimize the molecular weight and yield of the polymer. The reactions required to generate a lanthanide containing conjugated polymer will be attempted when there is a sufficient amount of the material available for use in a quantitative study.

Figure 3-12. Proton NMR spectra of 1-(2,5-Dibromo-phenyl)-3-phenyl-propane-1,3-dione, inset is an expansion of the aromatic region of the larger spectrum.

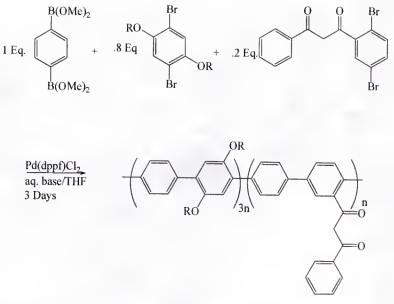

Figure 3-13. Synthesis of Diketone containing polymer.

Diketonate Exchange Reaction

When the diketone polymer was initially being synthesized, there were no lanthanide compounds available that would react to generate the lanthanide containing polymeric complex. One possible method of attaching a rare earth metal to the diketone containing polymer would be the exchange reaction between a trisdiketonate complex and the diketone on the polymer (Figure 3-14). To determine which diketones would undergo the exchange process, several ytterbium tris(β diketonate)s were combined with DBM in NMR scale reactions.

The experiments were run in deuterated chloroform at room temperature and NMR was used to monitor the progress of the reaction. The TTFA, acac, TMHD, and the DNM complexes of ytterbium were combined with 1, 2, and 3 equivalents of DBM. It was felt that DBM would successfully model the diketone containing polymer.

Alkyl substituted diketonates exchanged rapidly with DBM and the reaction was completed before the NMR spectrum could be recorded. For experiments with one

equivalent of the DBM, it was observed that there was a mixture of three species in the solution: the starting material, the monosubstituted complex and the disubstituted complex. Upon the addition of the second equivalent of the DBM, the starting material peak disappeared and peaks appeared that were assigned to the trisubstituted complex. Integration of the peaks corresponding to the mono complex and the disubstituted complex exhibit a shift in their relative integration ratio so that it appears there was more disubstituted material than mono. Upon addition of the third equivalent, the monosubstituted peak disappeared and the disubstituted peak's integration was significantly reduced relative to the trisubstituted peaks. The TTFA and DNM diketonate complexes demonstrated no propensity for exchanging with the DBM.

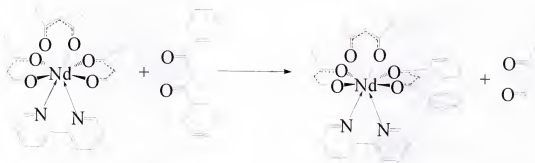

Figure 3-14. Example of the proposed exchange reaction that could be used to attach a lanthanide complex to the conjugated diketone polymer

These results lead us to conclude that the acac and TMHD complexes would be effective in a possible exchange reaction. Additionally, the complexes appear to be unstable to the type of exchange reaction shown in Figure 3-15. A disproportionation reaction of this type would complicate isolation the polymer/lanthanide complex. The aromatic diketonate complexes do not appear to under go any exchange reactions regardless of conditions and are thus excluded from applicability. Ideally, what is needed to generate the complex is one labile ligand on the Ln starting material that could be

displaced by the diketone on the polymer. The remaining ligands on the lanthanide would need to be resistent to further exchange reactions to ensure that the polymer/lanthanide complex would be stable.

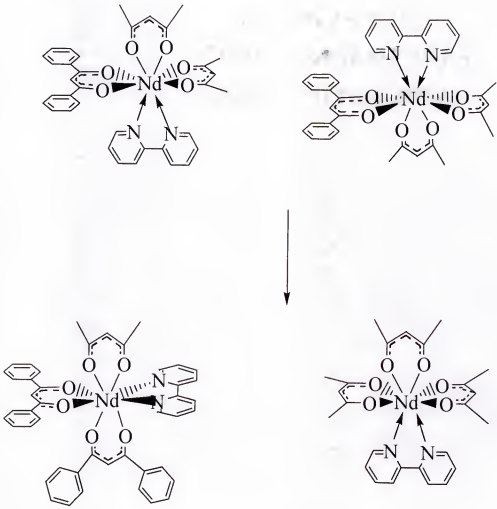

Figure 3-15. Further exchange reaction leading to possible crosslinking in polymer/lanthanide complexes.

Summary and Conclusion

Lanthanide trisdiketonates have been successfully employed as NIR EL and PL sources. It has been determined experimentally that the spectral overlap of the polymer emission with the absorption of the ligands on the rare earth metal has a direct effect on the emission properties of the devices. It appears that a loading of 20 mol% for the Ln

(DNM) Phen complexes produces the most light while requiring the least amount of current. Attempts to attach a lanthanide complex to a polymer have yet to be successful but progress towards that goal is continuing. Chapter 4 will present new complexes whose properties differ significantly from the β diketonates.

CHAPTER 4
SYNTHESIS AND CHARACTERIZTION OF LANTHANIDE TETRAPHENYLPORPHYRIN COMPLEXS

Work discussed in this chapter will focus on the development of lanthanide containing tetraphenylporphyrin compounds as an alternative to the diketonate complexes used in the previous chapter. New synthetic routes to the porphyrin complexes will be presented along with subsequent reactions of those complexes to yield new, more efficient lumiphores for EL and PL. Particular attention will be paid to the methods by which the structures of these compounds were elucidated and the effects of the structure on their physical properties.

It has been observed by several researchers that the spectral overlap of conjugated polymers (CPs) and the absorption wavelength of lumiphores plays a role in the EL and PL efficiency of these polymer blends.[49] It appears that this relationship is accurately described by the Förester energy transfer equation, which specifies that the efficiency for the transfer is dependant on the fluorescence efficiency of a donor molecule at a specific wavelength and the molar absorptivity of an acceptor at that wavelength.[50] To improve the energy transfer and thus the luminescence performance of the rare earth ions, the ligands on the lanthanide would need to have a high molar absorptivity at the fluorescence wavelength of the CP. Conjugated polymers used in our studies have their fluorescence maxima at approximately 400 nm, therefore the complexes that would meet this requirement would need to strongly absorb in this region of the visible spectrum.

A survey of the literature provided a limited number of complexes that have been isolated, which have absorptions with high molar absorptivities at the desired wavelengths. Of the possibilities available, lanthanide tetraphenylporphyrin pentane 2,4 dione (LnTPP(acac)) compounds exhibited an absorption band at 420 nm with an ε of ~300,000 M^{-1} cm^{-1} making them interesting materials to investigate for blending with several of our available CPs.[51]

Prior Investigations of LnTPP Complexes

Several researchers investigating EL in the near infrared have made use of diketonate based materials because they are ease to prepare, can be generated from any β–diketone, and require little effort to isolate cleanly in high yields. This stands in stark contrast to the original preparation of the LnTPP(acac) complexes, which required a complicated synthesis and an extensive purification.[52] The metalloporphyrin was generated by the reaction between a free base porphyrin and a $Ln(acac)_3$ in refluxing trichlorobenzene (Figure 4-1). Progress of the reaction was monitored by UV-visible spectroscopy and indicated that the yield of the reaction was 90% or higher. During the course of the reflux, the solution was sparged with an inert gas to facilitate the removal of the acetylacetone and to prevent oxidation reactions at the elevated temperature. Isolation of the product is achieved by column chromatography, during which decomposition of the product occurs leading to isolated yields that range from 10-30 %. In spite of the low yield associated with this procedure, it has been the standard method for producing LnTPP complexes for 25 years.

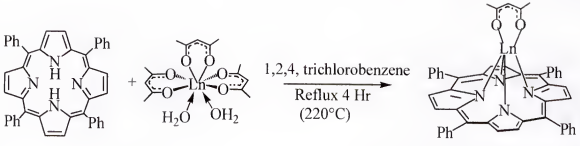

Figure 4-1. Commonly used synthetic pathway to LnTPP(acac) complexes

Utilizing this method, we generated the Yb and Er versions of the LnTPP(acac) complexes and found them to be competent at generating NIR photons.[53] From this work, we were interested in determining if replacing the acac with other ligands would help to improve the luminescent properties of the complexes. We were also interested in finding a route to the LnTPP complexes that would not require column chromatography and would allowed the isolation of the complexes in high yield.

Recently, an alternate route to LnTPP complexes was published that involved a simplified synthesis of these materials.[54] The procedure begins with the reaction of a $LnCl_3$ with three equivalents of lithium 1,1,1,3,3,3-Hexamethyl-disilazide ($LiN(SiMe_3)_2$) in THF generating a $Ln(N(SiMe_3)_2)_3$ complex. After a series of synthetic manipulations requiring several days to perform, crystals of the hydrated LnTPP(Cl) complex were isolated in moderate yields by filtration (Figure 4-2). This procedure had several advantages over the standard method, namely column chromatography was not needed to isolate the product, the reported isolated yield was higher than 50 %, and the chloride counter ion could be replaced to generate new complexes.

While this new procedure had many attractive features, the isolated complex coordinated several equivalents of water, which could be problematic. The LnTPP(acac)

complexes are not exceptionally stable to hydrolysis, with complexes containing larger ions such as Pr^{3+} decomposing in the span of a few days. This observation should apply equally to the chlorides, precluding their long-term stability. Stable porphyrin complexes would need to be anhydrous and any viable synthetic route for these materials would take this into consideration.

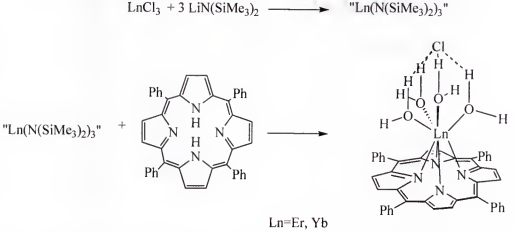

Figure 4-2. Recently developed alternate synthetic path to a LnTPP complex

Lanthanide Amides as Precursors to LnTPP Complexes

As may be observed from the synthetic scheme in Figure 4-2, the product of the reaction contains a chloride whose origin was not ascertained. The authors of the work proposed that the $Ln(N(SiMe_3)_2)_3$ that was used was not a neutral compound but was in fact ionic, coordinating three amides and a chloride. Complexes of this nature have been observed for other lanthanide complexes making this a reasonable hypothesis.[55] The reaction between the porphyrin and this compound would then generate the anionic amide-porphyrin-chloride complex, which when exposed to the atmosphere would be hydrolyzed to generate the isolated product. The proposed pathway was left unconfirmed, as isolation of the anhydrous anionic intermediate was not reported.

In an attempt to clarify the nature of the precursor to the product, we generated and isolated the lithium chloride free versions of the $Ln(N(SiMe_3)_2)_3$ complexes.[56] The intended purpose for these compounds was to use them in a reaction with the $TPPH_2$ in an attempt to generate and isolate a $LnTPP(N(SiMe_3)_2)$ complex. Initial reactions were attempted on small scales in resealable NMR tubes, with the progress of the reaction being followed by proton NMR spectroscopy.

For this reaction, a $Ln(N(SiMe_3)_2)_3$ complex and tetraphenylporphyrin were dissolved in dueterated benzene. Initially, the spectrum showed little change but over the course of 144 hours the reaction proceeded. The relative integration of the peaks for the N-H protons on the pyrrole nitrogens decreased with the concurrent appearance of peaks that were tentatively assigned to the paramagnetically shifted hydrogens on the phenyl rings. Additionally, a large singlet appeared at 0.11 ppm and this resonance was assigned to $HN(SiMe_3)_2$. These results indicated that the amine exchange reaction was occurring and producing the anticipated compound. Attempts to grow crystals of the products of the NMR tube reactions were not successful. The reaction was then attempted multiple times on a larger scale, but when the scale of the reaction was increased, the NMR spectra of the isolated materials did not match the spectra of the NMR scale experiments.

Interactions between the methyl groups on the $-N(SiMe_3)_2$ and the porphyrin ring could decrease the stability of the complexes and this would increase the difficulty of isolating of the product. A complex with a less sterically demanding amide might be more stable and thus improve the chance of its being isolated. An alternate amine that was investigated was 1,1,3,3-tetramethyl-disilazane($HN(SiMe_2H)$).[57] Lanthanide complexes with this amide are synthesized by the same procedure as previously discussed

$Ln(N(SiMe_3)_2)_3$. In the structures of these complexes, the reduced number of methyls on the silyls opens up the coordination sphere around the metal allowing the complexation of two equivalents of THF. This difference in the number of coordinated molecules indicated that this ligand is not as sterically demanding as the $N(SiMe_3)_2$ and might allow for a more stable product.[58] Upon reacting this material with $TPPH_2$ the UV-Visible spectrum of the solution was consitent with the metal coordinating to the porphyrin, but attempts to isolate and characterize this compound have been unsuccessful.

Having little success in isolating the silyl amide derivitized LnTPP complexes, we turned our attention to other reports on the preparation of LnTPP (amide) complexes. In a communication published by Wong, work was presented on the use of Ln tris(diphenylamide) ($Ln(NPh_2)_3$) in the synthesis of LnTPP complexes.[59] Following a procedure similar to the $Ln(N(SiMe_3)_2)_3$ based synthesis, the amide was generated *in situ* and allowed to react with $TPPH_2$. The product of the reaction was not isolated but instead was treated with half an equivalent of water producing the oxo-bridged LnTPP complex (TPPLn-O-LnTPP). The authors asserted that the precursor to this complex was a monomeric, neutral $LnTPP(NPh_2)$. As before, there was no report on the isolation of the proposed intermediate, leaving the true nature of the precursor to the oxo-bridged complex undetermined. In our efforts to isolate a LnTPP(amide) complex, we repeated this work and focused our efforts on isolating the precursor to the oxo-bridged complex.

Synthesis, Isolation and Characterization of Bistetrahydrofuran Ln Tris(diphenylamide) ($Ln(NPh_2)_3 \cdot 2$ THF

Researchers had reported generating Ln tris(diphenylamide) complexes and using them *in situ*, but these compounds had not been isolated or structurally characterized.[60] To better understand the reactivity of these compounds and the possible products they

might generate after reacting with a porphyrin, we decided to determine their true structure. Our work was mainly concerned with Er and Yb and these are the two metals that were examined.

The complexes were synthesized by the reaction between $KNPh_2$ and anhydrous $YbCl_3$ or $ErCl_3$. The complexes were isolated in moderate yields and characterized by elemental analysis and X-ray crystallography. The complexes are extremely reactive and are prone to decomposition. When being manipulated by Schlenk techniques, the inert gas being used must be passed over a drying column. Failure to use a gas that has been dried appropriately leads to the formation of a forest green substance that is insoluble in organic solvents. Additionally, prolonged exposure to high vacuum induces decomposition, but in this instance, an insoluble, white powder forms. It is presumed that under vacuum one or both of the THF molecules are removed from the coordination sphere of the metal inducing decomposition. The NMR spectrum of the materials had several broad peaks varying in width from 2 to 10 ppm, complicating their assignment. The broad nature of the peaks is attributed to fluxional processes that rapidly change the geometry of the molecule coupled with the paramagnetic character of the metals.

Thermal ellipsoid plots of the structures for complex **8** and **9** are shown in Figure 4-3. As expected the two compounds are almost isostructrual, manifesting themselves as distorted trigonal bipyramids. The angles between the amides around the equatorial region of the Yb complex are 130.6°, 118.5°, and 110.8°, for the Er complex the angles are 131.1°, 121.5°, and 107.0°. The angle between the axial THF molecules is 167.1° and 160.3° for the Yb and Er complexes, respectively. It appears that the approach of the ethers towards each other forces the amides apart and is responsible for the asymmetry in

the equatorial angles. The main difference between the structures is that the bond lengths in the Er complex are slightly longer, reflecting the slightly larger ionic radius of metal. In the Yb molecule, the average bond distances are Yb-N 2.22(9) Å and Yb-O 2.32(2) Å. For the Er complex, the observed average distances for the Er-N, Er-O bonds are 2.252(6) Å and 2.361(5) Å, respectively.

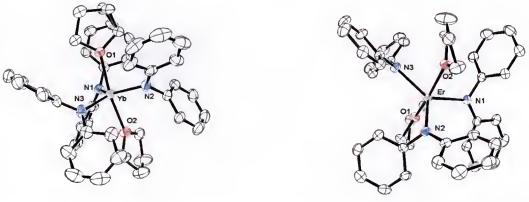

Figure 4-3. Thermal ellipsoid plots of **8** (left) and **9** (right) with the hydrogen atoms excluded for clarity.

Reaction of the LnTDPA Complexes with TPP

As before, an NMR scale reaction was run to determine if the amides would react with the porphyrin. Within an hour of assembling the reactants, it was evident that a reaction had occurred. Paramagnetically shifted peaks for the metalloporphyrin and free diphenylamine were observed, indicating that the expected amine exchange had proceeded. Attempts to isolate the product from the NMR scale reaction were not successful, and efforts to produce the complex on a larger scale have been met with mixed results.

Lanthanide Tetraphenylporphyrin Chloride Synthesis

Another synthetic path to the LnTPP materials would be to use a salt metathesis reaction. Combining an alkali metal salt of the porphyrin dianion and a lanthanide

trihalide in anhydrous solvents should produce an LnTPP complex. We had initially discounted this path, because in work published by Wong, it was stated that this approach did not lead to the desired product.[61] We decided to try the reaction using anhydrous, air free conditions to determine if a LnTPPCl complex could be generated and isolated by this means.

We focused our efforts on the salt metathesis reaction of $LnCl_3 \cdot 3(THF)$ with dilithiotetraphenylporphyrin bisdimethoxyethane (Figure 4-4).[62] Reaction of the two components in refluxing toluene gave complete conversion to the lanthanide tetraphenylporphyrin chloride dimethoxyethane complex (LnTPPCl(DME)). Progress of the reaction was conveniently monitored by following the appearance of the Soret band of the metalloporphyrin at 422 nm and by the increase of the Q band absorbance at 551 nm. The resulting mixture was cloudy with lithium chloride, which was separated from the solution by hot filtration. The solution was then reduced to 1/3 its original volume and cooled to 0° C, whereupon the LnTPPCl(DME) precipitates in approximately 75-85% yield.

This synthetic approach has been successfully applied to ytterbium, thulium, erbium, and holmium, though we expect that it will be applicable to the larger lanthanide metals (it is possible that the larger size of the early Ln metals may result in the formation of dimers or complexes with higher coordination numbers). The formation of anionic complexes that coordinate lithium chloride, which have been observed for other lanthanide salt metathesis reactions, are presumably suppressed due to the low polarity of toluene.[63] Attempts to repeat this reaction in ethereal solvents produced less than satisfactory results, (low yields with the material contaminated with lithium chloride).

Once the complexes have been isolated there is no change in their spectral properties on standing for several days under an inert atmosphere or when exposed to alcohols. Exposure to 1M HCl in diethyl ether produces the 416 nm Soret band of the free tetraphenylporphyrin, suggesting the complex has been demetallated. The stability of these complexes to ambient conditions is not known, but exposure to water should result in the displacement of the DME and the subsequent coordination of 2 or more water molecules to the metal center of the LnTPP.

Figure 4-4. Synthesis of anhydrous LnTPP complex

Thermal ellipsoid plots of the solid-state structures of the ytterbium and holmium complexes, in conjunction with selected atom labels, are presented in Figure 4-5. The ytterbium ion sits 1.105(1) Å above the centroid of the least squares plane defined by the four pyrrole nitrogens and has an average Yb-N bond distance of 2.324(2) Å. The angle between the line perpendicular to the N4 mean plane passing through the N4 mean plane centroid and the line passing through the metal and the centroid is 0.8°, placing the ytterbium directly above the center of the porphyrin cavity. To accommodate the metal and the steric bulk of the other ligands, the ring loses planarity and adopts a saddle shape. The shape of the ring is such that the N1 and N2 containing pyrrole rings are on one side of the saddle with the other side consisting the pyrrole rings containing the N3 and N4 nitrogen atoms. A dihedral angle of 21.36°(1) exists between the N1-C1-C2-C3-C4 plane

and the-N4-C16-C17-C18-C19 plane; likewise, an angle of 16.71°(1) exists between the N2-C6-C7-C8-C9 plane and the N3-C11-C12-C13-C14 plane. In contrast, the angles between the planes containing N1-N2 and N3-N4 are 4.0°(2) and 6.5°(4).

The seven coordinate Ho atom lies 1.154(3) Å above the centroid of the pyrrole nitrogen mean plane and has an average Ho-N distance of 2.357(1) Å, as is consistent with its slightly larger ionic radius. The angle between the line perpendicular to the N4 mean plane passing through the N4 mean plane centroid and the line going through the metal and the centroid is 0.7°, placing the holmium above the center of the ring. The porphyrin ring adopts a domed conformation with the mean planes defined by the pyrrole rings having dihedral angles of N1-N2 13.02°(21), N2-N3 14.95°(13), N3-N4 8.97°(17), and N4-N1 15.09° (16).

Dilithioporphyrins have been used as the starting material for various other metal porphyrin complexes.[64] Most notably dilithiooctaethylporphyrin reacts with one equivalent of scandium trichloride to produce the scandium chloride octaethylporphyrin complex in a good yield.[65] The complex lacks any coordinating solvents such as those observed in our system. This is in all likelihood due to the much smaller size of scandium relative to lanthanide metals. In addition, the metal is much closer to the plane of the porphyrin ring, being only displaced from the centroid of the nitrogen mean plane by 0.68 Å.[66] It can be expected that the porphyrin ring also provides some amount of steric hindrance to the coordination environment around the metal center. More recently, a seven coordinate ytterbium tetra(p-tolyl)porphyrin complex has been generated which has a metal to porphyrin centroid displacement of 1.090 Å.[67]

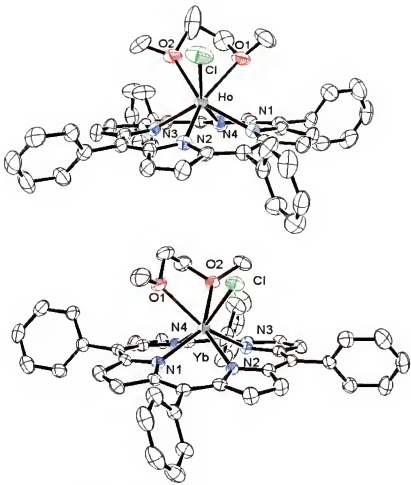

Figure 4-5. Thermal ellipsoid plots of **10** (top) and **13** (bottom) drawn at the 50% probability level, hydrogen atoms have been excluded for clarity.

The remaining chloride on the complexes can be easily replaced by a second salt metathesis reaction. Addition of potassium acetylacetonoate to the Yb complex in dimethoxyethane at room temperature leads to the YbTPP(acac) complex in 91% isolated yield, giving an overall yield of 72% based on $LnCl_3 \cdot 3(THF)$. This yield is a substantial improvement on the literature method used to synthesize the LnTPP(acac) compounds.

Mass Spectrometry of the Chloride Complexes

To further explore the nature of the chloride complexes in more detail a series of electrospray ionization (ESI) mass spectrometry experiments were performed.[68] In ESI, solvated ions are injected into the spectrometer and excess solvent is evaporated by the high vacuum necessary for the experiment, leaving behind only the ions present in the solution. Because no other ionizing sources are used in this experiment, it is considered a soft technique suitable for large, fragile ions.[69] This technique is typically performed on air stable materials, but due to the hydroscopic nature of our compounds, precautions were taken to prevent the introduction of water.

Solvent choice for this experiment is critical; solvents must not undergo electrochemical reactions at the spray tip when the potential is applied. In our investigation, a solvent mixture of methylene chloride and acetonitrile was used to dissolve the complex. A mixed solvent system was used because the complex was soluble in methylene chloride and the acetonitrile was capable of solvent separating the chloride from the complex.

The main ion observed in the experiment is shown in Figure 4-6. Below the spectrum of the observed peaks is the calculated isotopic distribution for the $[(CH_3CN)YbTPP]^+$ ion. A difference between the predicted values and the observed values of less than 0.005 mass units coupled with the unique isotope distribution pattern of the ytterbium provides a high degree of confidence that the predicted structure accurately describes the structure of the observed ion. Ions were also observed that were assigned as the YbTPP complex coordinated to 2,3 and 4 acetonitriles, but these had smaller intensities in the spectrum. As a *caveat,* it must be stated that the intensity of an

observed ion is not related to the actual quantity of that material in the solution but only to the ability of that ion to fly in the mass spectrometer. It is fully expected that the coordination number of the material in solution is not five but more likely the higher number of seven or eight.

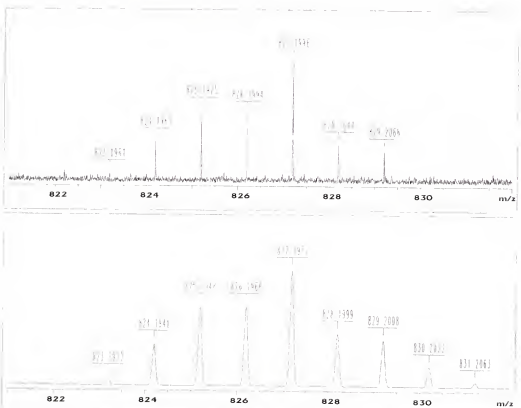

Figure 4-6. Results of electrospray ionization mass spectroscopy of **13**

The effect of water on the mass spectrum was provided by a set of experiments in which a small quantity of water was introduced into the samples. The premise behind this inquiry was to determine what effect water would have on the observed peaks. When water was introduced into the samples, peaks observed did not correspond to observed peaks in the previous set of experiments. The ions still consisted of a lanthanide and tetraphenylporphyrin and these masses were subtracted from the mass of the observed ions providing a pattern of peaks that varied by multiples of 59.04 mass units, the mass of

acetamide. When the acetamide was added into the calculation for the isotopic distribution it was in agreement with the observed distribution. Since this molecule was not present previously, it is assumed that it was generated from the addition of water to the nitrile. The proposed mechanism for this reaction is shown in Figure 4-7. Experiments to repeat this reaction on a larger scale or catalytically have not been performed. These results demonstrate that when water is present in the samples, under these conditions, it reacts with acetonitrile to produce acetamide that in turn can be observed in the mass spectrum.

Synthesis and Crystal Structure of LnTPP(TP) Complexes

We believed that if the steric bulk of the axial ligand on the lanthanide complex were increased it might prevent quenching agents from interacting with the metal and thereby enhance the luminescence properties of the LnTPP. Ligands to be investigated would need to be monoanionic to make neutral complexes, multidentate to be resistant to exchange reactions, and not quench the NIR emission of the lanthanide. Additionally, the ligands would need to be air stable because 90% of the EL device fabrication occurs on the bench top. The first ligand that was investigated was the hydrido tris(pyrazoyl) borate anion(TP).[70]

Synthesis of the lanthanide compounds was performed under inert atmosphere to preclude the hydrolysis of the LnTPP bonds. The reaction between KTP and the LnTPP(Cl)(DME) was carried out in room temperature DME and allowed to proceed for 12 hours. After a standard workup procedure, the complexes were isolated in moderate yields. The molecular structure of the compounds was determined by X-ray

crystallography and the purity of the bulk material was confirmed by elemental analyses (Figure 4-8).

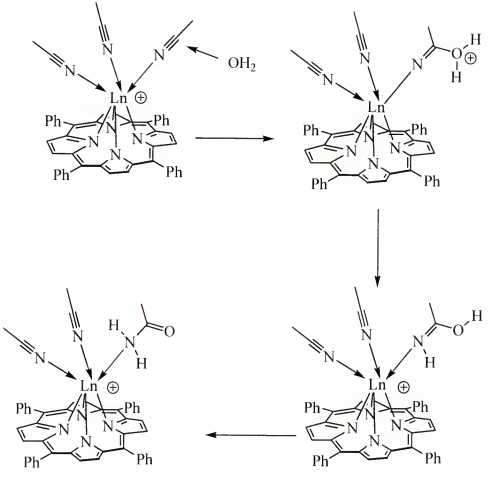

Figure 4-7. Proposed mechanism accounting for the observation of acetamide in the mass spectra

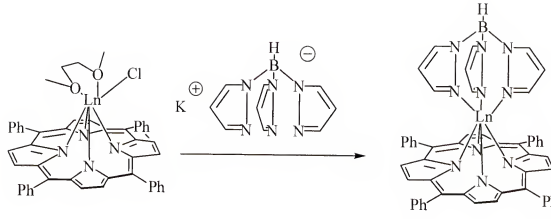

Ln = Ho(**14**), Er(**15**), Tm(**16**), Yb(**17**)

Figure 4-8. Synthesis of LnTPP(TP) complexes

Slow evaporation of a chloroform solution of **16,** under an inert atmosphere, yielded an X-ray diffraction quality crystal of the complex. Figure 4-9 displays the thermal ellipsoid plot of **16** along with selected atom labels. The material is monomeric with no coordinating solvents or ions. The geometry about the metal center is best described as a distorted capped trigonal prism. Due to the anisotropy in the Tm-N^{TPP} bond distances, the molecule has a slightly distorted appearance with the metal more closely bound to the N2 and N3 containing portion of the macrocycle. The center of the Tm atom is 1.187(1) Å above the center of the mean plane defined by the pyrrole nitrogens and 1.782(8) Å below the mean plane defined by N5, N7, and N9. The angle between the two planes defined by the nitrogen atoms on the ligand is 0.5°, making the planes nearly parallel. To accommodate the large size of the metal and the steric demands of the TP ligand, the porphyrin ring adopts a domed conformation with the mean planes defined by the pyrrole rings deviating from the mean plane defined by the four pyrrole nitrogens by 14.9°, 13.7°, 10.8°, 10.9° for the rings containing N1, N2, N3, N4, respectively.

Single crystals of **17** were grown by cooling a toluene solution of the complex to -78 ° C. A thermal ellipsoid plot of the compound is shown in Figure 4-9. The structure is, as expected, similar to **16** with the bond distances slightly contracted due to the smaller ionic radius of the Yb. The distance from the metal to the N^{TPP} plane is 1.156(3) Å and the Yb is located 1.796(6) Å from the pyrazole nitrogen plane.

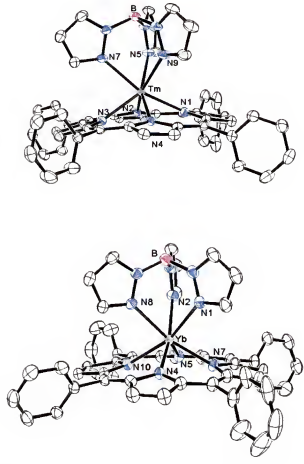

Figure 4-9. Thermal ellipsoid plots of **16** (top) and **17** (bottom) drawn at the 50% probabilities level, hydrogen atoms and disordered solvent molecules have been excluded for clarity.

Synthesis of LnTPP(Klaui) Complexes

In an effort to expand the repertoire of compounds that could be derived from the LnTPP(Cl)DME complexes, we attempted the synthesis of a complex that would contain the (cyclopentadienyl)tris(diethylphosphinito)cobaltate(I) anion or as it is colloquially known the Klaui ligand.[71] The use of this ligand in LnTPP complexes has already been partially investigated.

The synthesis and crystal structures of the erbium and ytterbium versions of the LnTPP(Klaui) complex have been previously reported.[72] The Klaui ligand is a mutlidentate, monoanionic, organometallic compound that binds readily to other metals and is stable to hydrolysis and oxidation.[72] The starting material for the complexes was the hydrated chloride discussed in the section on LnTPP chlorides. The chloride from that preparation was refluxed with the Klaui ligand in THF for 24 hours. Subsequently, the target molecule was isolated and purified by column chromatography

In an effort to produce these complexes with out the need for column chromatography, a synthetic method similar to the to LnTPP(TP) was attempted. When the extraction with toluene was performed, there was no residue left behind, indicating that the true nature of the lanthanide complex generated by this method was an anion with sodium as the counter ion. To generate a neutral version of the material, pentane was added to the toluene solution decreasing its polarity and forcing the precipitation of sodium chloride. Cooling the toluene/pentane mixture caused the deposition of analytically pure, purple crystals of the LnTPP(Klaui) complex (Figure 4-10). Elemental analysis, UV-visible spectroscopy, and proton NMR spectroscopy were used to characterize this set of compounds. The results of the first two analytical methods were

in agreement with those of the previously published syntheses for the compounds, but the proton NMR had not been used in their identification. The specifics of the NMR spectra along with a disscusion of the assignment will be presented in the next section.

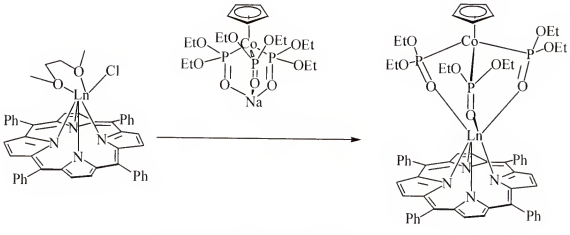

Ln= Ho(**18**), Er(**19**), Tm(**20**), Yb(**21**)

Figure 4-10. Numbering and synthesis of the LnTPP(Klaui) compounds

Proton NMR Analysis LnTPP(L) (L=TP or Klaui)

Typically, the NMR spectra of lanthanide containing complexes have not been reported. Papers published containing this information usually dealt with the use of lanthanide compounds as shift reagents, this being the first intended use for the LnTPP(acac) complexes.[73] Building on that work, and using the crystallographic data obtained from the structures of **16** and **17,** we were able to assign the proton NMR spectra for complexes **14-21**. Uncertainty about the magnitude of the psuedocontact shift in paramagnetic complexes prevents the *a priori* assignment of the proton resonances. Utilizing the relative integration of the peaks in the one-dimensional spectrum coupled with simple two-dimensional experiments, the resonances can be assigned to the correct proton in the structure.[74] While this provides limited predictive power, it affords the

researcher a tool to analyze the purity of a previously characterized material rapidly and efficiently.

Unpaired *f* electrons on the lanthanides are responsible for the isotropic paramagnetic shifts and the enhanced nuclear relaxation rates.[75] Increasing paramagnetism results in shorter T_1 times and large spectral dispersions. These effects vary with the distance and the angle of the nuclei relative to the magnetic axes of the metal, and with the identity of the lanthanide. In the following discussion, Yb will be used as an example because the crystallographic data is available for both the TP and Klaui complexes and the spectral dispersions are small. While Yb is the only metal discussed, the techniques described have been applied to the remaining compounds with equal success. Peak positions and their relative assignments for the remaining complexes are provided in Chapter 6 along with the other pertinent experimental details.

NMR Spectroscopy of YbTPP(TP)

The one-dimensional proton NMR of **17** is shown in Figure 4-11. Integration of the peak areas provides a ratio of 3:4:8:4:4:4:4:3:3 for the peaks moving from downfield to up (peaks labeled A-I). Additionally, some minor peaks are observed but evaluation of their relaxation times and line widths reveals them to be diamagnetic impurities. Using the crystallographic information and assuming the rotation of the phenyl rings on the porphyrin is slow on the time scale of the experiment, 9 peaks should be observed. Three peaks integrating for three protons for the TP ligand, five peaks integrating for four protons for the phenyl ring on the TPP, and one peak integrating for eight protons for the hydrogen atoms on the pyrrole rings. The proton attached to the borate on the TP ligand should not be observed due to the quadrapolar relaxation effect of the boron. The

spectrum agrees with this expectation, with peaks A, H, I integrating for 3 hydrogen atoms. The largest integration at 14.00 ppm (8H) (peak C) is assigned to the pyrrole protons, peaks labeled B, D, E, F, and G each integrates to 4 hydrogen atoms and are assigned to the phenyl ring protons. Assigning the peak identity based on a relative integration of four to three is tenuous and needs to be further verified.

To substantiate the identity of the peaks in the proton NMR, a COSY experiment was performed on the sample. Peaks on the diagonal traversing the center of Figure 4-12 correspond to the peaks observed in the one-dimensional spectrum. Off diagonal cross peaks indicate that the peaks on the diagonal have scalar couplings and that the hydrogen atoms giving rise to the peaks on the diagonal are adjacent in the molecular structure. Peaks H and I have a cross peak confirming that they are in the same spin system. Based on the relative integrations, peaks A, H, and I were assigned to the TP ligand. Peak A does not appear on the diagonal and does not exhibit a cross peak. The broadness of peak A in Figure 4-11 suggests that it has a short relaxation time, and when a proton relaxes faster than the time scale of the experiment its signal can not be distinguished from the baseline noise in the 2D spectrum. It may be for this reason that peak A is not observed in this experiment. The linewidth and large downfield shift of this proton is consistent with it being assigned as the proton closet to the metal center.

An expansion of the contour map from ~16 to 7 ppm (Figure 4-13) provides a detailed view of the cross peaks in that region. Peak B shows a correlation only with D, and due to the large paramagnetic shift exhibited, B is assigned as the *ortho*-proton that is pointing towards the TP ligand. Using cross peaks to establish the connectivities peak D, is assigned as the *meta* proton that is pointing towards the TP, E is assigned as the *para*

proton, and peaks F and G are assigned as the *meta*, and *ortho* protons pointing away from the TP ligand, respectively.

NMR Spectrtoscopy of YbTPP(Klaui)

The one dimensional proton spectrum of **21**, shown in Figure 4-15, has ten peaks that can be assigned to a paramagnetic molecule. Peaks at 7.16 ppm and 0.31 ppm are attributed to the residual protons on the deuterated benzene and to silicon grease impurities. From the structure of the complex, it can be expected that the methylene protons of the ethyl on the Klaui ligand should be diastereotopic. The absence of a peak integrating for 12 hydrogen atoms and the observation of two peaks that each integrate for six, further confirmed this expectation. Determing the identity of the remaining peaks by the relative integration, the methyl on the ethyl, the protons on the pyrrole, and the cyclopentadienide are assigned to the peaks at 2.88 ppm(18 H), 15.64 ppm (8 H), and -4.83 ppm(5 H). The phenyl protons on the tetraphenylporphyrin were then assigned and nature of the methylene peaks was confirmed using two-dimensional NMR spectroscopy.

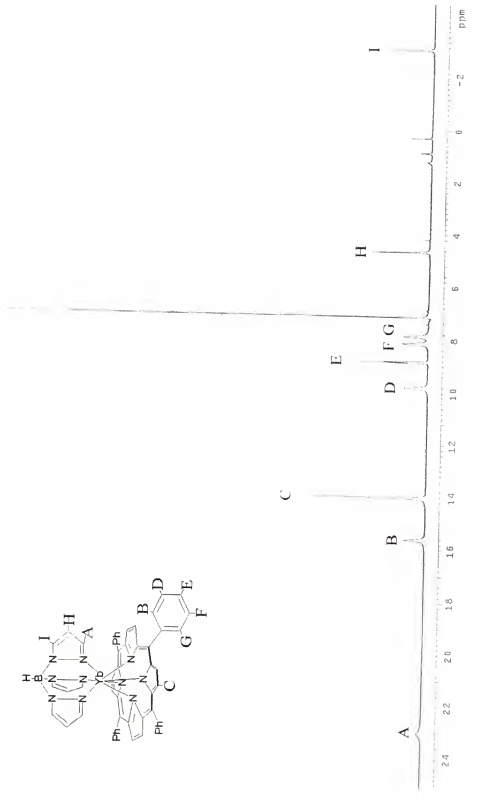

Figure 4-11. One-dimensional proton NMR spectrum of **16**

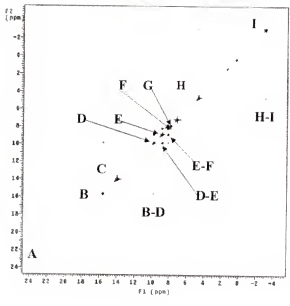

Figure 4-12. COSY spectrum of **16**

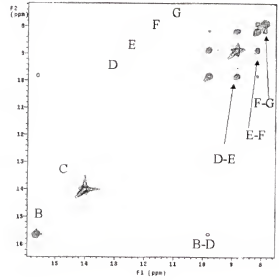

Figure 4-13. Expansion of Figure 4-12 from 7 to 16 ppm

As in the previous section, a COSY experiment was used to determine the relative positions of the protons on the phenyl rings. The contour map, shown in Figure 4-16, shows that the general pattern observed in **17** is preserved in this complex with the *ortho* proton directed towards the TP at the lower field and the protons then proceed around the ring to higher field in the order *meta, para, meta, ortho*. An expansion of the region from

0 to 9 ppm, clarifies the nature of the peaks at 8.28 and 7.50 ppm. A correlation is present between the two peaks and both peaks are related to the peak at 2.88 ppm. Since the peak at 2.88 has been unambiguously assigned to the methyl on the ethyl, it is certain that the peaks are the hydrogen atoms on the methylene portion on the ethyl. The protons can be correlated to each other and the methyl protons only when they are geminal diastereotopic protons.

Comparing the spectra of these two complexes with the published spectra of other Yb porphyrin complexes reveals an interesting trend. Horrocks reported that the porphyrin peaks in the Yb tetraparatolylporphyrin (1,1,3,3 tetramethylheptanedionate) complex have the same relative order as the peaks in our complexes.[76] Additionally, the peak positions in our materials are not significantly shifted from the peak positions reported for that complex. The peak positions observed by Horrocks, have been used to calculate the metal to pophyrin plane distance and suggest that the metal is ~1.2 Å above the nitrogen plane of the porphyrin.[77] The calculated distance in this work compares favorably with the crystallographically observed distance of ~1.15 Å for **17** and **21**. Results from our work experimentally confirm that the distances predicted by calculations using NMR peak positions are accurate.

Synthesis of LnTPP(Diketonates)

Chapter 3 finished with a brief description of a diketone containing conjugated polymer that could attach a lanthanide complex. As discussed in the synthetic section on Ln TPP chlorides, the acac complex has been synthesized by a simple salt metathesis reaction to yield the LnTPP(acac)complex in ~72% yield. Capitalizing on this reactivity, the potassium salt of the polymer and the porphyrin chloride complex could be combined

to generate the LnTPP/polymer complex. This reaction will be attempted when there is a sufficient quantity of the diketone polymer available to perform quantitive measurements on the resulting combination.

Synthesis and Isolation of YbTPP(Cp*) (22)

After successfully generating several LnTPP based coordination complexes, we endeavored to prepare an organometallic complex. There are several examples in the literature of pentamethylcyclopentadienide (Cp*) lanthanide complexes that have been shown to be stable, because of this it was chosen as the first ligand to be investigated.[78]

To generate the organometallic complex KCp* and YbTPP(Cl)DME were combined in DME and after stirring for several hours the reaction work up by a standard procedure. The complex was isolated in an ~ 65% yield as X-ray diffraction quality crystals. The material was characterized by X-ray crystallography, elemental analysis, and proton NMR.

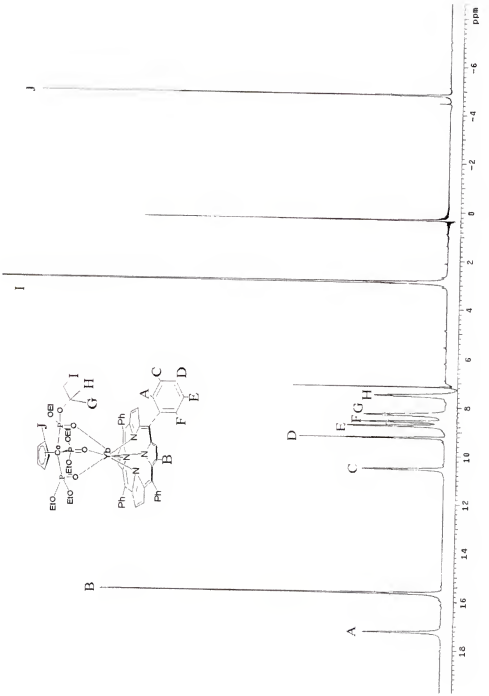

Figure 4-15. One-dimensional proton NMR of **21**

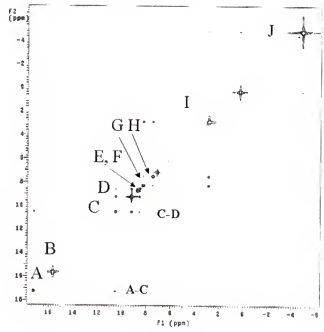

Figure 4-16. COSY spectrum of **21**

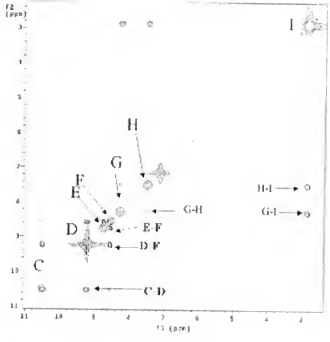

Figure 4-17. Expansion of Figure 4-15 from 2 to 11 ppm

In the crystal structure of **22** the distance from the Yb to the Cp* centroid is 2.312(3) Å, and the Yb is 0.965(9) Å from the TPP^N mean plane centroid. Angles between the nitrogen mean plane and the pyrrole ring mean plane for the rings containing N1, N2, N3, and N4 are 7.6°, 5.0°, 10.4°, and 4.4°, respectively. These angles are approximately half the value of what has been observed in previously recorded YbTPP crystal structures. The carbons on the Cp* are coplanar within 0.009(1) Å of the defined mean plane and there is a 0.5° angle between the TPP^N plane and the Cp* plane, making the planes virtually parallel. The average N-Yb bond distance is 2.281(1) Å and the average C-Yb distance is 2.608(2) Å.

The ytterbium to porphyrin ring centroid distances and the angles between the pyrrole ring and the nitrogen mean plane in this structure indicate that the steric properties of the Cp* ligand differ greatly from those of the ligands on other complexes whose structures have been solved. The average distance for the Yb-N bond is approximately the same in all of the complexes but the distance from the metal to the nitrogen plane centroid is smaller than the shortest observed distance to date by ~0.1 Å. The approach of the lanthanide to the plane is accompanied by an increase of the porphyrin ring planarity as evidenced by the reduced angle between the TPP^N plane and the pyrrole rings. This indicates that the Yb-N bond distance is a fixed quantity, and that the doming of the porphyrin ring observed in other structures is an attempt to accommodate the axial ligand/ porphyrin ring steric repulsions.

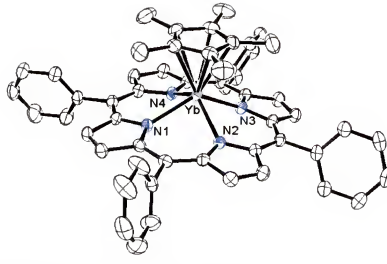

Figure 4-18. Thermal ellipsoid plot of **22** drawn at the 50% probability level, hydrogen atoms and occluded solvent have been omitted for clarity.

If the increase in planarity of the porphyrin ring in this complex were due to solid state crystal packing effects, it would be expected that when this complex were dissolved its UV visible spectrum would be similar to the other YbTPP complexes. In the UV-visible spectrum the complex absorbs blue of the acac complex by ~ 2 nm. The results appear to be contrary to what is expected, which would be that the spectrum would be red shifted because an increase in the conjugation as the ring becomes more planar. [79] It has recently been calculated that a blue shift in the absorption of a tetrarylporphyrin should be expected as it becomes more planar. This is due to a decrease in the interaction of the *meso*-phenyl rings with the porphyrin ring as the macrocycle becomes more planar.[80] This theoretical prediction thus explains why the absorption of **22** is at a higher energy than the other complexes. From this explanation, it can be expected that the porphyrin ring maintains the more planar structure in solution.

The proton NMR spectrum of the complex is similar to the spectra for the Klaui and the TP complexes. Peaks were assigned based on their relative integrations, by

comparison to the other spectra of YbTPP complexes, and by COSY NMR. The *ortho* and *meta* peaks are slightly broadened while the *para* peak and the pyrrole ring peak are well resolved. The *para* peak is sharp enough that upon inspection, the coupling to the *meta* protons is observed. The Cp* hydrogens appear at 1.83 ppm (15 H) as a broad singlet. This spectrum confirms that the structure of the complex in solution is consistent with the solid-state structure.

To determine the reactivity of the complex it was exposed to various conditions and its response was monitored by NMR spectroscopy. Under an inert atmosphere, the complex did not decompose when heated to 100°C for 4 days. Even after exposure to the atmosphere, the complex maintained its integrity for ~2 days but it ultimately decomposed by what is presumed to be hydrolysis of the Cp*-Yb bond. From this work, it is observed that this compound is a surprisingly robust material. Future work in this area will focus on the synthesis of the Er, Ho, and Tm versions of this complex.

Unexpected Reactions of the Chloride Complexes

This section of the chapter is devoted to reactions that produced unexpected results. It is hoped that by the inclusion of this information similar reactions will not be attempted, preventing the loss of valuable time and resources.

Lithio N-benzyltetraphenylpoprphyrin (23)

In an attempt to generate what would be a tetraphenylporphyrin sandwich compound, one equivalent of compound **13** was allowed to react with one equivalent of dilithiotetraphenylporphyrin. (Figure 4-19) The reaction was worked up in a standard fashion and crystals were grown of the Lithio N-benzyltetraphenylpoprphyrin (Figure 4-20). It is assumed that the product was formed by the reduction of the ytterbium metal by

the dilithioporphyrin generating Yb^{2+} and the porphyrin radical. The Yb^{2+} is a strong reducing agent that could abstract a hydrogen from the reaction solvent, toluene, generating a benzyl radical. Combination of the partially oxidized porphyrin and the aromatic radical would then generate the compound shown in the crystal structure. Results similar to these have been reported for transition metal complexes but not for lanthanide compounds.[81] The series of events leading to the isolated product are speculative at best, but to avoid repeating these results strongly reducing ligands should avoided with Yb.

Magnesium Tetraphenylporphyrin

To further explore the organometallic chemistry of the LnTPP complexes a reaction was run between compound **13** and allyl grignard (Figure 4-21). Upon addition of the grignard to a DME solution of the chloride an immediate color change occurred from a red to a dark purple solution. Proton NMR spectroscopy and X-ray crystallography allowed us to determine that the product of the reaction was actually the magnesium containing TPP.

It is expected that the product of the reaction is a result of the magnesium displacing the lanthanide from the porphyrin ring, forming the isolated compound and an undetermined ytterbium complex. Similar reactivities are expected from the remaining LnTPP materials and as such the use of magnesium based alkylating reagents should be avoided

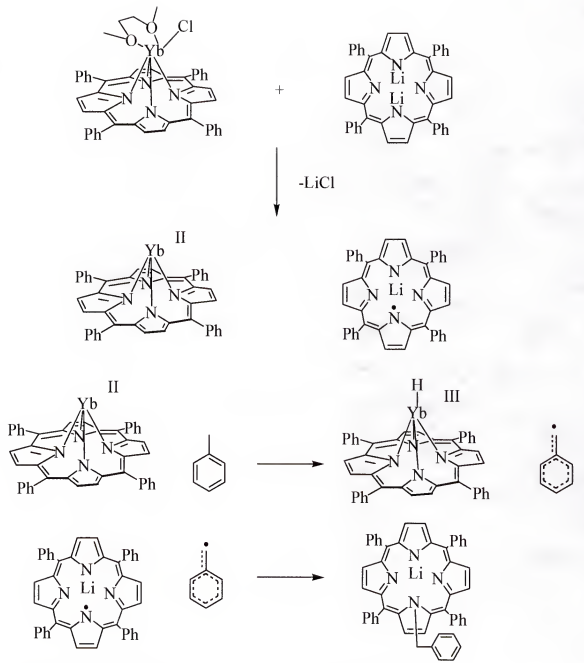

Figure 4-19. Proposed reaction accounting for the observation of **22**

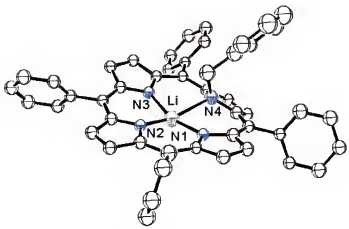

Figure 4-20. Thermal ellipsoid plot of **23** drawn at the 50% probability level, hydrogen atoms have been eliminated for clarity.

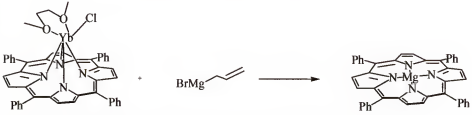

Figure 4-21. Reaction generating the MgTPP complex.

LnTPP PL and EL

After having fully characterized the LnTPP coordination complexes, their luminescent properties were examined. It has been shown in our research that the diketonate complexes with strong PLs could also be expected to luminesce in EL devices. Because the construction of EL devices is time consuming, PL is therefore useful in determing which complexes may provide the strongest EL emission.

Table 4-1. Photophysical Properties of LnTPPL measured in CH_2Cl_2.

	L= TP			L= Klaui		
n	λ_{abs} /nm (log ε)	λ_{em} /nm	IR ϕ	λ_{abs} /nm (log ε)	λ_{em} /nm	IR ϕ
o	423(5.69), 510(3.54), 552(4.27), 590(3.61), 627(3.32)	649, 715	-	427(5.72), 519(3.58), 597(3.85), 626(3.40), 649(3.31)	614, 656, 717	-
m	423(5.80), 513(3.55), 551(4.43), 588(3.70), 626(3.28)	652, 718	-	405(4.62), 426(5.71), 517(3.48), 557(4.27), 595(3.76), 624(3.15)	611, 655, 717	-
r	422(5.60), 514(3.71), 551(4.21), 590(3.63), 648(3.30)	653, 717, 1426, 1526	-	427(5.68), 520(3.72), 596(3.79), 625(3.06)	611, 655, 720	-
b	421(5.72), 513(3.58), 551(4.41), 588(3.77), 624(3.46)	652, 718, 929, 952, 974, 989, 1002, 1014, 1022, 1037	.032	427(5.73), 521(3.67), 596(3.76)	612, 655, 719, 923, 958s, 977	.024

Quantum yields were measured relative to ZnTPP (ϕ = 0.033, CH_2Cl_2)

The results of the PL study, performed by Ben Harrison, on these complexes , with other important photophysical measurements, are shown in Table 4-1. These measurements indicate that the Yb containing compounds have the highest quantum yields of the complexes studied. While the Er, Tm, and Ho complexes have extremely low quantum yields. Experiments performed on the erbium containing complexes have determined they are luminescent, but the typically observed 1550 nm emission appears to be absent from the spectrum.

It should be noted that recent experiments performed on the fluorescence detectors have shown that there is a sharp decrease in the sensitivity of our instrument at ~1550 nm. This would indicate that the intensity of the transition for the erbium containing complexes might be much higher than what we are currently reporting. This

issue will need to be resolved before any definitive numbers can be supplied for erbium containing complexes.

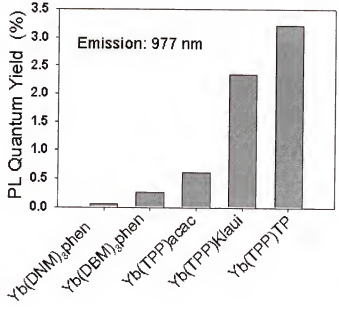

Figure 4-22. Performance of the various Yb complexes

The porphyrin complexes have a significantly increased quantum yields compared to the diketonate materials (Figure 4-22). The YbTPP(acac) is twice as efficient as the best diketonate complex. The quantum yield from the YbTPP(TP) complex is 2.5% or seven times more intense than the YbTPP(acac) complex. The seven coordinate compounds, which this chapter has focused on, affirm our hypothesis that the increased steric bulk around the metal does allow for better NIR light production.

Results from these experiments indicate that the porphyrin-based materials have a significantly higher PL quantum yield than the diketonate complexes. From these results it was expected that EL devices using these complexes as the luminescent centers would also outperform devices that used diketonate complexes. Due to the strong fluorescence

of the Yb-based complexes, devices utilizing them in the active layer will be discussed. The devices that will be discussed were constructed with PPP-OR11 as the host polymer and YbTPP complexes as the luminescent centers. The architecture of the devices is identical to the devices discussed in Chapter 3.

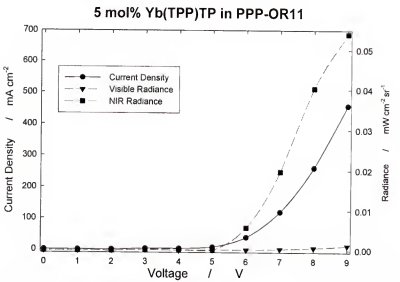

Figure 4-23. Performance of a device utilizing YbTPP(TP)/ PPP/OR11 in the active layer

Figure 4-23 shows the characteristics of a device that utilized **17** as the luminescent center. The turn on voltage was at 5.5 V with a break down voltage of 9 V similar to the LEDs detailed in Chapter 3. The device produced 0.058 mw/cm^2 while drawing 415 ma/cm^2. Production of NIR light with these numbers represents a quantum efficiency of 0.04% for this device, which is 0.03 % or four times more efficient than our best diketonate based device. The emission of visible light by the device was reduced to less than 5% at a 10% by weight loading of the porphyrin complex. Similar results to these were observed when complex **21** was used in the active layer of the device.

Nonconjugated Polymer Based Devices

To demonstrate the effect of the conjugated polymer on the quantum efficiencies of the devices, a device was constructed where the PPP-OR11 was replaced with polystyrene. It was expected that the voltage at which the device would begin to emit light would be much higher than the CP containing LED, if there were any NIR emission at all. Instead, the device had a turn on voltage of 7 V and had a current density 1/10 that of the previously discussed devices. The device had an irradiance measurement of 0.8 mW/cm^2, which is ~16 times more intense than the best CP based device, coupled with the low current density indicates that the device should have a quantum efficiency of 3-4%. To ensure that this was not an error, this experiment was repeated several times and in each case the results were identical. If these numbers are correct, then this represents an increase of an order of magnitude in the QE of the device over the best previously recorded results. The complex used in this device was **21** but in experiments performed with **17** as the luminescent center, the results were similar.

We believe that the dramatic increase in efficiency may be attributed to the means by which charge is transported through the active layer of the device. It is possible that the conjugated polymer was providing a nonproductive pathway for the charge migration. In eliminating the CP from the active layer this route would be excluded thus resulting in a much lower current density. Current flow that did occur would have to find an alternate route, which is proposed to be through a ring hopping mechanism involving the porphyrins. Charge recombination would occur exclusively on the porphyrin ring, which should lead to an increased probability of the excited state energy being transferred to the lanthanide metal. Porphyrin based transport mechanisms of this sort have been proposed

by other researches.[82] Considering this, it may be advantageous to investigate replacing the porphyrin with ring systems, such as phthalocyanine, whose conducting properties have been more thoroughly investigated. Exploration of the synthesis of such compounds will form the basis of the ensuing chapter.

Summary and conclusion

Several lanthanide compounds have been used in attempts to isolate a LnTPP amide. While these methods have provided less than satisfactory results, a new path to LnTPP complexes has been developed that does not rely on the use on Ln amide compounds. Instead it relies on the reaction of the dianion of the porphyrin and the chlorides of the lanthanides to produce LnTPP(Cl) DME complexes. These complexes can then be readily converted into known and previously unknown compounds. Spectroscopic techniques have been developed to analyze these compounds thus allowing rapid determinations of the materials identity and purity.

The use of sterically demanding ligands has been shown to enhance the luminescing ability of the LnTPP complexes. Recent work has demonstrated that the most efficient and intense EL devices do not require the incorporation of a conjugated polymer in the active layer.

CHAPTER 5
LANTHANIDE PHTHALOCYANINE COMPLEXES

In chapter 4, the discussion focused on the use of tetraphenylporphyrin as a sensitizing chromophore for lanthanide NIR luminescence. While this work demonstrated that a porphyrin could be an effective ligand for this purpose, it is important that other ligands are investigated, to determine if they might provide better properties. Characteristics that would be advantageous to maintain in any new ligands would be a large molar absorptivity, high denticity, and an uncomplicated synthesis. An aromatic, macrocycle that has many of these desired properties is phthalocyanine (Pc). It is easily synthesized by a variety of methods, has a strong absorption at ~720 nm, and is a tetradentate ligand.[83] Work described in this chapter will cover the synthesis of complexes incorporating this ligand and the preliminary results on their photoluminescence capabilities.

There are many of examples of $LnPc_2$ sandwich complexesin the literature where the metal is situated between the two Pc rings.[84] These compounds are characterized by a strong interligand charge transfer band at ~1550 nm. This absorption would effectively quench many of the lanthanide NIR transitions that we are interested in investigating, thereby precluding these complexes as potential candidates for NIR luminescent materials. An alternative to this sandwich structure would be a mono ring complex similar to the LnTPP complexes of Chapter 4. The chemistry of these compounds is relatively unexplored with few examples in the literature.[85] The majority of reports focused on the reaction between dilithiophthalocyanine and Ln tris (β-diketonate)

complexes in an attempt to generate an LnPc (diketonate) complex. When this strategy was employed, the complexes formed were not neutral, as anticipated, but retained two diketonates after complexing the Pc and were anionic (Figure 5-1).

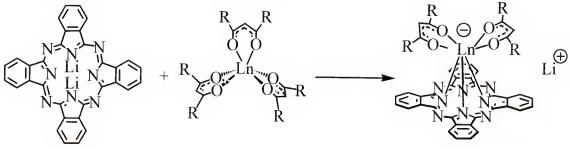

Ln=Yb, Pr, La, Eu
R= Me, C_2F_5, C_4F_9

Figure 5-1. Examples of common mono-ring LnPc complexes

These complexes are typified by their insolubility in many common organic solvents leading to a lack of knowledge about their molecular structures. It has been shown by work in our group that the identity of the axial ligand on LnTPP complexes plays a substantial role in determining their solubility. In the compounds we have explored thus far, the Klaui derivitized porphyrin complexes are the most soluble. It was therefore expected that this ligand might alleviate some of the solubility issues that have been associated with LnPc containing compounds.

Synthesis of LnPc(Cl)

The dilithio salt of tetraphenylporphyrin was only isolated in the last 10 years but dilithiophthalocyanine has been known and used for almost 70 years. One of the first preparations for Pc involved the reflux of 1,2 dicyanobenzene with lithium in pentanol to produce the phthalocyanine dianion.[86] A synthetic procedure published in the patent literature, relies on refluxing this anion with anhydrous lanthanide trichlorides to produce

Ln (Pc)Cl complexes.[87] In this procedure, the product is sparingly soluble in the reaction solvent, allowing the complex to be isolated by filtration. Because no column chromatography is required to purify the product, the compounds can be generated efficiently in multigram quantities (Figure 5-2).

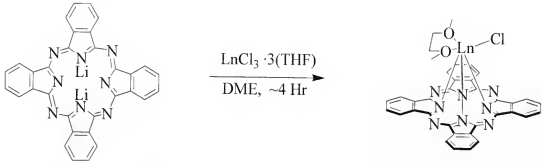

Figure 5-2. Synthesis of LnPc(Cl)DME

Synthesis and Characterization of LnPc(Klaui)

To generate the Ln(Pc)Klaui complexes, a THF slurry of Ln(Pc)Cl is combined with the sodium salt of the Klaui ligand in THF. For this reaction, the solvent choice does not appear to be critical in determining the outcome of the reaction as several other sets of reaction conditions have been used with equal success. Once the axial ligand is added to the solution, the Pc complex can be seen to dissolve in a matter of minutes, indicating a new complex has formed. After a standard purification procedure an electric blue crystalline material, that is soluble in most organic solvents, is isolated in moderate yields. A methylene chloride solution of this material when layered with pentane produces analytically pure, X-ray diffraction quality crystals of the title compound (Figure 5-3).

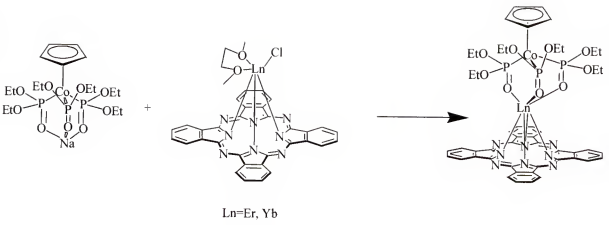

Figure 5-3. Synthetic scheme to generate LnPc(Klaui) complex

The molecular structures of the complexes were determined by X-ray diffraction studies. The thermal ellipsoid plot of Yb(Pc)Klaui (**24**) is shown in Figure 5-4. In the structure there is considerable disorder associated with the ethyl portion of the Klaui ligand, but this has been model accurately, with R1 = 0.0256 and wR2 = 0.0639. The Yb atom is 1.247(4) Å from the least squares mean plane defined by the phthalocyanine nitrogens that are coordinated to the Yb and the metal is positioned 1.466(8) Å below the Klaui ligand oxygen mean plane. There is an angle of 6.8° between the oxygen plane and the nitrogen plane. In the structure, 3 of the rings that compose the Pc ligand are bent out of nitrogen plane by ~ 12°, with the remaining ring being displaced by 2.7°. This anisotropy makes the complex appear to cant in one direction. It is not clear why one ring does not bend as much as the others do, but it may be caused by to a solid-state crystal packing effect

As expected, the crystal structure of compound **25** is identical to the structure of **24**, including the distortion in the ring plane. The only difference is that the lanthanide bonds are elongated by 0.015 Å. In all other respects, the structure and packing diagram are identical.

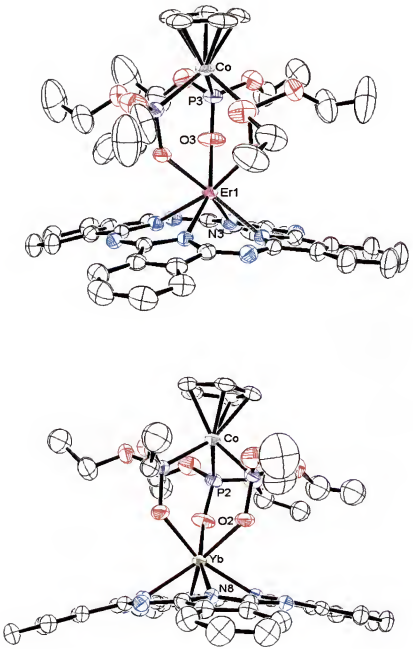

Figure 5-4. Thermal ellipsoid plots of **25** (top) and **24** (bottom) drawn at the 50% probability level; hydrogen atoms have been excluded for clarity.

As was demonstrated in Chapter 4, one-dimensional and multi-dimensional proton NMR can be used as means to identify paramagnetic complexes. In this section, the results of the NMR experiments on **24** and **25** will be discussed. In addition, a

complication to the assignment of the peaks in the erbium complex will be described along with the manner in which this problem was solved. Readers unfamiliar with the particulars of paramagnetic NMR are referred back to the section in Chapter 4 pertaining to these experiments.[88]

In the proton NMR spectrum of **24,** six peaks are observed (Figure 5-5). The peaks at 14.78 and 10.43 ppm integrate for 8 hydrogen atoms and are assigned as the two protons on the phenyl portion of the phthalocyanine. Given the symmetry of the complexes and observations made for the LnTPP(Klaui) complexes, it is expected that the protons on the methylene of the ethyl portion of the Klaui ligand would contain two diastereotopic protons accounting for two peaks that integrate for 6 H. From this assumption, the peaks labeled as C and D at 8.94 (6 H) and 8.53 (6 H) ppm respectively are assigned as the diastereotopic hydrogen atoms. The peak at 4.20 ppm integrates for 18 hydrogen atoms and is thus readily assigned to the methyl protons on the ethyl of the Klaui ligand. Finally, the peak at -6.46 ppm is assigned to the cyclopentadienide protons because of its relative integration of five hydrogen atoms.

To further confirm the assignment of the peaks, a COSY experiment was performed on this sample (Figure 5-6). In the spectrum the peaks labeled as A and B in the 1D spectrum are strongly coupled to each other as anticipated. Examination of an expansion of the spectrum from 9 to 1 ppm reveals that the peaks labeled as C and D are coupled to each other as well as to the peak labeled E (Figure 5-7). In the 1D spectrum the peak, E was unambiguously assigned as the methyl on the ethyl because of its integration. This information confirms that the peaks C and D are the diastereoscopic protons.

The 1D proton NMR spectrum of **25**, when first recorded, did not conform to the pattern observed for **24** (Figure 5-8). It was expected that 6 peaks would be observed similar to **24**, instead only 5 peaks were present with a relative integration ratio of 18:14:8:6:5. The peak at 36 ppm appeared to have a shoulder indicating that it might actually be two peaks superimposed on each other.

To determine if the peak was compromised of two peaks, we decided to take advantage of the fact that paramagnetic NMR peak positions have a strong temperature dependence. If no significant structural changes occur upon changing the temperature, the peak position of each proton will vary linearly with the temperature. The magnitude of the change in peak position versus temperature is dependant on the identity of the proton; therefore, if two peaks appear as being superimposed at one temperature raising or lowering the temperature should cause the peaks to separate.[75]

Raising the temperature to 332 K caused the peak observed at 36 ppm to separate and the expected number of resonances was then be observed. Peaks at 31.42 (8 H) and 18.68 ppm (8 H) were assigned to the protons on the phenyl ring on the Pc; the diastereotopic protons on the Klaui ligand were assigned to the peaks at 29.98 (6 H) and 27.83 ppm (6 H). The methyl on the ethyl protons were at 16.15 ppm (18 H), with the cyclopentadienide protons being attributed to the peak at –42 ppm (5 H).

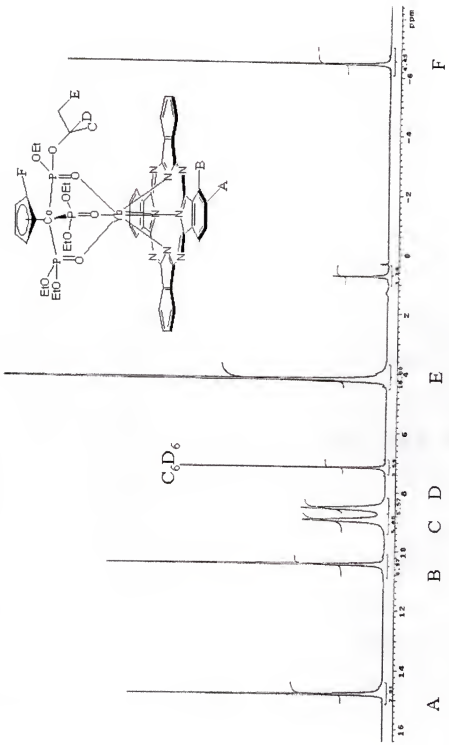

Figure 5-5. One-dimensional proton NMR of **24**

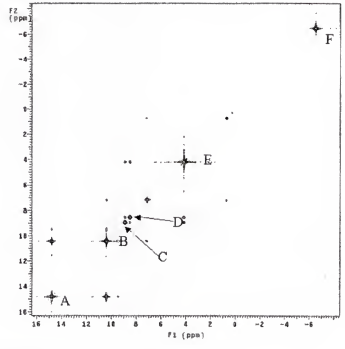

Figure 5-6. COSY spectrum of **24**

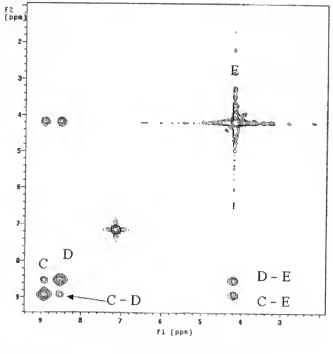

Figure 5-7. Expansion of Figure 5-6 from 2 to 9.5 ppm

Synthesis of LnPc(Tp)

Following the successful synthesis of the Klaui ligated LnPc complex, an attempted was made to generate the Tp version of the complex. A similar procedure was followed, but the material resulting from the reaction was virtually insoluble in common organic solvents. Due to the limited solubility of the complexes, purification and characterization of the materials was complicated and has not been completed.

Photoluminescence Experiments

As discussed at the beginning of the chapter the Pc ligand has a strong absorption similar to a porphyrin. Shown in Figure 5-10 is the absorption spectrum of **24**, the transition with the highest molar absorptivity is red of the porphyrin Soret band by almost 300 nm. We hypothesized that the longer wavelength of the excitation may lead to more efficient stimulation of the longer wavelength transitions in the lanthanide ions because there would be a smaller difference in energy levels. Additionally, the longer wavelength absorption of the ligand would effectively quench any lanthanide transition in the visible. This quenching effect would eliminate the possibility for competing radiative relaxation pathways, ensuring that the maximum amount of NIR photons would be produced.[89]

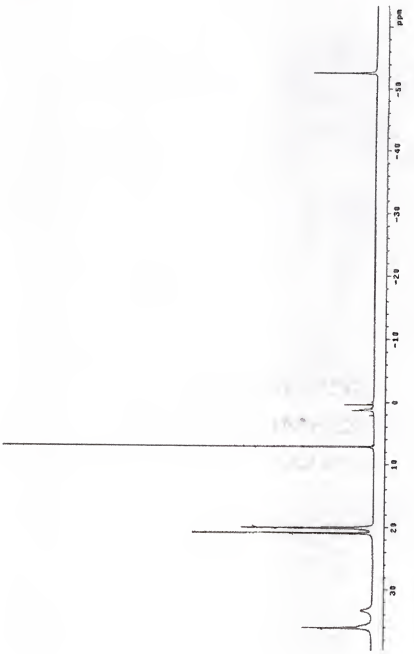

Figure 5-8. One dimensional proton spectrum of **25** at 292 K.

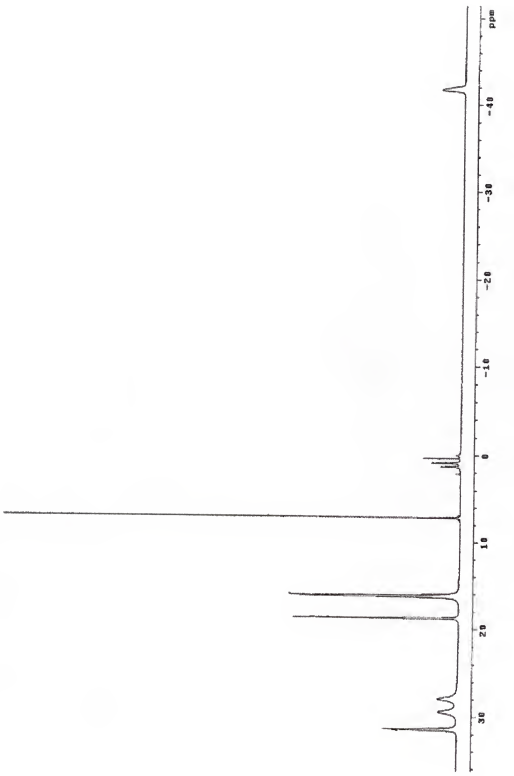

Figure 5-9. One-dimensional proton NMR spectrum of **25** at 332 K

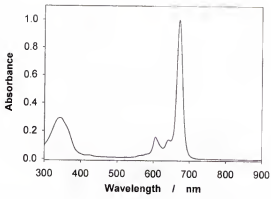

Figure 5-10. Absorption spectrum of YbPc(Klaui) in methylene chloride.

Complex **24** shows no propensity for NIR PL. This has been attributed to the triplet state energy of the Pc being lower in energy than the Yb transition, the emission wavelength of Yb is 970 nm and the triplet state of the Pc ligand extends to ~1050 nm.[90] When complex **23** was examined, the expected emission starting at 1500 nm was observed (Figure 5-11). The true value of the luminescence intensity has not been determined, but it can be observed that the ratio of the signal to the background noise is highest for the ErPc(Klaui) complex as compared to other Er containing complexes that have been studied indicating that it may be strongly luminescent. From this work, it is expected that the EL of a device using this complex should follow the observed trend where complexes with strong PL act as efficient luminescent centers in PLEDs.

Summary

Lanthanide containing phthalocyanine complexes have been generated in moderate yields and their solubility in organic solvents has been improved by the coordination of the Klaui ligand. Near infrared PL from the Yb complex does not occur due to electronic transitions on the Pc that are lower in energy the *f-f* transition of the lanthanide. Emission has been observed for the Er containing compound and it appears

be more intense than any previously documented. Future work will focus on using the Pc ligand to stimulate the lanthanides that emit at longer wavelengths, quantifying the PL quantum yield, and developing NIR PLEDs using these complexes as the luminescent centers.

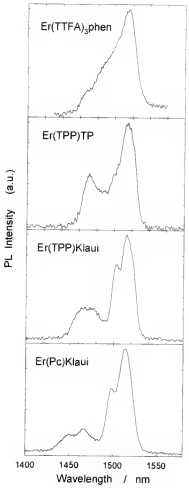

Figure 5-11. Photoluminescence spectra of selected Er containing coordination complexes

CHAPTER 6
EXPERIMENTAL PROCEDURES

General Synthetic Procedures

Unless otherwise stated synthetic manipulations were carried out on a double manifold Schlenk line under an atmosphere of nitrogen or in an atmosphere of nitrogen in a glovebox. Glassware was oven dried at no less than 110 °C prior to use. Toluene, pentane, diethyl ether, and tetrahydrofuran were purchased from Aldrich Chemicals and dried by passage through a column of activated alumina. Following dehydration, the solvents were degassed, and stored over 4 Å sieves in resealable ampoules fitted with Teflon valves. All other solvents were purchased from Fisher Scientific and dried according to literature procedures.[91] Elemental analyses were performed by Complete Analysis Laboratories Inc. of Parsippany, NJ or the University of Florida Spectroscopic Services. Starting materials used for this work were generated according to literature procedures, with the references for the preparation of the specific compounds provided in the sections where those compounds are discussed.

Photophysical Measurements

All photophysical studies were conducted by Ben Harrison unless otherwise noted. All absorption, emission, and lifetime measurements were made in CH_2Cl_2, in 1 cm square quartz cuvettes. Absorption spectra were obtained on a double-beam Cary-100 UV-visible spectrometer. Fluorescence spectra were measured on a SPEX Fluorolog-2 equipped with a water-cooled PMT detector or on a spectrometer consisting of an ISA-SPEX Triax 180 spectrograph equipped with a LN_2 cooled CCD detector (Hamamatsu

CCD, 1024x64 pixel, 400-1100 nm). NIR measurements were measured on a SPEX Fluorolog-2 equipped with a LN_2 cooled InGaAs detector (800-1600 nm). All measurements were corrected for detector response. Emission quantum yields were measured by relative actinometry with H_2TPP (ϕ=0.11, CH_2Cl_2) or ZnTPP (0.033, CH_2Cl_2). Time-resolved emission decays were obtained by time-correlated single photon counting on an instrument that was constructed in-house. Excitation was effected by using either a pulsed LED source or a blue-pulsed diode laser (IBH instruments, Edinburgh, Scotland). The pulsed LED and diode laser sources have pulse widths of ca. 1 ns. Time-resolved emission was collected using a red sensitive, photon-counting PMT (Hamamatsu R928), and the light was filtered using 10 nm band-pass interference filters.

Nuclear Magnetic Resonance Experimental

Spectra were recorded in 5 mm Kontes resealable NMR tubes. Proton NMR spectra were measured at 300 MHz on a Varian Gemini 300, VXR 300, or Mercury 300 with C_6D_6 as the solvent unless otherwise noted. Chemical shifts in the spectra were referenced to the residual protons on the deuterated solvent and are reported in parts per million downfield from tetramethylsilane (δ=0). For paramagnetic complexes, the acquisition times were varied according to the relaxation rate enhancement provided by the lanthanide, spectral window width was determined by expanding the scope of the spectrum until the peak positions remained invariant to further expansions. The number of transients collected for an individual spectrum varied with the nature of the metal, with minimum being determined by the noise in the particular spectrum. COSY spectra were collected using the standard parameters that accompanied the Varian operating software.

ESI Mass Spectroscopy

The acquisition of the spectra and calibration of the machine were performed by Lidia Mateeva under the direction of Dave Powell. All samples analyzed by this technique were dissolved in a 1: 3 acetonitrile: methylene chloride solution. The solvent mixture was used to dissolve 1 mg/ 10 ml under an inert atmosphere. Samples were then taken directly to the Finnigan LCQ mass spectrometer in the Chemistry Department at the University of Florida. A syringe that had been washed with three aliquots of the sample was used to inject the sample into the spectrometer. After the anhydrous samples had been analyzed, 1 μl of deionized water was added to the sample and the spectrum was then taken again. The software provided by Finnigan generated the predicted isotopic distributions.

Synthesis Bis(2,3-dihydro-thieno[3,4-b][1,4]dioxine) 1,4-divinyl-benzene (1)

Potassium hydride (0.105 g, 2.64 mmol)was added to ~50 ml of DME with vigorous stirring. Into this slurry was added the [4-(diethoxy-phosphorylmethyl)-benzyl]-phosphonic acid diethyl ester (0.500g, 1.32 mmol) and the 2,3-dihydro-thieno[3,4-b][1,4]dioxine-5-carbaldehyde (0.446 g, 2.64 mmol), hydrogen gas was immediately evolved as the solvent turn a pumpkin orange color.[26] The reaction was then brought to reflux, and allowed to proceed for 12 hours. The resulting dark-brown solution was concentrated under vacuum to $^{1}/_{3}$ of its original volume and cannulated into a stirring solution of water and hydrochloric acid with a pH <2. A yellow-orange precipitate formed and was collected by suction filtration. The solid was dissolved in a minimum amount of chloroform, the solution was then dried with magnesium sulfate, and layered with pentane. The product of the reaction then precipitated and was dried under

vacuum to yield 0.292 grams(7.12×10^{-1} mmol, 54 %). It should be noted that NaH works equally well for this procedure, but the use of BuLi and $LiNMe_2$ have not been successful in producing the desired complex. ^1H NMR ($CDCl_3$) δ 7.42 (s, 4H, C_6H_4), 7.18 (d, 2H, C_6H_4-C*H*=CH), 6.85 (d, 2H, C_6H_4-CH=C*H*), 6.23(s, 2H, *H*C-S), 4.36 (m, 8H, CH_2CH_2)

Synthesis of Ru (η^5-C_5Me_5)(Bis(2,3-dihydro-thieno[3,4-b][1,4]dioxine) 1,4-divinyl-benzene) triflate (2)

A solution of **1** (0.100 g, 2.44×10^{-1} mmol) in ~25 ml of THF was stirred at room temperature, to this was added a slurry of [Ru(η^5-C_5Me_5)(CH_3CN)$_3$] [OTf] in ~25 ml THF (0.124 g ,2.44×10^{-1} mmol).[18] This solution was then heated to reflux and allowed to react for 12 hours. The reaction was then allowed to cool to room temperature. During the course of the reaction a brown ppt formed and was isolated from the reaction mixture by filtration. The filtrate volume was then reduced by half, was layered with pentane, and allowed to stand for an additional 12 hours. A crystalline material was deposited on the walls of the flask and was isolated by cannula filtration. The material was then dissolved in a minimum amount of dichloromethane and layered with diethyl ether, giving the complex in a yield of 43% (8.47×10^{-2}g, 1.06×10^{-1} mmol). ^1H NMR ($CDCl_3$) δ 7.05 (d, 2H, C_6H_4-C*H*=CH), 6.27 (d, 2H, C_6H_4-CH=C*H*), 6.30 (s, 2H, *H*C-S), 6.00 (s, 4H, C_6H_4), 4.38 (m, 8H, CH_2CH_2), 1.79 (s, 15H, (η^5-C_5Me_5))

Synthesis of Ru(η^5-C_5Me_5)([4-(diethoxy-phosphorylmethyl)-benzyl]-phosphonic acid diethyl ester) triflate (3)

A colorless, solution of the [4-(diethoxy-phosphorylmethyl)-benzyl]-phosphonic acid diethyl ester (0.500 g, 1.32 mmol)in 25 ml of THF was added to a slurry of the [Ru(η^5-C_5Me_5)(CH_3CN)$_3$] [OTf] (0.672, 1.32 mmol) in THF (~ 25 ml). The solution was brought to reflux and stirred for 4 hours. The solvent was removed *in vacuo* and the residue was dissolved in ~ 10 ml dichloromethane and then layered with 50 ml of pentane. The ensuing tan, crystalline precipitate was then isolated by cannula filtration, yielding 0.768 g of product (1.00 mmol, 76%).^{1}H NMR ($CDCl_3$) δ 5.92 (s, 4H, C_6H_4), 4.15 (q, 8H, OCH_2CH_3), 2.70 (d, 4H, $C_6H_4CH_2P$), 1.92 (s, 15H, (η^5-C_5Me_5)), 1.36 (t, 12H, OCH_2CH_3)

Alternate Synthesis of Ru (η^5-C_5Me_5)(Bis(2,3-dihydro-thieno[3,4-b][1,4]dioxine) 1,4-divinyl-benzene) triflate (2)

The synthetic procedure for this complex is the same as for **1** using 0.200 g (2.617×10^{-1} mmol) of the [Ru(η^5-C_5Me_5)([4-(diethoxy-phosphorylmethyl)-benzyl]-phosphonic acid diethyl ester)] [OTf], 0.089 g (5.23×10^{-4} mol) of 2,3-dihydro-thieno[3,4-b][1,4]dioxine-5-carbaldehyde, and 0.012 g (5.23×10^{-1} mmol) of NaH. The product of the reaction was isolated by the same procedure used in the original synthesis. This method then gave an isolated yield of 0.266 g of **2** (3.35×10^{-1} mmol, 64%).

Synthesis of Rh (η^5-C_5Me_5)(Bis(2,3-dihydro-thieno[3,4-b][1,4]dioxine) 1,4-divinyl-benzene) bis(tetrafluoroborate) (4)

Silver tetraflouroborate(0.125 g, 6.48 x 10^{-1} mmol) was added to a suspension of the complex [Rh(η^5-C_5Me_5)Cl_2]$_2$ (0.100 g, 1.62 x 10^{-1} mmol) in deoxygenated 25 ml acetone.[35] Upon addition of the silver reagent, a voluminous precipitate immediately formed and after stirring for an additional 30 min, was separated from the solution by means of a centrifuge. The resulting orange solution was then filtered and reduced in volume to ~ 5 ml and added to a 10 ml solution of EVPVE (0.133 g, 3.24 x 10^{-1} mmol) in methylene chloride. It appeared that the two phases were not miscible, but stirring was continued for two days. After the allotted time the solution was passed through a filter cannula and then layered with pentane. The resulting precipitate was isolated by filter cannula to yield 0.095 g of product (1.15 x 10^{-1} mmol, 35%).^{1}H NMR ($CDCl_3$) δ 7.90 (d, 2H, C_6H_4-C*H*=CH), 7.88 (s, 4H, C_6H_4), 6.90 (d, 2H, C_6H_4-CH=C*H*), 6.84 (s, 2H, *H*C-S), 4.62 (m, 8H, CH_2CH_2), 2.18 (s, 15H, η^5-C_5Me_5)

Synthesis of the - Bis(2,3-dihydro-thieno[3,4-b][1,4]dioxine) 1,4-divinyl-2,5-Bis-dodecyloxy benzene (5)

The procedure outlined by Kubo was used to generate 2,5 bis-dodecyloxy [4-(Diethoxy-phosphorylmethyl)-benzyl]-phosphonic acid diethyl ester was generated following the procedure outlined by Kubo.[23] Utilizing that compound, a reaction was run that was identical to the synthesis of **1**. Combining 0.500g (6.69 x 10^{-1} mmol) of diphosphonate, 0.226g (1.33 x 10^{-3} mmol) of aldehyde, and 0.0503g (1.33 x 10^{-3} mmol) of potassium hydride in ~100 ml of DME , 0.224 g (2.87 x 10^{-1} mmol, 46%) of **5** was produced. The material was purified by fractional crystallization from chloroform and

acetonitrile to yield 0.205 g of product. ^{1}H NMR ($CDCl_3$) δ 7.33 (d, 2H, C_6H_2-C*H*=CH), 7.26 (s, 2H, C_6H_2), 7.00 (d, 2H, C_6H_2-CH=C*H*), 6.20 (s, 2H, *H*C-S), 4.27, 4.23 (m, 8H, CH_2CH_2), 4.15 (t, 4H, OCH_2CH_2) 1.85 (m, 4, OCH_2CH_2) 1.6-1.2 (m, 36H, alkoxy side chain), 0.95 (t, 6H, -CH_2CH_3)

General Synthesis of Ln Diketone Complexes

The synthetic procedure used to generate any of the lanthanide diketonate complexes has been detailed in several excellent references, but will be outlined here.[42] Researchers interested in a particular diketone are advised to investigate its synthesis using the resources provided in Chapter 3.

Into refluxing ethanol is added 3 equivalents of a diketone, 3 equivalents of sodium hydroxide and if desired 1 equivalent of a bidentate Lewis base(not adding the Lewis base leads to a product where two equivalents of water are coordinated to the product). After the added reagents have dissolved and the solution turns to the color of the diketonate anion (usually a yellow to golden color) an ethanol solution of the desired lanthanide trichloride is added in a dropwise fashion. In most instances, the product begins to precipitate immediately, but if this does not occur after the addition of the lanthanide solution is completed, heating should be continued until a sufficient amount the solvent has been removed such that the solution begins to appear cloudy. At that point, the reaction vessel should be removed from the heat and allowed to cool. Products from the reaction were typically isolated by vacuum filtration, and were recrystallized from chloroform/ pentane solutions. Yields for the material following purification were typically between 25 – 75 %.

Synthesis of 5,5'-Bis-[2-(4-bromo-2,5-bis-hexyloxy-phenyl)-vinyl]-[2,2']bipyridine (6)

The synthesis of the diphosphonate followed the procedure outlined by Yu.[44] The synthesis of 4-bromo-2,5-bis-hexyloxy-benzaldehyde, also followed the literature precedent. The coupling reaction between the phosphonate and the aldehyde followed the procedure used to generate complex **1.** Utilizing 2.00 g (4.38×10^{-1} mmol) of the diphosphonate, 3.36 g (8.76×10^{-1} mmol) of the aldehyde, and 0.035 g(8.76×10^{-1} mmol) of potassium hydride in 150 ml of DME, 0.218 g (2.73×10^{-1} mmol) of **6** was isolated representing a yield of 54 %. The product was purified by precipitation from chloroform and pentane solution.

Synthesis of 1-(2,5-Dibromo-phenyl)-3-phenyl-propane-1,3-dione (7)

Into a reaction vessel with 0.11 g of NaH (1.14×10^{1} mmol) mixed with 50 ml of DME was slowly syringed of acetophenone (1.304 g ,1.14×10^{1} mmol), hydrogen gas immediately evolved from the reaction and the solution turned yellow. After the solution had been allowed to stir for 1 hour, a solution of 2,5-dibromo-benzoyl chloride (1.50 g, 5.07 mmol) in 25 ml of DME was slowly added.[46] The reaction grew warm with the addition and after the all the acid chloride was added the reaction the solution was then stirred for an additional 12 hours. The solution was then concentrated under vacuum to $^{1}/_{3}$ of its it original volume and cannulated into a stirring solution of water and hydrochloric acid with a pH <2. A yellow-orange precipitate formed and was collected by suction filtration. The product was purified by several recrystillazations from hot ethanol and water to give 1.437 g of product (3.785 mmol, 74%).. ^{1}H NMR ($CDCl_3$)

δ 16.24 (s, 1H, O-*H*-O), 8.01 (m, 1H, CBrC*H*C-C=O), 7.97 (m, 2H, CBrC*HCH*CBr) 7.6-7.4 (m, 5H, C_6H_5), 6.73 (s, 1H, O=CC*H*C=O)

Synthesis of $Yb(NPh_2)_3 \cdot 2THF$ (8)

Into a stirred solution of 2.00 g(1.182×10^1 mmol) of diphenylamine in 25 ml of THF, was added 0.461 g (1.182×10^1 mmol) of potassium hydride. Immediately after the addition began the evolution of hydrogen gas was evident and the solution became warm to the touch. After stirring for ~30 minutes the golden yellow solution was combined with 1.091 g (3.94 mmol) of anhydrous $YbCl_3$. The color of the solution then changed from yellow to colorless to purple over the span of 15 minutes. Stirring of the solution was then continued for 12 hours, after which time the solvent was removed *in vacuo*. Toluene was then used to extract the residue (3 x 20 ml), and the extract was separated from the potassium chloride by means of a filter cannula. The combined filtrates were then reduced to half of its original volume and was then layered with pentane to yield X-ray diffraction quality crystals after standing overnight. The crystals were dissolved in THF and layered with pentane to yield analytically pure crystals of **7** (2.31 g ,2.82 mmol) in a 71% yield. Anal. Calcd.For: $C_{44}H_{46}N_3O_2Yb$ C, 64.30; H, 5.64; N, 5.11;. Found C, 64.25; H, 5.12; N, 5.65

Synthesis of $Er(NPh_2)_3 \cdot 2THF$ (9)

The procedure used to generate this complex was identical to that for **8**. In this reaction 2.00 g (1.182×10^1 mmol) of diphenylamine, 0.461 g (1.182×10^1 mmol) of potassium hydride, and 1.091 g (3.94 mmol) of $ErCl_3$ were used to yield 1.80 g (2.20 mmol, 55%) of product. Anal. Calcd. For: $C_{44}H_{46}N_3O_2Er$ C, 64.75; H, 5.68; N, 5.15;. Found C, 64.29; H, 6.02; N, 5.25

Synthesis of YbTPPCl(DME). (13)

In the glove box, $YbCl_3 \cdot 3(THF)$[92a] (2.755 g, 5.99 mmol) and $(LiDME)_2TPP$ (4.861 g, 5.99 mmol)[92b] were combined in a 250 ml Schlenk tube equipped with a sidearm.[92] The reaction mixture was brought out to the Schlenk line where 150 ml of toluene was added and the reaction was then heated to reflux under a flow of nitrogen. After 4 hours, a precipitate formed and was separated from the solution by filtration of the hot reaction mixture. The residue in the reaction flask was washed with dichloromethane (2x with *ca.* 35 ml), the combined filtrates were combined with the toluene solution. The solvent mixture was then reduced to *ca.* 50 ml *in vacuo* and cooled to 0 °C, where upon red purple crystalline **13** (3.930 g, 4.313 mmol) precipitated and was isolated by filtration. The mother liquor was then concentrated to *ca.* 25 ml and cooled to −78 ° C affording a second crop of (0.4340 g, 4.744×10^{-1} mmol) of product. The two fractions were combined and dissolved in hot toluene, the solution was then cooled to room temperature, layered with pentane, and cooled to 0 °C yielding 4.364g of product(79%). X-ray quality crystals were grown by the slow evaporation of a chloroform solution under an inert atmosphere. Anal. Calcd. For $C_{48}H_{38}ClN_4O_2Yb$: C, 63.26; H, 4.20; N, 6.15. Found: C, 64.25; H, 3.62; N, 5.85 UV-Visible CH_2Cl_2 [λ_{max}, nm (log ε)] 421(5.71), 514(3.59), 550 (4.40), 586 (3.77), 624 (3.44)

Synthesis of TmTPPCl(DME). (12)

Procedure is the same as that for the Yb complex, using 2.80 g (6.16 mmol) of $TmCl_3 \cdot 3(THF)$ and 4.99 g (6.16 mmol) of $(LiDME)_2TPP$ to give 4.72g (5.21 mmol, 84%) of the porphyrin complex. Anal. Calcd. For $C_{48}H_{38}ClN_4O_2Tm$: C, 63.55; H, 4.22;

N, 6.18 Found: C, 65.11; H, 4.48; N, 5.90 UV-Visible CH_2Cl_2 [λ_{max}, nm (log ε)] 420 (5.62), 514 (3.75), 551 (4.41), 586 (3.63), 624 (3.30)

Synthesis of ErTPPCl(DME) (11)

Procedure is the same as that for the Yb complex, using 2.78 g (6.16 mmol) of $ErCl_3$•3(THF) and 4.99 g (6.16 mmol) of $(LiDME)_2TPP$ to give 4.21g (4.65, 76%) of the porphyrin complex. Anal. Calcd. For V $C_{48}H_{38}ClN_4O_2Er$: C, 63.66; H, 4.23; N, 6.19 Found: C, 63.59; H, 4.14; N, 5.94 UV-Visible CH_2Cl_2 [λ_{max}, nm (log ε)] 420 (5.80), 514 (3.55), 551 (4.21), 586 (3.63), 624 (3.28)

Synthesis of HoTPPCl(DME). (10)

Procedure is the same as that for the Yb complex. Starting with 2.778 g (6.16 mmol) of $HoCl_3$•3(THF) and 4.99 g (6.16 mmol) of $(LiDME)_2TPP$ to give 4.14g (4.57 mmol, 74%) of the porphyrin complex. Crystals of this compound were also grown by slow evaporation of a chloroform solution under an inert atmosphere. Anal. Calcd. for $C_{48}H_{38}ClN_4O_2Ho$: C, 63.83; H,4.24; N, 6.20 Found C, 63.92; H, 4.17; N, 6.24 UV-Visible CH_2Cl_2 [λ_{max}, nm (log ε)] 420 (5.69), 513 (3.54), 551 (4.27), 587(3.61), 624 (3.32)

Synthesis of Yb(TPP)TP (17).

A solution of YbTPP(Cl)(DME) (0.300 g, $3.31x10^{-1}$ mmol) in toluene (*ca.* 65 mL) was stirred vigorously while potassium hydridotris(1-pyrazolyl)borate (KTP) (0.084 g, $3.31x10^{-1}$ mmol) was added.[69] Following addition, the solution was allowed to stir at room temperature for 12 hr. The solvent was then removed *in vacuo* and the purple residue was extracted with *ca.* 30 ml of methylene chloride, leaving behind a brown residue. The solution was then reduced to *ca.* 10 ml and was layered with *ca.* 30 ml of

pentane. Purple crystals formed on standing overnight. The supernatant was filtered, concentrated, and cooled to -78 °C whereupon an additional amount of product precipitated. The fractions were then combined, dissolved in *ca.* 20 ml of methylene chloride, and cooled to -78 ° C. Crystals then formed, which were isolated by cannula giving 0.265g of product (81%). Anal. Calcd for $C_{53}H_{38}BN_{10}Yb$: C, 63.73; H, 3.83; N, 14.02; Found C, 64.23; H, 3.91; N, 13.89; ^{1}H NMR (C_6D_6) 22.71 ($\nu_{1/2}$= 53.24 Hz, 3H, H-TP), 15.48 ($\nu_{1/2}$= 40.81 Hz, 4H, *o*-C_6H_5 TPP), 13.88 ($\nu_{1/2}$= 25.90, 8H, H-pyrrole), 9.73 ($\nu_{1/2}$= 39.55 Hz, 4H, *m*-C_6H_5 TPP), 8.77 ($\nu_{1/2}$= 26.74, 4H, *p*-C_6H_5 TPP), 8.09 ($\nu_{1/2}$= 43.17 Hz, 4H, *m*-C_6H_5 TPP), 7.83 ($\nu_{1/2}$= 44.39 Hz, 4H, *o*-C_6H_5 TPP), 4.62 ($\nu_{1/2}$= 23.34 Hz, 3H, H-TP), -3.03 ($\nu_{1/2}$= 23.81 Hz, 3H, H-TP)

Synthesis of Tm(TPP)TP (16).

The procedure used to generate this complex was the same as that was used for **17** with TmTPP(Cl)(DME) (0.300 g, $3.31x10^{-1}$ mmol) and K TP (0.084 g, $3.31x10^{-1}$ mmol) reacting to give 0.244 g of **16** (73%). Anal. Calcd for $C_{53}H_{38}BN_{10}Tm$ C, 64.00; H, 3.85; N, 14.08. Found: C, 64.52; H, 3.83; N, 14.11; ^{1}H NMR (C_6D_6): 122.96 (113.08 Hz) (bs, 3H, H-TP), 55.33 (58.73 Hz) (bs, 4H, *o*-C_6H_5 TPP), 38.92 ($\nu_{1/2}$= 38.16 Hz, 8H, H-pyrrole), 22.81 ($\nu_{1/2}$= 31.80 Hz, 4H, *m*-C_6H_5 TPP), 16.11 ($\nu_{1/2}$= 22.84 Hz, 4H, *p*-C_6H_5 TPP), 11.97 ($\nu_{1/2}$= 30.49 Hz, 4H, *m*-C_6H_5 TPP), 7.28 ($\nu_{1/2}$= 79.37 Hz, 3H, H-TP), 3.72 ($\nu_{1/2}$= 25.72 Hz, 3H, H-TP), -55.91 ($\nu_{1/2}$= 30.92 Hz, 4H, *o*-C_6H_5 TPP),

Synthesis of Er (TPP)TP (15).

The procedure used to generate this complex was the same as that was used for **17** with ErTPP(Cl)(DME) (0.084 g, $3.31x10^{-1}$ mmol) and K TP (0.300 g, $3.31x10^{-1}$ mmol) reacting to give 0.271 g of **15** (82%). Anal. Calcd. for $C_{53}H_{38}BN_{10}Er$ C, 64.10; H, 3.86;

N, 14.11. Found: C, 63.85; H, 3.12; N, 14.69; ^{1}H NMR (C_6D_6): 61.76 ($\nu_{1/2}$= 493.43 Hz, 3H, H-TP), 32.13 ($\nu_{1/2}$= 94.73 Hz, 4H, *o*-C_6H_5 TPP), 20.90 ($\nu_{1/2}$= 72.68 Hz, 8H, H-pyrrole), 15.14 ($\nu_{1/2}$= 30.38 Hz, 4H, *m*-C_6H_5 TPP), 11.84 ($\nu_{1/2}$= 18.77 Hz, 4H, *p*-C_6H_5 TPP), 9.63 ($\nu_{1/2}$= 28.32 Hz, 4H, *m*-C_6H_5 TPP), 7.66 ($\nu_{1/2}$= 55.83 Hz, 4H, *o*-C_6H_5 TPP), 2.82 ($\nu_{1/2}$= 48.22 Hz, 3H, H-TP), -24.79 ($\nu_{1/2}$= 59.67 Hz, 3H, H-TP),

Synthesis of Ho(TPP)TP (14).

The procedure used to generate this complex was the same as that was used for **17** with HoTPP(Cl)(DME) (0.300 g, 3.31x10^{-1} mmol) and K TP (0.084 g, 3.31x10^{-1} mmol) reacting to give 0.255 g of **14** (77%). Anal. Calcd for $C_{53}H_{38}BN_{10}Ho$ C, 64.26; H, 3.87; N, 14.14. Found: C, 63.75; H, 3.77; N, 13.75 ^{1}H NMR (C_6D_6): 40.30 ($\nu_{1/2}$= 139.20 Hz, 3H, H-TP), 8.90 ($\nu_{1/2}$= 84.74 Hz, 4H, *o*-C_6H_5 TPP), 4.62 ($\nu_{1/2}$= 40.08 Hz, 4H, *m*-C_6H_5 TPP), 3.11 ($\nu_{1/2}$= 95.88 Hz, 3H, H-TP), 2.43 ($\nu_{1/2}$= 26.86 Hz, 4H, *p*-C_6H_5 TPP), 1.36 ($\nu_{1/2}$= 38.59 Hz, 3H, H-TP), -1.90 ($\nu_{1/2}$= 43.16 Hz, 4H, *m*-C_6H_5 TPP), -14.98 ($\nu_{1/2}$= 113.24 Hz, 8H, H-pyrrole), -19.90 ($\nu_{1/2}$= 121.76 Hz, 4H, *o*-C_6H_5 TPP)

Synthesis of Yb(TPP)Klaui (21).

A solution of YbTPP(Cl)(DME) (0.150 g, 1.65x10^{-1} mmol) in DME (*ca.* 50 ml) was stirred vigorously while Na Klaui (0.088 g, 1.65x10^{-1} mmol) was added neat.[70] The solution was stirred at room temperature for 12 hr, after which time the DME was removed *in vacuo* leaving a purple amorphous solid. The solid was extracted twice with *ca.* 15 ml of toluene leaving behind a slight amount of brown residue. The two extracts were combined and reduced to *ca.* 10 ml to which was added *ca.* 30 ml of pentane producing a small amount of brown precipitate. The solution was filtered to remove the precipitate and then cooled to – 78 ° C. Purple crystals of the material formed on

standing for 5 hr, the purple supernatant was separated from the crystals via cannula filtration. Residual solvents were removed from the crystals *in vacuo*, giving 0.200 grams of product (90%). Anal. Calcd. For $C_{62}H_{65}CoN_4O_9P_3Yb$: C, 55.78; H, 4.91; N, 4.20. Found: C, 55.40; H, 4.65; N, 4.08;. ^{1}H NMR (C_6D_6): 17.41($\nu_{1/2}$= 18.27 Hz, 4H, *o*-C_6H_5 TPP), 15.81 ($\nu_{1/2}$= 8.22, 8H, H-pyrrole), 10.68 ($\nu_{1/2}$= 8.03 Hz, 4H, *m*-C_6H_5 TPP), 9.40 ($\nu_{1/2}$= 4.43 Hz, 7 Hz, 4H, *p*-C_6H_5 TPP), 8.91 ($\nu_{1/2}$= 17.09 Hz, 6H, OCH_2CH$_3$), 8.63 ($\nu_{1/2}$= 18.20 Hz, 4H, *o*-C_6H_5 TPP), 8.45 ($\nu_{1/2}$= 28.34 Hz, 4H, *m*-C_6H_5 TPP), 7.67 ($\nu_{1/2}$= 29.31 Hz, 6H, OCH_2CH$_3$), 3.05 ($\nu_{1/2}$= 10.45 Hz, 18H, OCH$_2$CH_3), -4.67($\nu_{1/2}$= 4.10 Hz, 5H, Cp*H*)

Synthesis of Tm(TPP)Klaui (20).

The synthetic procedure was the same as that used for **21** with TmTPP(Cl)(DME) (0.150 g, 1.65x10^{-4} mol) reacting with Na(Klaui) (0.088 g, 1.65x10^{-4} mol) to give 0.133 g of **20** (60.6%). Anal. Calcd for $C_{62}H_{65}CoN_4O_9P_3Tm$: C, 55.95; H, 4.92; N, 4.21. Found: C, 51.92; H, 5.45; N, 3.37. ^{1}H NMR (C_6D_6): 67.59 ($\nu_{1/2}$= 49.68 Hz, 4H, *o*-C_6H_5 TPP), 52.41 ($\nu_{1/2}$= 34.64 Hz, 8H, H-pyrrole), 40.92 ($\nu_{1/2}$= 70.14 Hz, 6H, OCH_2CH$_3$), 35.49 ($\nu_{1/2}$= 74.76 Hz, 6H, OCH_2CH$_3$), 27.22 ($\nu_{1/2}$= 21.01 Hz, 4H, *m*-C_6H_5 TPP), 18.95 ($\nu_{1/2}$= 19.63 Hz, 4H, *p*-C_6H_5 TPP), 14.72 ($\nu_{1/2}$= 21.20 Hz, 5H, Cp*H*) 14.52 ($\nu_{1/2}$= 14.77 Hz, 18H, OCH$_2$CH_3), 11.58 ($\nu_{1/2}$= 23.59 Hz, 4H, *m*-C_6H_5 TPP), -55.78 ($\nu_{1/2}$= 14.47 Hz, 4H, *o*-C_6H_5 TPP)

Synthesis of Er(TPP)Klaui (19).

The synthetic procedure was the same as that used for **21** with ErTPP(Cl)(DME) (0.150 g, 1.65x10^{-1} mmol) reacting with Na(Klaui) (0.088 g, 1.65x10^{-1} mmol) to give 0.155 g of **19** (70 %). Anal. Calcd for $C_{62}H_{65}CoN_4O_9P_3Er$: C, 56.02; H, 4.93; N, 4.21.

Found: C, 56.04; H, 4.84; N, 4.08. ^{1}H NMR (C_6D_6): 46.29 ($\nu_{1/2}$= 82.29 Hz, 4H, *o*-C_6H_5 TPP), 34.74 ($\nu_{1/2}$= 77.14 Hz, 8H, H-pyrrole), 27.39 ($\nu_{1/2}$= 170.34 Hz, 6H, OCH_2CH$_3$), 23.10 ($\nu_{1/2}$= 185.68 Hz, 6H, OCH_2CH$_3$), 20.08 ($\nu_{1/2}$= 22.69 Hz, 4H, *m*-C_6H_5 TPP), 14.73 ($\nu_{1/2}$= 16.91 Hz, 4H, *p*-C_6H_5 TPP), 11.92 ($\nu_{1/2}$= 20.65 Hz, 4H, *m*-C_6H_5 TPP), 10.23 ($\nu_{1/2}$= 52.65 Hz, 5H, Cp*H*), 9.71 ($\nu_{1/2}$= 32.28 Hz, 18H, OCH$_2$CH_3), -34.72 ($\nu_{1/2}$= 21.95 Hz, 4H, *o*-C_6H_5 TPP)

Synthesis of Ho(TPP)Klaui (18).

The synthetic procedure was the same as that used for **21** with HoTPP(Cl)(DME) (0.150 g, 1.65x10^{-1} mmol) reacting with Na(Klaui) (0.088 g, 1.65x10^{-1} mmol) to give 0.146 g of **18**(66%). Anal. Calcd for $C_{62}H_{65}CoN_4O_9P_3Ho$: C, 56.12; H, 4.44; N, 4.22. Found: C, 55.67; H, 4.46; N, 4.65. ^{1}H NMR (C_6D_6): 40.39 ($\nu_{1/2}$= 65.17 Hz, 4H, *o*-C_6H_5 TPP), 6.77 ($\nu_{1/2}$= 90.51 Hz, 5H, Cp*H*), 3.10 ($\nu_{1/2}$= 28.32 Hz, 4H, *m*-C_6H_5 TPP), 0.61 ($\nu_{1/2}$= 16.20 Hz, 4H, *p*-C_6H_5 TPP), -4.63 ($\nu_{1/2}$= 29.23 Hz, 4H, *m*-C_6H_5 TPP), -7.98 ($\nu_{1/2}$= 60.87 Hz, 18H, OCH$_2$CH_3), -17.77 ($\nu_{1/2}$= 478.58 Hz, 12 H, OCH_2CH$_3$), -20.81 ($\nu_{1/2}$= 125.81 Hz, 8H, H-pyrrole), -28.52 ($\nu_{1/2}$= 138.57 Hz, 4H, *o*-C_6H_5 TPP)

Synthesis of YbTPP(η^5-C_5Me_5)(22)

A solution of 0.100 g (7.35x10^{-1} mmol) of pentamethylcyclopentadiene (HC_5Me_5) in 30 ml of DME was combined with potassium hydride(0.026 g, 7.35x10^{-1} mmol). The solution immediately evolved hydrogen gas and turned a golden yellow. After the solution had stirred for ~30 min. **13** (0.661g, 7.35x10^{-1} mmol) was added to the reaction. The solution then stirred for 12 hours, after which time the solvent was removed *in vacuo* to yield a purple residue. The residue was then extracted of toluene (3 x 10 ml) and the combined filtrates were reduced in volume by half and layered with pentane (~50 ml).

Upon sitting overnight, X-ray diffraction quality crystals of the material were deposited on the walls of the reaction tube. Crystals were isolated by filtration in a yield of 64% (0.492, $4.72x10^{-1}$ mmol). ^1H NMR (C_6D_6): 18.22 ($\nu_{1/2}$= 48.78 Hz, 4H, *o*-C_6H_5 TPP) 16.63 ($\nu_{1/2}$= 13.54 Hz, 8H, H-pyrrole), 10.87 ($\nu_{1/2}$= 46.50 Hz, 4H, *m*-C_6H_5 TPP), 9.61 ($\nu_{1/2}$= 6.41 Hz, 7 Hz, 4H, *p*-C_6H_5 TPP), 9.18 ($\nu_{1/2}$= 48.59 Hz, 4H, *m*-C_6H_5 TPP), 8.89 ($\nu_{1/2}$= 60.08 Hz, 4H, *o*-C_6H_5 TPP), 1.84 ($\nu_{1/2}$= 19.51 Hz, 15H, η^5-C_5Me_5)

Synthesis of Lithio N-benzyltetraphenylpoprphyrin (23)

To a solution of **13** (0.100g, $1.10x10^{-1}$ mmol) in toluene was added neat dilithiotetraphenylporphyrin (0.068g, $1.10x10^{-1}$ mmol). The solution was then stirred for 12 hours after which time an off-white precipitate formed. The precipitate was separated from the solution by cannula filtration, the filtrate was condensed, and then layered with pentane. X-ray diffraction quality crystals then formed on the walls of the reaction vessel in a 33% yield(0.0275g, $3.332x10^{-2}$ mmol).

Synthesis of YbPc(Klaui) (24)

To a stirred suspension of the YbPc(Cl)DME (0.500g, $6.16*10^{-1}$ mmol) in 40 ml of THF was added Na(Klaui) (.344 g, $6.16*10^{-1}$ mmol) as a powder.[86] The solid immediately dissolved and the solution turned a dark, electric blue. The reaction mixture was then allowed to stir overnight, after which time the THF was removed *in vacuo*. The residue was then extracted with methylene chloride (3 x 10 ml). The extracts were combined and reduced to half of the initial volume. The solution was then layered with an equal or greater volume of pentane and allowed to stand at room temperature. Crystals then formed after 48 hours. Isolation of the product was achieved by filtration. In subsequent syntheses the pentane/ methylene chloride phases were combined with

stirring and the crystal formation was completed in 12 hours, yielding an analytically pure sample **24** in 56.8% yield(0.434g, $3.49*10^{-1}$ mmol). Anal. Calcd. For $C_{51}H_{50}CoN_8O_9P_3Yb$: C, 48.21; H, 4.21; N, 9.18; Found: C, 47.09; H, 4.49; N, 8.59 Proton NMR, ^1H NMR (C_6D_6): 14.80 ($\nu_{1/2}$= 12.75 Hz, 8H, *H*-Pc), 10.43 ($\nu_{1/2}$= 11.35 Hz, 8H, *H*-Pc), 8.94 ($\nu_{1/2}$= 30.89 Hz, 6H, OC*H*$_2$CH$_3$), 8.53 ($\nu_{1/2}$= 30.41 Hz, 6H, OC*H*$_2$CH$_3$), 4.20 ($\nu_{1/2}$= 12.27 Hz, 18H, OCH$_2$C*H*$_3$), -6.46 (4.97 Hz)(s, 5H, Cp*H*)

ErPc(Klaui) (25)

The procedure used to synthesize this material was identical to that for the previous complex. In this procedure (0.500g, $6.16*10^{-1}$ mmol) of the ErPc(Cl)DME was combined with Na(Klaui) (0.344 g, $6.16*10^{-1}$ mmol) to yield 0.353 g of product ($2.84*10^{-1}$ mmol, 46%) Anal. Calcd. For $C_{51}H_{50}CoN_8O_9P_3Er$: C, 48.43; H, 4.23; N, 9.22; Found: C, 48.63; H, 4.49; N, 9.05; Proton NMR spectrum recorded at 332 K, ^1H NMR (C_6D_6): 31.42 ($\nu_{1/2}$= 64.73 Hz, 8H, *H*-Pc), 29.42 ($\nu_{1/2}$= 148.51 Hz, 6H, OC*H*$_2$CH$_3$), 27.83 ($\nu_{1/2}$= 136.24 Hz, 6H, OC*H*$_2$CH$_3$), 18.68 ($\nu_{1/2}$= 18.68 Hz, 8H, *H*-Pc), 16.15 ($\nu_{1/2}$= 59.78 Hz, 18H, OCH$_2$C*H*$_3$), -41.67 ($\nu_{1/2}$= 148.03 Hz, 5H, Cp*H*)

Xray Diffraction Experimental

Data collection, structure solutions and refinements were performed by or under the direction of Dr. Khalil A Abboud.

Compound 2

Data were collected at 173 K on a Siemens SMART PLATFORM equipped with A CCD area detector and a graphite monochromator utilizing MoK_α radiation (λ = 0.71073 Å). Cell parameters were refined using up to 8192 reflections. A hemisphere of data (1381 frames) was collected using the ω-scan method (0.3° frame width). The first

50 frames were remeasured at the end of data collection to monitor instrument and crystal stability (maximum correction on I was < 1 %). Absorption corrections by integration were applied based on measured indexed crystal faces.

The structure was solved by the Direct Methods in *SHELXTL5,* and refined using full-matrix least squares. The non-H atoms were treated anisotropically, whereas the methyl hydrogen atoms were calculated in ideal positions and were riding on their respective carbon atoms. The asymmetric unit consisted of the molecule of interest and one triflate ion. A total of 429 parameters were refined in the final cycle of refinement using 5407 reflections with $I > 2\sigma(I)$ to yield R_1 and wR_2 of 10.25% and 19.63%, respectively. Refinement was done using F^2.

Compound 8

Data were collected at 173 K on a Siemens SMART PLATFORM equipped with A CCD area detector and a graphite monochromator utilizing MoKα radiation (λ = 0.71073 Å). Cell parameters were refined using up to 7162 reflections. A hemisphere of data (1381 frames) was collected using the ω-scan method (0.3° frame width). The first 50 frames were remeasured at the end of data collection to monitor instrument and crystal stability (maximum correction on I was < 1 %). Absorption corrections by integration were applied based on measured indexed crystal faces.

The structure was solved by the Direct Methods in *SHELXTL5,* and refined using full-matrix least squares. The non-H atoms were treated anisotropically, whereas the hydrogen atoms were calculated in ideal positions and were riding on their respective carbon atoms. One of the CH2 units of the O1 THF ligand is disordered and was refined in two parts. Their site occupation factors were dependently refined to 0.71(1) for the

major parts (C38) and consequently 0.29 for the minor part (C38'). A total of 709 parameters were refined in the final cycle of refinement using 6700 reflections with $I > 2\sigma(I)$ to yield R_1 and wR_2 of 4.21% and 11.06%, respectively. Refinement was done using F^2.

Compound 9

Data were collected at 173 K on a Siemens SMART PLATFORM equipped with A CCD area detector and a graphite monochromator utilizing MoK_α radiation (λ = 0.71073 Å). Cell parameters were refined using 4431 reflections. A hemisphere of data (1381 frames) was collected using the ω-scan method (0.3° frame width). The first 50 frames were remeasured at the end of data collection to monitor instrument and crystal stability (maximum correction on I was < 1 %). Absorption corrections by integration were applied based on measured indexed crystal faces.

The structure was solved by the Direct Methods in *SHELXTL5,* and refined using full-matrix least squares. The non-H atoms were treated anisotropically, whereas the hydrogen atoms were calculated in ideal positions and were riding on their respective carbon atoms. A total of 503 parameters were refined in the final cycle of refinement using 7169 reflections with $I > 2\sigma(I)$ to yield R_1 and wR_2 of 4.12% and 7.98%, respectively. Refinement was done using F^2.

Compound 10

Data were collected at 173 K on a Siemens SMART PLATFORM equipped with A CCD area detector and a graphite monochromator utilizing MoK_α radiation (λ = 0.71073 Å). Cell parameters were refined using 4431 reflections. A hemisphere of data (1381 frames) was collected using the ω-scan method (0.3° frame width). The first 50

frames were remeasured at the end of data collection to monitor instrument and crystal stability (maximum correction on I was < 1 %). Absorption corrections by integration were applied based on measured indexed crystal faces.

The structure was solved by the Direct Methods in *SHELXTL5,* and refined using full-matrix least squares. The non-H atoms were treated anisotropically, whereas the hydrogen atoms were calculated in ideal positions and were riding on their respective carbon atoms. A total of 503 parameters were refined in the final cycle of refinement using 7169 reflections with $I > 2\sigma(I)$ to yield R_1 and wR_2 of 4.12% and 7.98%, respectively. Refinement was done using F^2.

Compound 13

Data were collected at 173 K on a Siemens SMART PLATFORM equipped with A CCD area detector and a graphite monochromator utilizing Mo$K\alpha$ radiation (λ = 0.71073 Å). Cell parameters were refined using up to 8192 reflections. A full sphere of data (1850 frames) was collected using the ω-scan method (0.3° frame width). The first 50 frames were remeasured at the end of data collection to monitor instrument and crystal stability (maximum correction on I was < 1 %). Absorption corrections by integration were applied based on measured indexed crystal faces.

The structure was solved by the Direct Methods in *SHELXTL5,* and refined using full-matrix least squares. The non-H atoms were treated anisotropically, whereas the hydrogen atoms were calculated in ideal positions and were riding on their respective carbon atoms. A total of 507 parameters were refined in the final cycle of refinement using 6742 reflections with $I > 2\sigma(I)$ to yield R_1 and wR_2 of 3.32% and 6.37%, respectively. Refinement was done using F^2.

Compound **16** Data were collected at 173 K on a Siemens SMART PLATFORM equipped with A CCD area detector and a graphite monochromator utilizing $MoK\alpha$ radiation ($\lambda = 0.71073$ Å). Cell parameters were refined using up to 8192 reflections. A full sphere of data (1381 frames) was collected using the ω-scan method (0.3° frame width). The first 50 frames were remeasured at the end of data collection to monitor instrument and crystal stability (maximum correction on I was < 1 %). Absorption corrections by integration were applied based on measured indexed crystal faces.

The structure was solved by the Direct Methods in *SHELXTL5,* and refined using full-matrix least squares. The non-H atoms were treated anisotropically, whereas the hydrogen atoms were calculated in ideal positions and were riding on their respective carbon atoms; except the Boron H atom, which was obtained from a Difference Fourier map and refined freely. The asymmetric unit consists of the Tm complex and two chloroform molecules of crystallization. A total of 663 parameters were refined in the final cycle of refinement using 10920 reflections with $I > 2\sigma(I)$ to yield R_1 and wR_2 of 3.40% and 7.28%, respectively. Refinement was done using F^2.

Compound 17

Data were collected at 173 K on a Siemens SMART PLATFORM equipped with A CCD area detector and a graphite monochromator utilizing $MoK\alpha$ radiation ($\lambda = 0.71073$ Å). Cell parameters were refined using up to 8192 reflections. A full sphere of data (1381 frames) was collected using the ω-scan method (0.3° frame width). The first 50 frames were remeasured at the end of data collection to monitor instrument and crystal stability (maximum correction on I was < 1 %). Absorption corrections by integration were applied based on measured indexed crystal faces.

The structure was solved by the Direct Methods in *SHELXTL5,* and refined using full-matrix least squares. The non-H atoms were treated anisotropically, whereas the hydrogen atoms were calculated in ideal positions and were riding on their respective carbon atoms. The asymmetric unit consists of the complex and four benzene molecules. Two of the solvent molecules were disordered in their respective planes and each was refined in two parts. The site occupation factors of the minor and major parts in each disordered molecule were dependently refined to 0.54(2) and 0.53(1) for the C80 and the C90 benzene molecules major parts, respectively. The disordered molecules were restrained to maintain equivalent geometries throughout the refinement and their C atoms were refined with isotropic thermal parameters. A total of 797 parameters were refined in the final cycle of refinement using 12598 reflections with $I > 2\sigma(I)$ to yield R_1 and wR_2 of 2.69% and 6.50%, respectively. Refinement was done using F^2.

Compound 22

Data were collected at 173 K on a Siemens SMART PLATFORM equipped with A CCD area detector and a graphite monochromator utilizing MoK_α radiation (λ = 0.71073 Å). Cell parameters were refined using up to 8192 reflections. A full sphere of data (1381 frames) was collected using the ω-scan method (0.3° frame width). The first 50 frames were remeasured at the end of data collection to monitor instrument and crystal stability (maximum correction on I was < 1 %). Absorption corrections by integration were applied based on measured indexed crystal faces.

The structure was solved by the Direct Methods in *SHELXTL5,* and refined using full-matrix least squares. The non-H atoms were treated anisotropically, whereas the methyl hydrogen atoms were calculated in ideal positions and were riding on their

respective carbon atoms. The asymmetric unit contains one Yb complex and one toluene solvent molecule. A total of 601 parameters were refined in the final cycle of refinement using 8380 reflections with $I > 2\sigma(I)$ to yield R_1 and wR_2 of 2.33% and 5.28%, respectively. Refinement was done using F^2.

Compound 24

Data were collected at 173 K on a Siemens SMART PLATFORM equipped with A CCD area detector and a graphite monochromator utilizing $MoK\alpha$ radiation (λ = 0.71073 Å). Cell parameters were refined using up to 8192 reflections. A full sphere of data (1381 frames) was collected using the ω-scan method (0.3° frame width). The first 50 frames were remeasured at the end of data collection to monitor instrument and crystal stability (maximum correction on I was < 1 %). Absorption corrections by integration were applied based on measured indexed crystal faces.

The structure was solved by the Direct Methods in *SHELXTL5,* and refined using full-matrix least squares. The non-H atoms were treated anisotropically, whereas the methyl hydrogen atoms were calculated in ideal positions and were riding on their respective carbon atoms. Atoms C35 and C36 were disordered over two positions C35' and C36'. The site occupation factor refined to 0.48 (0.02). A total of 666 parameters were refined in the final cycle of refinement using 10008 reflections with $I > 2\sigma(I)$ to yield R_1 and wR_2 of 2.45% and 6.19%, respectively. Refinement was done using F^2.

Compound 25

Data were collected at 173 K on a Siemens SMART PLATFORM equipped with A CCD area detector and a graphite monochromator utilizing $MoK\alpha$ radiation (λ =

0.71073 Å). Cell parameters were refined using up to 8192 reflections. A full sphere of data (1381 frames) was collected using the ω-scan method (0.3° frame width). The first 50 frames were remeasured at the end of data collection to monitor instrument and crystal stability (maximum correction on I was < 1 %). Absorption corrections by integration were applied based on measured indexed crystal faces.

The structure was solved by the Direct Methods in *SHELXTL6,* and refined using full-matrix least squares. The non-H atoms were treated anisotropically, whereas the hydrogen atoms were calculated in ideal positions and were riding on their respective carbon atoms. Five of the six ethoxy groups were found to be disordered and each was refined in two parts. Their site occupation factors were dependently refined to 0.52(2), 0.54(4), 0.52(3), 0.56(3) and 0.64(1) for the major part of the O5-O9 ethyl groups. Atoms of the disordered species were refined with isotropic thermal paramteres. A total of 637 parameters were refined in the final cycle of refinement using 9437 reflections with $I > 2\sigma(I)$ to yield R_1 and wR_2 of 2.56% and 6.39%, respectively. Refinement was done using F^2.

APPENDIX
CRYSTALLOGRAPHIC INFORMATION

Table A-1. Information for the crystal structure of **2**

University of Florida Chemistry department identification code	tjf9
Temperature	173(2) K
Wavelength	0.71073 Å
Crystal system	Monoclinic
Space group	P2(1)/n
Unit cell dimensions	
	a = 8.577(1) Å α= 90°.
	b = 41.086(5) Å β= 104.298(2)°.
	c = 11.582(2) Å γ = 90°.
Volume	3954.9(9) $Å^3$
Z	4
Density (calculated)	1.594 Mg/m^3
Absorption coefficient	0.852 mm^{-1}
F(000)	1928
Crystal size	0.42 x 0.19 x 0.12 mm^3
Theta range for data collection	2.50 to 25.00°.
Index ranges	-10≤h≤10, -48≤k≤40, -13≤l≤12
Reflections collected	21514
Independent reflections	6846 [R(int) = 0.0687]
Completeness to theta =	25.00° 98.5 %
Absorption correction	None
Refinement method	Full-matrix least-squares on F^2
Data / restraints / parameters	6846 / 37 / 557
Goodness-of-fit on F^2	1.158
Final R indices [I>2sigma(I)]	R1 = 0.0665, wR2 = 0.1614 [5981]
R indices (all data)	R1 = 0.0748, wR2 = 0.1662
Largest diff. peak and hole	0.813 and -0.976 $e.Å^{-3}$

$R1 = \Sigma(||F_o| - |F_c||) / \Sigma|F_o|$

$wR2 = [\Sigma[w(F_o^2 - F_c^2)^2] / \Sigma[w(F_o^2)^2]]^{1/2}$

$S = [\Sigma[w(F_o^2 - F_c^2)^2] / (n-p)]^{1/2}$

$w = 1/[\sigma^2(F_o^2)+(0.0370*p)^2+0.31*p]$,

$p = [\max(F_o^2,0)+ 2* F_c^2]/3$

Table A-2 Atomic coordinates (x 10^4) and equivalent isotropic displacement parameters ($Å^2$x 10^3) for **2**. U(eq) is defined as one third of the trace of the orthogonalized U^{ij} tensor.

	x	y	z	U(eq)
Ru	1062(1)	1237(1)	7152(1)	34(1)
S1	2393(2)	51(1)	3992(1)	40(1)
O1	3337(5)	-330(1)	7149(4)	46(1)
O2	4632(5)	-717(1)	5499(4)	47(1)
O3	-3955(11)	2455(2)	6810(7)	84(2)
O4	-5271(8)	2799(1)	8535(7)	69(2)
C1	3478(7)	-301(2	4072(5)	41(1)
C2	3812(7)	-437(1)	5184(5)	39(1)
C3	3156(7)	-246(1)	5980(5)	37(1)
C4	2346(7)	27(1)	5481(5)	35(1)
C5	1577(6)	268(1)	6050(5)	34(1)
C6	925(7)	545(1)	5575(5)	38(1)
C7	100(20)	780(3)	6157(13)	34(4)
C8	-614(14)	1064(2)	5531(11)	43(3)
C9	-1415(10)	1297(2)	6076(10)	46(2)
C10	-1517(8)	1264(2)	7269(9)	39(2)
C11	-790(9)	979(2)	7901(8)	36(2)
C12	-3(15)	749(3)	7360(9)	33(2)
C13	-2244(8)	1502(2)	7920(7)	44(2)
C14	-2813(9)	1786(2)	7531(8)	51(2)
C15	-3514(9)	2019(2)	8217(9)	50(2)
C16	-4042(10)	2321(2)	7856(8)	55(2)
C17	-4670(17)	2494(2)	8690(13)	59(4)
C18	-4706(9)	2318(2)	9699(8)	46(2)
S2	-3853(3)	1941(1)	9607(3)	51(1)
C19	4567(8)	-581(2)	7519(6)	47(2)
C20	4405(8)	-842(2)	6605(6)	51(2)
C21	-4870(20)	2758(3)	6501(13)	119(7)
C22	-4632(16)	2954(3)	7612(10)	96(4)
C23	3128(6)	1326(1)	8630(5)	35(1)
C24	2313(7)	1627(1)	8279(5)	38(1)
C25	2351(7)	1690(2)	7075(6)	46(2)
C26	3194(7)	1430(2)	6681(5)	43(1)
C27	3669(6)	1202(1)	7629(5)	37(1)
C28	3435(8)	1175(2)	9838(6)	46(1)
C29	1586(8)	1841(2)	9056(7)	54(2)
C30	1699(11)	1993(2)	6399(8)	75(2)
C31	3562(10)	1407(2)	5484(6)	64(2)
C32	4660(8)	899(2)	7635(6)	49(2)

Table A-2. Continued

	x	y	z	U(eq)
O3'	-3200(70)	2344(15)	7140(50)	88(19)
O4'	-5350(80)	2752(15)	7890(50)	90(20)
C7'	-20(160)	800(20)	5970(60)	30(40)
C8'	-680(100)	1069(14)	5220(40)	30(20)
C9'	-1330(70)	1344(10)	5700(40)	22(14)
C10'	-1540(80)	1344(11)	6860(50)	40(19)
C11'	-980(50)	1066(10)	7590(30)	4(10)
C12'	-260(110)	803(13)	7150(50)	30(20)
C13'	-2290(40)	1635(9)	7180(30)	12(8)
C14'	-2790(40)	1656(8)	8270(30)	10(8)
C15'	-3610(40)	1940(7)	8730(30)	5(7)
C16'	-4190(90)	2221(11)	8180(40)	60(20)
C17'	-4760(90)	2444(9)	8900(50)	16(14)
C18'	-5240(170)	2280(20)	9810(90)	300(140)
S2'	-4150(20)	1920(4)	10065(19)	53(5)
C21'	-4440(90)	2436(17)	6080(60)	80(30)
C22'	-4750(100)	2714(17)	6820(60)	51(19)
O10	-5630(30)	2365(6)	3040(20)	70(6)
S3	8834(2)	1172(1)	1401(1)	45(1)
C33	10371(8)	871(2)	1983(6)	49(2)
F1	9777(5)	631(1)	2532(4)	65(1)
F2	11598(6)	997(1)	2766(5)	92(2)
F3	10919(6)	737(1)	1122(4)	75(1)
O11	7620(6)	986(1)	586(5)	68(1)
O12	9671(7)	1406(1)	843(5)	64(1)
O13	8407(8)	1286(1)	2443(5)	71(2)
C34	2346(11)	-155(2)	9647(6)	62(2)
Cl1	1900(3)	-200(1)	11026(2)	77(1)
Cl2	3108(3)	233(1)	9481(2)	68(1)
C35	-3789(14)	1877(4)	3100(10)	89(4)
Cl3	-5506(4)	1788(1)	2274(3)	106(1)
Cl4	-3757(5)	2128(1)	4372(3)	90(1)

Table A-3. Crystal data and structure refinement for **8**.

University of Florida Chemistry department identification code	tf12
Empirical formula	C44 H46 N3 O2 Yb
Formula weight	821.88
Temperature	173(2) K
Wavelength	0.71073 Å
Crystal system	Monoclinic
Space group	P2(1)/n
Unit cell dimensions	
	a = 12.0306(5) Å α= 90°.
	b = 19.0747(8) Å β= 91.997(1)°.
	c = 16.3710(7) Å γ = 90°.
Volume	3754.5(3) $Å^3$
Z 4	
Density (calculated)	1.454 Mg/m^3
Absorption coefficient	2.531 mm^{-1}
F(000)	1668
Crystal size	0.32 x 0.13 x 0.06 mm^3
Theta range for data collection	2.00 to 27.50°.
Index ranges	-15≤h≤15, -21≤k≤24, -17≤l≤21
Reflections collected	25040
Independent reflections	8589 [R(int) = 0.0483]
Completeness to theta = 27.50°	99.6 %
Absorption correction	Integration
Refinement method	Full-matrix least-squares on F^2
Data / restraints / parameters	8589 / 0 / 457
Goodness-of-fit on F^2 1.047	
Final R indices [I>2sigma(I)]	R1 = 0.0289, wR2 = 0.0691 [6700]
R indices (all data)	R1 = 0.0454, wR2 = 0.0792
Extinction coefficient	0.00026(8)
Largest diff. peak and hole	0.553 and -0.652 e.$Å^{-3}$

$R1 = \Sigma(||F_o| - |F_c||) / \Sigma|F_o|$

$wR2 = [\Sigma[w(F_o^2 - F_c^2)^2] / \Sigma[w(F_o^2)^2]]^{1/2}$

$S = [\Sigma[w(F_o^2 - F_c^2)^2] / (n-p)]^{1/2} w = 1/[\sigma^2(F_o^2)+(0.0370*p)^2+0.31*p],$

$p = [\max(F_o^2,0)+ 2* F_c^2]/3$

Table A-4. Atomic coordinates (x 10^4) and equivalent isotropic displacement parameters ($Å^2$x 10^3) for **8**. U(eq) is defined as one third of the trace of the orthogonalized U_{ij} tensor.

	x	y	z	U(eq)
Yb	4689(1)	2240(1)	3672(1)	27(1)
N1	2858(2)	2128(1)	3394(2)	33(1)
N2	5860(2)	1559(2)	4396(2)	34(1)
N3	5563(2)	3166(2)	3189(2)	37(1)
C1	2450(3)	1470(2)	3095(2)	34(1)
C2	2122(3)	1389(2)	2278(2)	39(1)
C3	1770(3)	746(2)	1978(2)	47(1)
C4	1723(3)	169(2)	2480(3)	48(1)
C5	2025(3)	240(2)	3290(3)	52(1)
C6	2381(3)	885(2)	3601(2)	43(1)
C7	2039(3)	2622(2)	3548(2)	33(1)
C8	2340(3)	3333(2)	3650(2)	40(1)
C9	1574(4)	3831(2)	3857(2)	48(1)
C10	472(4)	3654(2)	3967(2)	52(1)
C11	164(3)	2963(2)	3870(3)	49(1)
C12	929(3)	2456(2)	3655(2)	37(1)
C13	6884(3)	1285(2)	4180(2)	38(1)
C14	7400(3)	722(2)	4601(3)	46(1)
C15	8391(4)	440(2)	4341(3)	62(1)
C16	8889(4)	696(3)	655(3)	75(2)
C17	8405(3)	1244(3)	3248(3)	67(1)
C18	7413(3)	1546(2)	3497(2)	50(1)
C19	5510(3)	1382(2)	5189(2)	33(1)
C20	4666(3)	899(2)	5299(2)	39(1)
C21	4256(3)	774(2)	6065(2)	47(1)
C22	4683(4)	1129(2)	6739(2)	53(1)
C23	5536(3)	1602(2)	6652(2)	51(1)
C24	5943(3)	1728(2)	5882(2)	39(1)
C25	6330(3)	3576(2)	3649(2)	39(1)
C26	6425(3)	4296(2)	3539(3)	56(1)
C27	7119(4)	4692(3)	4042(4)	73(2)
C28	7735(4)	4394(3)	4674(3)	66(1)
C29	7662(3)	3688(3)	4780(3)	57(1)
C30	6985(3)	3278(2)	4277(2)	46(1)
C31	5408(3)	3328(2)	2353(2)	34(1)
C32	6315(3)	3468(2)	1861(3)	45(1)
C33	6164(4)	3569(2)	1033(3)	56(1)
C34	5116(4)	3527(2)	663(3)	56(1)
C35	4219(3)	3394(2)	1136(2)	49(1)
C36	4363(3)	3302(2)	1972(2)	40(1)

Table A-4. Continued

	x	y	z	U(eq)
O1	4967(2)	1475(1)	2598(1)	34(1)
C37	5053(3)	713(2)	2704(2)	43(1)
C38	4896(14)	431(7)	1860(8)	39(4)
C38'	5678(7)	472(3)	2005(4)	52(2)
C39	5250(4)	943(2)	1314(3)	62(1)
C40	5023(3)	1633(2)	1730(2)	45(1)
O2	4167(2)	2802(1)	4861(2)	36(1)
C41	3303(3)	2531(2)	5385(2)	40(1)
C42	3158(4)	3080(3)	6026(3)	77(2)
C43	4221(4)	3463(3)	6065(3)	66(1)
C44	4559(4)	3466(2)	5209(3)	64(1)

Table A-5. Crystal data and structure refinement for **9**

University of Florida Chemistry department identification code	tf11
Empirical formula	C44 H46 Er N3 O2
Formula weight	816.10
Temperature	173(2) K
Wavelength	0.71073 Å
Crystal system	Monoclinic
Space group	P2(1)/c
Unit cell dimensions	
	a = 15.3535(7) Å α= 90°.
	b = 12.5832(5) Å β= 107.086(1)°.
	c = 20.3459(9) Å γ = 90°.
Volume	3757.3(3) Å^3
Z	4
Density (calculated)	1.443 Mg/m^3
Absorption coefficient	2.274 mm^{-1}
F(000)	1660
Crystal size	0.21 x 0.17 x 0.11 mm^3
Theta range for data collection	1.93 to 27.50°.
Index ranges	-16≤h≤19, -14≤k≤16, -26≤l≤26
Reflections collected	26202
Independent reflections	8574 [R(int) = 0.0752]
Completeness to theta = 27.50°	99.4 %
Absorption correction	Integration
Max. and min. transmission	0.8113 and 0.6510
Refinement method	Full-matrix least-squares on F^2
Data / restraints / parameters	8574 / 0 / 451

Table A-5. Continued

Goodness-of-fit on F^2	1.039
Final R indices [I>2sigma(I)]	R1 = 0.0328, wR2 = 0.0841 [7666]
R indices (all data)	R1 = 0.0370, wR2 = 0.0881
Largest diff. peak and hole	0.776 and -1.832 e.Å^{-3}

$R1 = \sum(||F_o| - |F_c||) / \sum|F_o|$

$wR2 = [\sum[w(F_o^2 - F_c^2)^2] / \sum[w(F_o^2)^2]]^{1/2}$

$S = [\sum[w(F_o^2 - F_c^2)^2] / (n-p)]^{1/2}$

$w = 1/[\sigma^2(F_o^2)+(0.0370*p)^2+0.31*p]$,

$p = [\max(F_o^2,0)+ 2* F_c^2]/3$

Table A-6. Atomic coordinates (x 10^4) and equivalent isotropic displacement parameters ($Å^2$x 10^3) for **9**. U(eq) is defined as one third of the trace of the orthogonalized U^{ij} tensor.

	x	y	z	U(eq)
Er	2527(1)	2975(1)	6226(1)	19(1)
N1	3091(2)	2085(2)	7223(1)	25(1)
C1	2855(2)	998(2)	7234(1)	24(1)
C2	1965(2)	675(3)	7172(2)	31(1)
C3	1738(2)	-396(3	7147(2)	43(1)
C4	2403(3)	-1160(3)	7195(2)	47(1)
C5	3286(2)	-862(3)	7263(2)	40(1)
C6	3508(2)	204(2)	7277(2)	30(1)
C7	3622(2)	2516(2)	7837(1)	25(1)
C8	3755(2)	2025(2)	8484(2)	30(1)
C9	4245(2)	2523(4)	9085(2)	40(1)
C10	4635(2)	3513(3)	9075(2)	44(1)
C11	4540(2)	3999(3)	8450(2)	37(1)
C12	4053(2)	3510(3)	7838(2)	31(1)
N2	3701(1)	3760(2)	5992(1)	25(1)
C13	4604(2)	3419(2)	6064(1)	27(1)
C14	4943(2)	2513(3)	6446(2)	33(1)
C15	5791(2)	2106(3)	6475(2)	42(1)
C16	6328(2)	2599(3)	6124(2)	43(1)
C17	6015(2)	3525(3)	5763(2)	44(1)
C18	5165(2)	3941(3)	5736(2)	35(1)
C19	3506(2)	4855(2)	5927(1)	23(1)
C20	4098(2)	5626(3)	6316(2)	30(1)
C21	3844(2)	6682(3)	6295(2)	36(1)
C22	2988(2)	7013(2)	5878(2)	37(1)
C23	2404(2)	6258(3)	5488(2)	32(1)
C24	2655(2)	5202(2)	5505(1)	26(1)
N3	1108(2)	2989(2)	5459(1)	25(1)
C25	362(2)	3104(2)	5742(1)	23(1)
C26	-17(2)	2221(3)	5971(2)	31(1)
C27	-706(2)	2358(3)	6282(2)	37(1)
C28	-1029(2)	3358(3)	6364(2)	40(1)
C29	-666(2)	4229(3)	6128(2)	36(1)
C30	21(2)	4099(2)	5820(2)	29(1)
C31	888(2)	2926(2)	4752(2)	23(1)
C32	-8(2)	2820(2)	4311(2)	29(1)
C33	-180(2)	2776(3)	3603(2)	37(1)
C34	509(2)	2837(3)	3295(2)	38(1)
C35	1399(2)	2930(2)	3723(2)	30(1)
C36	1592(2)	2973(2)	4430(2)	25(1)

Table A-6. Continued

	x	y	z	U(eq)
O1	2050(1)	4188(2)	6927(1)	23(1)
C37	2206(2)	5323(2)	7029(2)	33(1)
C38	2039(2)	5555(3)	7716(2)	35(1)
C39	1277(2)	4782(2)	7710(2)	31(1)
C40	1572(2)	3791(2)	7407(2)	27(1)
O2	2648(1)	1380(2)	5636(1)	29(1)
C41	3374(2)	1043(3)	5357(2)	49(1)
C42	3057(8)	64(12)	4956(8)	56(3)
C42'	2878(4)	425(6)	4702(4)	37(2)
C43	2036(3)	33(4)	4839(2)	70(1)
C44	1961(2)	553(3)	5468(2)	43(1)

Table A-7. Crystal data and structure refinement for **10**

University of Florida Chemistry department identification code	tf21
Empirical formula	C48 H38 Cl Ho N4 O2
Formula weight	903.20
Temperature	193(2) K
Wavelength	0.71073 Å
Crystal system	Monoclinic
Space group	Cc
Unit cell dimensions	
	a = 12.1257(8) Å α= 90°.
	b = 24.960(2) Å β= 109.943(1)°.
	c = 14.1532(9) Å γ = 90°.
Volume	4026.7(5) $Å^3$
Z	4
Density (calculated)	1.490 Mg/m^3
Absorption coefficient	2.076 mm^{-1}
F(000)	1816
Crystal size	0.40 x 0.07 x 0.02 mm^3
Theta range for data collection	1.96 to 27.50°.
Index ranges -	$15\leq h\leq 15$, $-32\leq k\leq 32$, $-18\leq l\leq 18$
Reflections collected	17767
Independent reflections	8772 [R(int) = 0.0551]
Completeness to theta = 27.50°	99.4 %
Absorption correction	Integration
Max. and min. transmission	0.9590 and 0.7135
Refinement method	Full-matrix least-squares on F^2
Data / restraints / parameters	8772 / 2 / 503
Goodness-of-fit on F^2	1.065
Final R indices [I>2sigma(I)]	R1 = 0.0412, wR2 = 0.0798 [7169]
R indices (all data)	R1 = 0.0622, wR2 = 0.0898
Absolute structure parameter	-0.004(11)
Largest diff. peak and hole	1.072 and -0.697 $e.Å^{-3}$

$R1 = \Sigma(||F_o| - |F_c||) / \Sigma|F_o|$

$wR2 = [\Sigma[w(F_o^2 - F_c^2)^2] / \Sigma[w(F_o^2)^2]]^{1/2}$

$S = [\Sigma[w(F_o^2 - F_c^2)^2] / (n-p)]^{1/2}$

$w= 1/[\sigma^2(F_o^2)+(0.0370*p)^2+0.31*p]$,

$p = [\max(F_o^2,0)+ 2* F_c^2]/3$

Table A-8. Atomic coordinates (x 10^4) and equivalent isotropic displacement parameters ($Å^2$x 10^3) for **10**. U(eq) is defined as one third of the trace of the orthogonalized U^{ij} tensor.

	x	y	z	U(eq)
Ho	18(1)	446(1)	2514(1)	28(1)
N1	-1725(4)	451(2)	1138(4)	30(1)
N2	431(6)	1073(2)	1434(5)	32(1)
N3	1840(5)	177(2)	2415(4)	29(1)
N4	-281(4)-	466(2)	2014(4)	31(1)
C1	-2621(6)	83(3)	976(5)	32(2)
C2	-3701(6)	314(3)	363(5)	41(2)
C3	-3463(6)	817(3)	134(5)	37(2)
C4	-2229(6)	901(3)	607(5)	32(1)
C5	-1621(6)	1350(3)	454(5)	33(2)
C6	-402(6)	1424(3)	818(5)	33(2)
C7	216(7)	1856(3)	546(6)	43(2)
C8	1377(6)	1782(3)	996(5)	38(2)
C9	1515(6)	1289(3)	1558(5)	34(2)
C10	2586(6)	1059(3)	2085(5)	33(2)
C11	2740(6)	527(3)	2486(5)	34(2)
C12	3853(6)	263(3)	2983(5)	39(2)
C13	3620(6)	-240(3)	3160(5)	35(2)
C14	2367(6)	-303(2)	2791(5)	32(2)
C15	1769(6)	-790(3)	2770(5)	33(2)
C16	532(6)	-862(3)	2376(5)	31(2)
C17	-37(11)-	1377(3)	2289(7)	48(3)
C18	-1175(7)	-1286(3)	1908(6)	43(2)
C19	-1359(6)	-712(3)	1710(5)	34(2)
C20	-2448(6)	-465(3)	1268(4)	33(1)
C21	-2321(6)	1782(3)	-243(5)	36(2)
C22	-2619(7)	2242(3)	114(6)	50(2)
C23	-3255(7)	2637(3)	-545(7)	55(2)
C24	-3600(7)	2550(3)	-1561(6)	51(2)
C25	-3308(7)	2093(3)	-1929(6)	53(2)
C26	-2663(7)	1702(3)	-1272(6)	50(2)
C27	3671(6)	1377(3)	2213(5)	35(2)
C28	4567(7)	1196(3)	1882(6)	50(2)
C29	5584(8)	1508(4)	2044(7)	65(3)
C30	5685(10)	1993(5)	2525(8)	69(3)
C31	4790(9)	2182(3)	2849(7)	54(3)
C32	3812(7)	1876(3)	2684(6)	41(2)
C33	2484(6)	-1284(3)	3166(5)	35(2)
C34	2763(7)	-1638(3)	2533(6)	45(2)
C35	3400(7)	-2085(3)	2905(6)	49(2)

Table A-8. Continued

	x	y	z	U(eq)
C36	3755(7)	-2207(3)	3908(7)	50(2)
C37	3499(9)	-1863(4)	4539(6)	64(3)
C38	2874(9)	-1396(3)	4168(6)	61(3)
C39	-3532(6)	-796(3)	1070(5)	36(2)
C40	-4276(7)	-703(3)	1590(6)	52(2)
C41	-5278(8)	-1006(4)	1414(8)	74(3)
C42	-5530(7)	-1405(4)	726(8)	64(3)
C43	-4825(8)	-1498(4)	200(6)	61(2)
C44	-3819(8)	-1194(3)	355(6)	55(2)
C1	-258(3)	1296(1)	3476(2)	73(1)
O1	-1322(5)	113(2)	3364(4)	48(1)
O2	1093(5)	145(2)	4238(4)	55(2)
C45	-634(9)-	224(4)	4209(8)	72(3)
C46	380(7) 5(4)	5000(11)	95(5)	
C47	-2261(9)	395(4) 3526(8)	77(3)	
C48	2125(9)	398(6) 4855(7)	99(4)	

Symmetry transformations used to generate equivalent atoms:

Table A-9. Crystal data and structure refinement for **13**

University of Florida Chemistry department identification code	tf17
Empirical formula	C48 H38 Cl N4 O2 Yb
Formula weight	911.31
Temperature	193(2) K
Wavelength	0.71073 Å
Crystal system	Monoclinic
Space group	P2(1)/c
Unit cell dimensions	
	a = 12.5879(5) Å α= 90°.
	b = 24.955(1) Å β= 114.640(1)°.
	c = 14.0773(6) Å γ = 90°.
Volume	4019.5(3) $Å^3$
Z	4
Density (calculated)	1.506 Mg/m^3
Absorption coefficient	2.438 mm^{-1}
F(000)	1828
Crystal size	0.04 x 0.04 x 0.15 mm^3
Theta range for data collection	1.78 to 27.50°.
Index ranges	$-16\leq h\leq 16$, $-32\leq k\leq 32$, $-18\leq l\leq 18$
Reflections collected	35855
Independent reflections	9210 [R(int) = 0.0641]
Completeness to theta = 27.50°	99.6 %
Absorption correction	Integration
Max. and min. transmission	0.9085 and 0.7664
Refinement method	Full-matrix least-squares on F^2
Data / restraints / parameters	9210 / 0 / 507
Table A-9. Continued	
Goodness-of-fit on F^2	1.030
Final R indices [I>2sigma(I)]	R1 = 0.0332, wR2 = 0.0637 [6742]
R indices (all data)	R1 = 0.0599, wR2 = 0.0722
Largest diff. peak and hole	0.574 and -0.711 $e.Å^{-3}$

$R1 = \sum(||F_o| - |F_c||) / \sum|F_o|$

$wR2 = [\sum[w(F_o^2 - F_c^2)^2] / \sum[w(F_o^2)^2]]^{1/2}$

$S = [\sum[w(F_o^2 - F_c^2)^2] / (n-p)]^{1/2}$

$w= 1/[\sigma^2(F_o^2)+(0.0278*p)^2+0.27*p]$,

$p = [\max(F_o^2,0)+ 2* F_c^2]/3$

Table A-10. Atomic coordinates (x 10^4) and equivalent isotropic displacement parameters ($Å^2$x 10^3) for **13**. U(eq) is defined as one third of the trace of the orthogonalized U^{ij} tensor.

	x	y	z	U(eq)
Yb	2370(1)	2070(1)	6360(1)	22(1)
Cl	3185(1)	1290(1)	7701(1)	38(1)
O1	1143(2)	2167(1)	7307(2)	37(1)
O2	3325(2)	2580(1)	7930(2)	32(1)
N1	519(3)	1984(1)	4990(2)	24(1)
N2	2681(3)	1442(1)	5294(2)	24(1)
N3	3993(3)	2396(1)	6178(2)	23(1)
N4	1835(3)	2954(1)	5817(2)	26(1)
C1	-411(3)	2319(2)	4856(3)	26(1)
C2	-1485(3)	2046(2)	4254(3)	35(1)
C3	-1219(3)	1568(2)	3965(3)	32(1)
C4	40(3)	1523(2)	4429(3)	25(1)
C5	681(3)	1092(2)	4290(3)	26(1)
C6	1902(3)	1058(2)	4692(3)	27(1)
C7	2534(4)	608(2)	4542(3)	34(1)
C8	3682(4)	724(2)	5019(3)	35(1)
C9	3782(3)	1247(2)	5485(3)	26(1)
C10	4839(3)	1532(2)	5983(3)	24(1)
C11	4924(3)	2075(2)	6273(3)	25(1)
C12	5976(3)	2391(2)	6642(3)	30(1)
C13	5675(3)	2903(2)	6734(3)	31(1)
C14	4443(3)	2910(2)	6449(3)	27(1)
C15	3782(3)	3367(2)	6401(3)	29(1)
C16	2564(3)	3390(2)	6072(3)	27(1)
C17	1897(4)	3876(2)	5961(3)	35(1)
C18	772(4)	3725(2)	5644(3)	36(1)
C19	724(3)	3153(2)	5551(3)	27(1)
C20	-320(3)	2854(2)	5175(3)	28(1)
C21	-13(3)	649(2)	3588(3)	29(1)
C22	-734(4)	311(2)	3844(3)	38(1)
C23	-1358(4)	-93(2)	3176(4)	47(1)
C24	-1309(4)	-163(2)	2242(4)	49(1)
C25	-615(4)	166(2)	1960(4)	46(1)
C26	46(4)	566(2)	2631(3)	35(1)
C27	5941(3)	1234(2)	6176(3)	27(1)
C28	6279(4)	805(2)	6861(3)	38(1)
C29	7326(4)	540(2)	7089(4)	48(1)
C30	8037(4)	696(2)	6615(4)	45(1)
C31	7693(4)	1107(2)	5902(4)	44(1)
C32	6659(3)	1378(2)	5689(3)	35(1)

Table A-10. Continued

	x	y	z	U(eq)
C33	4426(4)	3887(2)	6726(3)	33(1)
C34	4390(5)	4268(2)	6005(4)	52(1)
C35	4982(5)	4756(2)	6343(6)	71(2)
C36	5589(5)	4864(2)	7390(6)	66(2)
C37	5648(5)	4487(2)	8096(5)	76(2)
C38	5056(4)	4004(2)	7768(4)	57(1)
C39	-1387(3)	3148(2)	5096(3)	29(1)
C40	-2327(4)	3253(2)	4148(3)	37(1)
C41	-3299(4)	3528(2)	4114(4)	45(1)
C42	-3343(4)	3711(2)	5016(4)	47(1)
C43	-2409(4)	3622(2)	5957(4)	46(1)
C44	-1454(4)	3334(2)	6005(3)	39(1)
C45	1700(4)	2389(2)	8335(3)	48(1)
C46	2521(4)	2807(2)	8310(4)	45(1)
C47	327(4)	1760(2)	7264(4)	58(1)
C48	4453(4)	2453(2)	8734(3)	43(1)

Table A-11. Crystal data and structure refinement for **16**

University of Florida Chemistry department identification code	tf25
Empirical formula	C55 H40 B Cl6 N10 Tm
Formula weight	1233.41
Temperature	193(2) K
Wavelength	0.71073 Å
Crystal system	Monoclinic
Space group	P2(1)/n
Unit cell dimensions	a = 18.4931(8) Å α= 90°. b = 14.6041(6) Å β= 98.808(2)°. c = 19.4154(9) Å γ = 90°.
Volume	5181.8(4) Å^3
Z	4
Density (calculated)	1.581 Mg/m^3
Absorption coefficient	2.071 mm^{-1}
F(000)	2464
Crystal size	0.21 x 0.15 x 0.14 mm^3
Theta range for data collection	1.42 to 27.50°.
Index ranges	23≤h≤23, -18≤k≤18, -25≤l≤25
Reflections collected	46178
Independent reflections	11868 [R(int) = 0.0432]
Completeness to theta	=27.50° 99.7 %
Absorption correction	Integration
Max. and min. transmission	0.7940 and 0.6590
Refinement method	Full-matrix least-squares on F^2
Data / restraints / parameters	11868 / 0 / 663
Goodness-of-fit on F^2	1.179
Final R indices [I>2sigma(I)]	R1 = 0.0340, wR2 = 0.0728 [10920]
R indices (all data)	R1 = 0.0382, wR2 = 0.0750
Extinction coefficient	0.00093(6)
Largest diff. peak and hole	1.162 and -1.833 e.Å^{-3}

$R1 = \sum(||F_o| - |F_c||) / \sum|F_o|$

$wR2 = [\sum[w(F_o^2 - F_c^2)^2] / \sum[w(F_o^2)^2]]^{1/2}$

$S = [\sum[w(F_o^2 - F_c^2)^2] / (n-p)]^{1/2}$

$w = 1/[\sigma^2(F_o^2)+(0.0154*p)^2+11.9*p]$,

$p = [\max(F_o^2,0)+ 2* F_c^2]/3$

Table A-12. Atomic coordinates (x 10^4) and equivalent isotropic displacement parameters ($Å^2$x 10^3) for **16**. U(eq) is defined as one third of the trace of the orthogonalized U^{ij} tensor.

	x	y	z	U(eq)
Tm	4751(1)	7386(1)	7677(1)	17(1)
N1	4092(1)	8604(2)	8104(1)	20(1)
N2	3544(1)	7223(2)	7088(1)	19(1)
N3	4880(1)	7340(2)	6491(1)	20(1)
N4	5426(1)	8723(2)	7504(1)	20(1)
C1	4374(2)	9402(2)	8429(2)	21(1)
C2	3849(2)	9808(2)	8810(2)	25(1)
C3	3240(2)	9285(2)	8700(2)	26(1)
C4	3376(2)	8563(2)	8235(2)	20(1)
C5	2826(2)	8002(2)	7889(2)	21(1)
C6	2902(2)	7403(2)	7340(2)	21(1)
C7	2304(2)	6911(2)	6942(2)	24(1)
C8	2584(2)	6447(2)	6444(2)	24(1)
C9	3350(2)	6658(2)	6517(2)	20(1)
C10	3791(2)	6424(2)	6021(2)	22(1)
C11	4493(2)	6772(2)	5997(2)	22(1)
C12	4899(2)	6630(2)	5431(2)	28(1)
C13	5520(2)	7124(2)	5572(2)	28(1)
C14	5510(2)	7568(2)	6236(2)	23(1)
C15	6059(2)	8159(2)	6555(2)	22(1)
C16	6010(2)	8710(2)	7135(2)	22(1)
C17	6512(2)	9441(2)	7370(2)	26(1)
C18	6205(2)	9934(2)	7838(2)	26(1)
C19	5526(2)	9495(2)	7917(2)	22(1)
C20	5038(2)	9819(2)	8344(2)	21(1)
C21	2064(2)	8121(2)	8055(2)	25(1)
C22	1794(2)	7572(3)	8538(2)	40(1)
C23	1059(3)	7671(3)	8638(3)	58(1)
C24	619(2)	8315(4)	8276(3)	57(1)
C25	886(2)	8873(4)	7806(2)	53(1)
C26	1607(2)	8779(3)	7694(2)	40(1)
C27	3446(2)	5841(2)	5420(2)	22(1)
C28	3407(2)	4897(2)	5477(2)	29(1)
C29	3054(2)	4375(3)	4928(2)	36(1)
C30	2744(2)	4795(3)	4320(2)	37(1)
C31	2778(2)	5733(3)	4255(2)	38(1)
C32	3129(2)	6259(2)	4803(2)	31(1)
C33	6717(2)	8257(2)	6194(2)	23(1)
C34	7301(2)	7666(2)	6346(2)	33(1)
C35	7893(2)	7712(3)	5979(2)	37(1)

Table A-12. Continued

	x	y	z	U(eq)
C36	7895(2)	8352(3)	5460(2)	35(1)
C37	7323(2)	8950(3)	5313(2)	49(1)
C38	6732(2)	8904(3)	5681(2)	44(1)
C39	5183(2)	10729(2)	8700(2)	23(1)
C40	5477(2)	10795(2)	9398(2)	33(1)
C41	5528(2)	11638(3)	9737(2)	37(1)
C42	5289(2)	12419(2)	9381(2)	36(1)
C43	5013(2)	12371(3)	8680(2)	42(1)
C44	4958(2)	11531(2)	8342(2)	35(1)
B	5563(2)	5623(3)	8867(2)	26(1)
N5	4272(2)	6179(2)	8403(1)	26(1)
N6	4725(2)	5589(2)	8814(1)	24(1)
N7	5536(2)	6006(2)	7587(1)	27(1)
N8	5772(2)	5454(2)	8146(1)	27(1)
N9	5624(2)	7362(2)	8795(1)	28(1)
N10	5839(2)	6565(2)	9136(1)	26(1)
C45	3593(2)	5923(3)	8478(2)	32(1)
C46	3598(2)	5183(3)	8929(2)	35(1)
C47	4327(2)	4995(2)	9128(2)	30(1)
C48	5807(2)	5638(2)	7049(2)	33(1)
C49	6221(2)	4860(3)	7253(2)	42(1)
C50	6183(2)	4771(3)	7956(2)	37(1)
C51	5978(2)	8024(3)	9185(2)	36(1)
C52	6411(2)	7676(3)	9772(2)	40(1)
C53	6307(2)	6748(3)	9721(2)	33(1)
C54	3602(3)	8481(3)	3503(3)	60(1)
Cl1	2703(1)	8519(2)	3661(1)	105(1)
Cl2	4206(1)	8251(1)	4266(1)	80(1)
Cl3	3706(1)	7668(1)	2863(1)	84(1)
C55	3838(2)	9415(3)	6378(2)	46(1)
Cl4	4505(1)	9984(1)	5988(1)	85(1)
Cl5	3211(1)	8840(1)	5750(1)	59(1)
Cl6	3377(1)	10180(1)	6855(1)	57(1)

Table A-13. Crystal data and structure refinement for **17**

University of Florida Chemistry department identification code	tf30
Empirical formula	C77 H62 B1 N10 Yb1
Formula weight	874.14
Temperature	193(2) K
Wavelength	0.71073 Å
Crystal system	Triclinic
Space group	P-1
Unit cell dimensions	a = 11.9673(5) Å α= 98.846(2)°. b = 14.0070(6) Å β= 100.017(2)°. c = 20.7721(8) Å γ = 106.862(2)°.
Volume	3203.5(2) $Å^3$
Z	3
Density (calculated)	1.359 Mg/m^3
Absorption coefficient	1.513 mm^{-1}
F(000)	1338
Theta range for data collection	1.02 to 27.50°.
Index ranges	$-15 \le h \le 15$, $-18 \le k \le 18$, $-26 \le l \le 26$
Reflections collected	29053
Independent reflections	14388 [R(int) = 0.0355]
Completeness to theta	= 27.50° 97.7 %
Absorption correction	Analytical
Max. and min. transmission	0.9068 and 0.6121
Refinement method	Full-matrix least-squares on F^2
Data / restraints / parameters	14388 / 120 / 797
Goodness-of-fit on F^2	1.066
Final R indices [I>2sigma(I)]	R1 = 0.0269, wR2 = 0.0650 [12598]
R indices (all data)	R1 = 0.0355, wR2 = 0.0718
Extinction coefficient	0.00137(15)
Largest diff. peak and hole	0.643 and -0.768 $e.Å^{-3}$

$R1 = \sum(||F_o| - |F_c||) / \sum|F_o|$

$wR2 = [\sum[w(F_o^2 - F_c^2)^2] / \sum[w(F_o^2)^2]]^{1/2}$

$S = [\sum[w(F_o^2 - F_c^2)^2] / (n-p)]^{1/2}$

$w = 1/[\sigma^2(F_o^2)+(0.0392*p)^2+0.00*p]$,

$p = [\max(F_o^2,0)+ 2* F_c^2]/3$

Table A-14. Atomic coordinates (x 10^4) and equivalent isotropic displacement parameters ($Å^2$x 10^3) for **17**. U(eq) is defined as one third of the trace of the orthogonalized U^{ij} tensor.

	x	y	z	U(eq)
Yb	4932(1)	8858(1)	1907(1)	20(1)
B	4406(3)	11124(2)	1458(2)	32(1)
N1	6846(2)	8964(2)	2484(1)	25(1)
N2	5547(2)	7788(2)	1157(1)	22(1)
N3	3325(2)	7308(2)	1594(1)	24(1)
N4	4632(2)	8454(2)	2931(1)	26(1)
N5	6211(2)	10678(2)	2001(1)	29(1)
N6	5752(2)	11380(2)	1764(1)	30(1)
N7	4141(2)	9331(2)	840(1)	26(1)
N8	4027(2)	10271(2)	832(1)	27(1)
N9	3724(2)	9959(2)	2243(1)	30(1)
N10	3686(2)	10789(2)	1974(1)	31(1)
C1	7317(2)	9355(2)	3158(1)	28(1)
C2	8607(2)	9671(2)	3299(1)	36(1)
C3	8911(2)	9457(2)	2709(1)	35(1)
C4	7813(2)	9008(2)	2200(1)	27(1)
C5	7746(2)	8643(2)	1522(1)	25(1)
C6	6693(2)	8052(2)	1050(1)	24(1)
C7	6666(2)	7548(2)	386(1)	25(1)
C8	5525(2)	6963(2)	102(1)	26(1)
C9	4826(2)	7096(2)	586(1)	23(1)
C10	3581(2)	6593(2)	483(1)	24(1)
C11	2904(2)	6680(2)	960(1)	25(1)
C12	1687(2)	6023(2)	891(1)	34(1)
C13	1406(2)	6215(2)	1487(2)	36(1)
C14	2428(2)	6999(2)	1930(1)	28(1)
C15	2518(2)	7320(2)	2614(1)	32(1)
C16	3556(2)	7981(2)	3075(1)	31(1)
C17	3648(3)	8236(2)	3787(1)	38(1)
C18	4782(3)	8841(2)	4072(1)	36(1)
C19	5414(2)	8952(2)	3544(1)	29(1)
C20	6658(2)	9388(2)	3653(1)	29(1)
C21	8904(2)	8853(2)	1300(1)	28(1)
C22	9339(3)	9733(3)	1077(2)	46(1)
C23	10403(3)	9935(3)	859(2)	57(1)
C24	11022(3)	9247(3)	863(2)	50(1)
C25	10602(3)	8383(3)	1088(2)	54(1)
C26	9544(3)	8180(2)	1306(2)	43(1)
C27	2945(2)	5932(2)	-193(1)	27(1)
C28	3229(3)	5070(2)	-440(1)	32(1)

Table A-14 Continued

	x	y	z	U(eq)
C29	2682(3)	4501(2)	-1083(2)	42(1)
C30	1840(3)	4779(2)	-1487(2)	46(1)
C31	1525(3)	5610(2)	-1250(2)	41(1)
C32	2070(2)	6180(2)	-603(1)	35(1)
C33	1444(3)	6870(2)	2887(1)	41(1)
C34	573(3)	7322(3)	2904(2)	50(1)
C35	-417(3)	6906(4)	3164(2)	72(1)
C36	-520(4)	6028(4)	3401(2)	86(2)
C37	334(5)	5578(4)	3384(2)	94(2)
C38	1326(4)	5985(3)	3127(2)	71(1)
C39	7362(2)	9794(2)	4364(1)	32(1)
C40	7766(3)	10826(2)	4658(2)	38(1)
C41	8432(3)	11172(3)	5309(2)	46(1)
C42	8693(3)	10507(3)	5679(2)	50(1)
C43	8291(4)	9486(3)	5401(2)	65(1)
C44	7634(4)	9131(3)	4741(2)	57(1)
C45	7390(2)	11174(2)	2236(2)	35(1)
C46	7690(3)	12176(2)	2150(2)	44(1)
C47	6627(3)	12267(2)	1849(2)	39(1)
C48	3756(2)	8828(2)	194(1)	28(1)
C49	3393(2)	9416(2)	-221(1)	32(1)
C50	3581(2)	10330(2)	201(1)	33(1)
C51	3024(3)	9936(2)	2683(2)	39(1)
C52	2542(3)	10725(3)	2699(2)	45(1)
C53	2988(3)	11255(2)	2241(2)	41(1)
C60	10734(5)	13108(4)	4680(3)	107(2)
C61	10265(4)	12600(4)	4035(3)	88(2)
C62	10989(4)	12554(4)	3611(2)	77(1)
C63	12197(4)	13008(4)	3829(3)	84(1)
C64	12697(4)	13513(4)	4492(3)	88(2)
C65	11962(5)	13553(4)	4921(3)	99(2)
C70	15145(6)	16216(4)	3373(4)	112(2)
C71	15000(6)	15428(5)	3677(3)	106(2)
C72	15325(5)	14627(4)	3456(3)	82(1)
C73	15760(6)	14567(5)	2923(3)	110(2)
C74	15944(7)	15405(8)	2614(4)	164(4)
C75	15638(6)	16242(5)	2863(4)	121(3)
C80	15808(11)	12865(9)	4772(5)	61(3)
C81	15215(9)	12114(7)	4190(6)	64(3)
C82	15806(11)	12109(7)	3693(4)	53(2)
C83	16953(11)	12808(9)	3785(4)	51(2)
C84	17558(9)	13547(8)	4387(7)	70(3)

Table A-14. Continued

	x	y	z	U(eq)
C85	16974(11)	13541(7)	4893(5)	61(3)
C80'	16579(14)	13402(9)	4923(5)	58(3)
C81'	15540(12)	12616(11)	4672(7)	68(4)
C82'	15409(11)	12105(8)	4022(7)	61(3)
C83'	16260(13)	12361(9)	3646(4)	42(2)
C84'	17362(12)	13128(11)	3920(6)	61(3)
C85'	17480(12)	13607(10)	4579(8)	77(4)
C90	2629(10)	4038(9)	1735(6)	85(3)
C91	1809(12)	3519(8)	2046(5)	76(3)
C92	783(11)	2818(9)	1652(7)	77(3)
C93	445(10)	2605(9)	951(7)	94(4)
C94	1271(12)	3175(9)	648(4)	65(2)
C95	2333(9)	3840(7)	1031(5)	52(2)
C90'	2639(11)	4107(10)	1322(9)	95(4)
C91'	2354(14)	3945(12)	1924(7)	107(5)
C92'	1236(12)	3273(9)	1913(5)	61(3)
C93'	421(10)	2711(8)	1340(8)	78(3)
C94'	695(13)	2860(10)	734(6)	82(4)
C95'	1785(13)	3564(10)	747(6)	62(3)

Table A-15. Crystal data and structure refinement for **22**

University of Florida Chemistry department identification code	tf33
Empirical formula	C61 H51 N4 Yb
Formula weight	1013.10
Temperature	193(2) K
Wavelength	0.71073 Å
Crystal system	Monoclinic
Space group	P2(1)/c
Unit cell dimensions	
	a = 18.5565(7) Å α= 90°.
	b = 11.6578(4) Å β= 94.672(2)°.
	c = 21.9195(8) Å γ = 90°.
Volume	4726.0(3) $Å^3$
Z	4
Density (calculated)	1.424 Mg/m^3
Absorption coefficient	2.024 mm^{-1}
F(000)	2060
Crystal size	0.33 x 0.09 x 0.07 mm^3
Theta range for data collection	1.86 to 27.50°.
Index ranges	$-24 \le h \le 24$, $-15 \le k \le 15$, $-28 \le l \le 27$
Reflections collected	41235
Independent reflections	10764 [R(int) = 0.0548]
Completeness to theta	= 27.50° 99.2 %
Absorption correction	Analytical
Max. and min. transmission	0.8693 and 0.5722
Refinement method	Full-matrix least-squares on F^2
Data / restraints / parameters	10764 / 0 / 601
Goodness-of-fit on F^2	0.951

Table A-15. Continued

Final R indices [I>2sigma(I)]	R1 = 0.0233, wR2 = 0.0528 [8380]
R indices (all data)	R1 = 0.0371, wR2 = 0.0557
Largest diff. peak and hole	0.857 and -0.639 e.$Å^{-3}$

$R1 = \sum(||F_o| - |F_c||) / \sum|F_o|$

$wR2 = [\sum[w(F_o^2 - F_c^2)^2] / \sum[w(F_o^2)^2]]^{1/2}$

$S = [\sum[w(F_o^2 - F_c^2)^2] / (n-p)]^{1/2}$

$w = 1/[\sigma^2(F_o^2)+(0.0256*p)^2+0.00*p]$,

$p = [\max(F_o^2,0)+ 2* F_c^2]/3$

Table A-16. Atomic coordinates (x 10^4) and equivalent isotropic displacement parameters ($Å^2$x 10^3) for **22**. U(eq) is defined as one third of the trace of the orthogonalized U^{ij} tensor.

	x	y	z	U(eq)
Yb	2479(1)	-2794(1)	4329(1)	21(1)
N1	2004(1)	-1403(2)	4907(1)	24(1)
N2	1272(1)	-3070(2)	4071(1)	23(1)
N3	2472(1)	-2995(2)	3297(1)	24(1)
N4	3189(1)	-1272(2)	4113(1)	25(1)
C1	2393(1)	-529(2)	5201(1)	25(1)
C2	1985(1)	-88(2)	5688(1)	29(1)
C3	1366(1)	-689(2)	5680(1)	30(1)
C4	1368(1)	-1507(2)	5189(1)	24(1)
C5	795(1)	-2246(2)	5001(1)	24(1)
C6	750(1)	-2964(2)	4482(1)	23(1)
C7	133(1)	-3653(2)	4277(1)	29(1)
C8	278(1)	-4142(2)	3743(1)	29(1)
C9	986(1)	-3774(2)	3606(1)	23(1)
C10	1328(1)	-4058(2)	3075(1)	24(1)
C11	2008(1)	-3669(2)	2929(1)	24(1)
C12	2313(1)	-3843(2)	2352(1)	30(1)
C13	2942(1)	-3278(2)	2370(1)	30(1)
C14	3047(1)	-2726(2)	2958(1)	24(1)
C15	3616(1)	-1971(2)	3136(1)	25(1)
C16	3677(1)	-1288(2)	3670(1)	26(1)
C17	4243(1)	-471(2)	3827(1)	31(1)
C18	4087(1)	56(2)	4350(1)	32(1)
C19	3420(1)	-432(2)	4527(1)	27(1)
C20	3055(1)	-92(2)	5036(1)	26(1)
C21	154(1) -	2244(2)	5377(1)	27(1)
C22	180(2)	-2839(2)	5925(1)	44(1)
C23	-408(2)	-2851(3)	6275(2)	54(1)
C24	-1027(2)	-2263(3)	6083(2)	50(1)
C25	-1060(2)	-1666(3)	5543(1)	55(1)
C26	-469(1)	-1659(3)	5190(1)	45(1)
C27	916(1)	-4782(2)	2602(1)	25(1)
C28	282(1)	-4379(2)	2295(1)	33(1)
C29	-93(2)	-5043(2)	1849(1)	39(1)
C30	160(2)	-6105(2)	1707(1)	40(1)
C31	784(2)	-6515(2)	2003(1)	40(1)
C32	1168(1)	-5859(2)	2451(1)	32(1)
C33	4185(1)	-1852(2)	2692(1)	25(1)
C34	4634(1)	-2769(2)	2584(1)	32(1)
C35	5144(1)	-2687(2)	2155(1)	36(1)

Table A-16. Continued

	x	y	z	U(eq)
C36	5201(1)	-1686(3)	1830(1)	37(1)
C37	4754(2)	-777(2)	1925(1)	39(1)
C38	4242(1)	-849(2)	2356(1)	33(1)
C39	3381(1)	863(2)	5423(1)	27(1)
C40	3678(1)	644(2)	6019(1)	36(1)
C41	3963(2)	1531(3)	6383(1)	45(1)
C42	3952(2)	2635(3)	6165(1)	47(1)
C43	3661(2)	2868(2)	5584(2)	53(1)
C44	3375(2)	1978(2)	5215(1)	44(1)
C45	3522(1)	-3576(2)	5093(1)	34(1)
C46	2866(1)	-3867(2)	5348(1)	32(1)
C47	2495(1)	-4686(2)	4961(1)	31(1)
C48	2924(1)	-4902(2)	4462(1)	32(1)
C49	3551(1)	-4227(2)	4547(1)	34(1)
C50	4105(2)	-2798(3)	5367(2)	59(1)
C51	2631(2)	-3419(3)	5947(1)	52(1)
C52	1801(2)	-5283(3)	5075(1)	50(1)
C53	2759(2)	-5760(2)	3955(1)	54(1)
C54	4184(2)	-4258(3)	4154(1)	55(1)
C61	1928(2)	100(3)	2413(1)	48(1)
C62	2039(2)	872(3)	1954(2)	65(1)
C63	2460(2)	1821(4)	2051(2)	87(1)
C64	2795(2)	2034(4)	2629(3)	91(2)
C65	2687(2)	1276(4)	3093(2)	86(2)
C66	2251(2)	328(3)	2985(2)	64(1)
C67	1472(2)	-952(3)	2294(2)	70(1)

Table A-17. Crystal data and structure refinement for **24**.

University of Florida Chemistry department identification code	tf28
Empirical formula	C49 H51 Co Er N8 O9 P3
Formula weight	1215.08
Temperature	193(2) K
Wavelength	0.71073 Å
Crystal system	Monoclinic
Space group	P2(1)/c
Unit cell dimensions	
	a = 11.9513(5) Å α= 90°.
	b = 23.5083(9) Å β= 107.703(2)°.
	c = 19.1408(7) Å γ = 90°.
Volume	5123.0(3) $Å^3$
Z	4
Density (calculated)	1.575 Mg/m^3
Absorption coefficient	2.107 mm^{-1}
F(000)	2452
Crystal size	0.28 x 0.18 x 0.08 mm^3
Theta range for data collection	1.73 to 27.50°.
Index ranges	-15≤h≤15, -29≤k≤30, -24≤l≤24
Reflections collected	46010
Independent reflections	11734 [R(int) = 0.0357]
Completeness to theta	= 27.50° 99.6 %
Absorption correction	Analytical
Max. and min. transmission	0.8489 and 0.6242
Refinement method	Full-matrix least-squares on F^2
Data / restraints / parameters	11734 / 0 / 666
Goodness-of-fit on F^2	1.025
Final R indices [I>2sigma(I)]	R1 = 0.0245, wR2 = 0.0619 [10008]
R indices (all data)	R1 = 0.0319, wR2 = 0.0663
Largest diff. peak and hole	0.655 and -0.606 $e.Å^{-3}$

$R1 = \Sigma(||F_o| - |F_c||) / \Sigma|F_o|$

$wR2 = [\Sigma[w(F_o^2 - F_c^2)^2] / \Sigma[w(F_o^2)^2]]^{1/2}$

$S = [\Sigma[w(F_o^2 - F_c^2)^2] / (n-p)]^{1/2}$

$w = 1/[\sigma^2(F_o^2)+(0.0373*p)^2+3.66*p]$,

$p = [\max(F_o^2,0)+ 2* F_c^2]/3$

Table A-18. Atomic coordinates (x 10^4) and equivalent isotropic displacement parameters ($Å^2$x 10^3) for **24**. U(eq) is defined as one third of the trace of the orthogonalized U^{ij} tensor.

	x	y	z	U(eq)
Er1	99(1)	7082(1)	7785(1)	27(1)
Co	517(1)	6620(1)	9959(1)	33(1)
P1	1962(1)	6883(1)	9574(1)	38(1)
P2	-593(1)	7310(1)	9392(1)	37(1)
P3	-127(1)	6049(1)	9031(1)	36(1)
O1	1681(2)	7073(1)	8792(1)	54(1)
O2	-821(2)	7377(1)	8579(1)	49(1)
O3	-171(2)	6239(1)	8272(1)	54(1)
O4	2890(2)	6371(1)	9715(1)	65(1)
O5	2756(2)	7359(1)	10076(1)	72(1)
O6	-61(2)	7897(1)	9780(1)	58(1)
O7	-1830(2)	7293(1)	9543(1)	61(1)
O8	-1407(2)	5854(1)	9030(1)	52(1)
O9	560(2)	5455(1)	9178(1)	58(1)
N1	1086(2)	7917(1)	7632(1)	28(1)
N2	-1323(2)	7720(1)	7078(1)	33(1)
N3	-899(2)	6612(1)	6686(1)	34(1)
N4	1519(2)	6806(1)	7223(1)	29(1)
N5	-425(2)	8619(1)	7572(1)	36(1)
N6	-2818(2)	7056(1)	6406(1)	43(1)
N7	611(2)	5957(1)	6576(1)	36(1)
N8	2993(2)	7539(1)	7660(1)	30(1)
C1	2272(2)	7948(1)	7746(1)	29(1)
C2	2667(2)	8532(1)	7921(1)	34(1)
C3	3772(3)	8779(1)	8079(2)	44(1)
C4	3845(3)	9358(1)	8213(2)	56(1)
C5	2853(3)	9681(1)	8182(2)	55(1)
C6	1755(3)	9435(1)	8016(2)	47(1)
C7	1676(2)	8851(1)	7890(1)	35(1)
C8	685(2)	8455(1)	7692(1)	32(1)
C9	-1337(2)	8275(1)	7286(1)	36(1)
C10	-2552(2)	8467(1)	7113(2)	46(1)
C11	-3034(3)	8984(2)	7235(2)	62(1)
C12	-4262(4)	9022(2)	6991(2)	81(1)
C13	-4952(3)	8572(2)	6641(2)	84(1)
C14	-4480(3)	8064(2)	6514(2)	65(1)
C15	-3254(2)	8014(1)	6764(2)	47(1)
C16	-2456(2)	7551(1)	6738(1)	39(1)
C17	-2090(2)	6641(1)	6356(1)	39(1)

Table A-18. Continued

	x	y	z	U(eq)
C18	-2474(3)	6134(1)	5901(1)	45(1)
C19	-3578(3)	5967(2)	5439(2)	58(1)
C20	-3622(4)	5461(2)	5060(2)	69(1)
C21	-2627(4)	5136(2)	5129(2)	67(1)
C22	-1541(3)	5306(1)	5571(2)	53(1)
C23	-1487(3)	5812(1)	5961(1)	42(1)
C24	-493(2)	6124(1)	6450(1)	36(1)
C25	1530(2)	6284(1)	6907(1)	34(1)
C26	2723(2)	6150(1)	6910(1)	38(1)
C27	3199(3)	5690(1)	6635(2)	53(1)
C28	4372(3)	5726(2)	6667(2)	63(1)
C29	5054(3)	6193(2)	6959(2)	59(1)
C30	4593(2)	6649(1)	7240(2)	45(1)
C31	3413(2)	6619(1)	7213(1)	36(1)
C32	2632(2)	7025(1)	7401(1)	30(1)
C33	3911(4)	6434(2)	9472(3)	103(2)
C34	4685(5)	5958(3)	9690(4)	153(3)
C35	2933(12)	7893(5)	9691(7)	73(4)
C35'	2666(8)	7943(4)	10047(10)	89(4)
C36	3221(18)	8368(8)	10098(12)	144(8)
C36'	3709(11)	8212(6)	9944(8)	90(5)
C37	-680(4)	8416(2)	9511(2)	74(1)
C38	92(5)	8897(2)	9583(3)	91(1)
C39	-2937(3)	7215(2)	9014(3)	92(2)
C40	-3829(4)	7538(3)	9161(4)	140(3)
C41	-2094(3)	5498(2)	8445(2)	71(1)
C42	-3182(4)	5332(2)	8601(3)	89(1)
C43	1242(4)	5221(2)	8734(3)	96(2)
C44	2203(6)	4875(3)	9184(5)	172(4)
C45	1487(3)	6750(2)	11044(1)	59(1)
C46	1525(3)	6170(2)	10867(1)	53(1)
C47	363(3)	5967(1)	10657(2)	50(1)
C48	-389(3)	6416(2)	10694(2)	53(1)
C49	322(4)	6907(2)	10940(2)	60(1)

Table A-19. Crystal data and structure refinement for **25**

University of Florida Chemistry department identification code	tf31
Empirical formula	C49 H51 Co N8 O9 P3 Yb
Formula weight	1220.86
Temperature	193(2) K
Wavelength	0.71073 Å
Crystal system	Monoclinic
Space group	P2(1)/c
Unit cell dimensions	
	a = 11.9103(5) Å α= 90°.
	b = 23.622(2) Å β= 107.458(2)°.
	c = 19.0387(8) Å γ = 90°.
Volume	5109.6(4) $Å^3$
Z	4
Density (calculated)	1.587 Mg/m^3
Absorption coefficient	2.300 mm^{-1}
F(000)	2460
Crystal size	0.20 x 0.20 x 0.04 mm^3
Theta range for data collection	1.72 to 27.50°.
Index ranges	-15≤h≤15, -30≤k≤30, -24≤l≤24
Reflections collected	45795
Independent reflections	11714 [R(int) = 0.0383]
Completeness to theta	= 27.50° 99.7 %
Absorption correction	Analytical
Max. and min. transmission	0.9142 and 0.6448
Refinement method	Full-matrix least-squares on F^2
Data / restraints / parameters	11714 / 0 / 637
Goodness-of-fit on F^2	1.030
Final R indices [I>2sigma(I)]	R1 = 0.0256, wR2 = 0.0639 [9437]
R indices (all data)	R1 = 0.0374, wR2 = 0.0684
Largest diff. peak and hole	0.708 and -0.558 e.$Å^{-3}$

$R1 = \Sigma(||F_o| - |F_c||) / \Sigma|F_o|$

$wR2 = [\Sigma[w(F_o^2 - F_c^2)^2] / \Sigma[w(F_o^2)^2]]^{1/2}$

$S = [\Sigma[w(F_o^2 - F_c^2)^2] / (n-p)]^{1/2}$

$w = 1/[\sigma^2(F_o^2)+(0.0346*p)^2+2.32*p]$,

$p = [\max(F_o^2,0)+ 2* F_c^2]/3$

Table A-20. Atomic coordinates (x 10^4) and equivalent isotropic displacement parameters ($Å^2$x 10^3) for **25**. U(eq) is defined as one third of the trace of the orthogonalized U^{ij} tensor.

	x	y	z	U(eq)
Yb	104(1)	7067(1)	7779(1)	25(1)
Co	508(1)	6610(1)	9956(1)	31(1)
P1	1959(1)	6869(1)	9569(1)	36(1)
P2	-585(1)	7302(1)	9389(1)	35(1)
P3	-139(1)	6046(1)	9022(1)	34(1)
O1	1680(2)	7045(1)	8777(1)	49(1)
O2	-792(2)	7371(1)	8574(1)	46(1)
O3	-201(2)	6241(1)	8256(1)	49(1)
O4	2903(2)	6364(1)	9728(1)	57(1)
O5	2739(2)	7356(1)	10063(1)	60(1)
O6	-57(2)	7880(1)	9784(1)	54(1)
O7	-1829(2)	7286(1)	9535(1)	57(1)
O8	-1412(2)	5844(1)	9031(1)	47(1)
O9	557(2)	5457(1)	9158(1)	52(1)
N1	2998(2)	7522(1)	7666(1)	28(1)
N2	1081(2)	7894(1)	7637(1)	26(1)
N3	-438(2)	8592(1)	7578(1)	33(1)
N4	-1323(2)	7696(1)	7081(1)	30(1)
N5	-2820(2)	7033(1)	6412(1)	38(1)
N6	-893(2)	6595(1)	6693(1)	32(1)
N7	624(2)	5940(1)	6585(1)	34(1)
N8	1523(2)	6792(1)	7229(1)	28(1)
C1	2274(2)	7927(1)	7749(1)	26(1)
C2	2663(2)	8507(1)	7926(1)	31(1)
C3	3770(3)	8756(1)	8089(2)	41(1)
C4	3837(3)	9330(1)	8221(2)	51(1)
C5	2839(3)	9654(1)	8189(2)	49(1)
C6	1738(3)	9405(1)	8024(2)	41(1)
C7	1668(3)	8825(1)	7898(2)	32(1)
C8	678(2)	8430(1)	7700(1)	28(1)
C9	-1346(2)	8247(1)	7291(2)	32(1)
C10	-2564(3)	8437(1)	7119(2)	41(1)
C11	-3051(3)	8950(2)	7244(2)	55(1)
C12	-4274(4)	8989(2)	6998(2)	69(1)
C13	-4969(3)	8542(2)	6645(3)	73(1)
C14	-4489(3)	8036(2)	6522(2)	56(1)
C15	-3264(3)	7986(1)	6768(2)	41(1)
C16	-2458(2)	7527(1)	6743(2)	35(1)
C17	-2087(2)	6621(1)	6358(2)	34(1)
C18	-2472(3)	6120(1)	5903(2)	40(1)

Table A-20. Continued

	x	y	z	U(eq)
C19	-3566(3)	5951(2)	5438(2)	52(1)
C20	-3605(4)	5449(2)	5058(2)	62(1)
C21	-2609(4)	5122(2)	5130(2)	59(1)
C22	-1522(3)	5293(1)	5575(2)	46(1)
C23	-1472(3)	5796(1)	5967(2)	38(1)
C24	-485(3)	6110(1)	6458(2)	32(1)
C25	1538(2)	6268(1)	6916(2)	32(1)
C26	2738(3)	6131(1)	6924(2)	36(1)
C27	3218(3)	5671(1)	6660(2)	49(1)
C28	4398(3)	5709(2)	6698(2)	59(1)
C29	5078(3)	6177(2)	6985(2)	53(1)
C30	4612(3)	6632(1)	7254(2)	42(1)
C31	3428(2)	6603(1)	7224(2)	33(1)
C32	2638(2)	7009(1)	7406(1)	28(1)
C33	3937(4)	6431(2)	9493(3)	91(2)
C34	4713(5)	5941(3)	9727(4)	135(3)
C35	2598(10)	7955(4)	9979(8)	75(4)
C35'	2890(8)	7884(3)	9664(6)	60(3)
C36	3716(10)	8199(5)	9936(6)	75(4)
C36'	3329(10)	8335(5)	10182(7)	83(4)
C37	-842(14)	8398(3)	9470(6)	44(3)
C37'	-470(20)	8408(5)	9603(9)	60(4)
C38	-89(18)	8881(4)	9515(9)	63(3)
C38'	330(20)	8879(4)	9687(9)	58(4)
C39	-2951(8)	7303(7)	8903(7)	67(3)
C39'	-2914(8)	7128(5)	9072(6)	50(3)
C40	-3868(8)	7454(6)	9263(8)	73(3)
C40'	-3795(10)	7625(7)	9006(9)	83(4)
C41	-2103(3)	5482(2)	8460(2)	63(1)
C42	-3054(14)	5200(9)	8740(11)	72(4)
C42'	-3249(8)	5363(5)	8549(6)	48(3)
C43	1260(20)	5259(10)	8674(14)	176(11)
C43'	1318(11)	5252(5)	8759(8)	37(3)
C44	2260(7)	4878(3)	9180(4)	88(3)
C44'	1000(30)	5026(15)	8338(18)	195(15)
C45	1474(3)	6741(2)	11045(2)	55(1)
C46	1517(3)	6166(2)	10869(2)	48(1)
C47	353(3)	5959(2)	10656(2)	48(1)
C48	-406(3)	6406(2)	10695(2)	52(1)
C49	300(4)	6893(2)	10939(2)	55(1)

LIST OF REFERENCES

1 *CRC Handbook of Materials Science and Engineering*, Eds. Schackelford, J.F.; Alexander, W.; Boca Raton, FL, CRC Press, **2001**

2 Kingsborough, R.P.; Swager, T.M.; *Progress in Inorganic Chemistry* **1999**, *48*, 123; Ed. Karlin, K.D.; New York, NY, John Wiley & Sons Inc.

3 *Handbook of Conducting Polymers* Skotheim, T.A.; Elsenbaumer, R.L.; Reynolds, J.R. Eds.; New York, NY, Marcel Dekker **1998**

4 Chien, J.C.W.; *Polyacetylene : Chemistry, Physics, and Materials Science* Orlando, FL Academic Press **1984**

5 Vanderberg, E.J.; *Contemporary Topics in Polymer Science Vol. 5* New York, NY, Plenum Press, **1984**

6 Diaz, A.F.; *Chem. Scripta.* **1981**, *17*, 142

7 Yamamoto, T.; *Prog. Poly. Sci.* **1992**, *17*,1153

8 Sugimoto, R.; Takeda; S. Gu, H.B.; Yoshino, K.; *Chem. Express.* **1986**, *1*, 635

9 Cotton, F.A.; Wilkinson, G.; *Advanced Inorganic Chemistry,* New York, NY, John Wiley & Sons, **1988**

10 Hueey, J.E.; Keiter, E.A.; Keiter, R.L.; *Inorganic Chemistry: Principles of Structure and Reactivity,* New York, NY, Harper Collins College, **1988**

11 Crabtree, R.H. *The Organometallic Chemistry of Transition Metals,* New York, NY, John Wiley & Sons, **1994**

12 (a) Manners, I. *Adv. Mater* **1994**, *6*,68; (b) Rulkens, R.; Resendes, R.;Verma, A.; Manners, I. Murti, K.; Fossum, E.; Miller, P.;Matyjaszewski, K.; *Macromolecules* **1997**, *16*, 8165 (c) Buretea, M.A.; Tilley, T.D.; *Organometallis* **1997**, *16*, 1507 (d) Compton, D.L.; Rauchfuss, T.B.; *Organometallics* **1994**, *13*, 4367 (e) Rulkens, R.; Lough, A.J.; Manners, I; Lovelace, S.R.; Grant, C.; Geiger, W.E.; *J. Am. Chem. Soc.* **1996**, *118*,12683

13 Samuel, I.D.W; Beeby, A. *Nature* **2000**, *403*, 710

14 Kraft, A.; Grimsdale, A.C.; Holmes, A.B.; *Angew. Chem. Int. Ed.* **1998**, *37*, 402

15 Segura, J.L.; *Acta Polym.* **1998**, *49*, 319

16 Yartsev, V.M.; Marcano, A; *Synthetic Metals* **2000**, *115,* 197

17 Bella, S.D.; Fragala, I; *Synthetic Metals* **2000**, *115*, 191

18 Plitzko, K.D.; Boekelheide, V.; *Organometallics* **1988**, *7*, 1573;

19 Fagan, P.J.; Ward, M.D. Calabrese, J.C.; Johnson, D.C.; *J. Am. Chem. Soc.* **1988**, *111*, 1698

20 Graf, D.D.; Day, Day, N.C.; Mann, K.R.; *Inorg. Chem.* **1995**, *34*, 1562

21 Graf, D.D.; Mann, K.R.; *Inorg. Chem.* **1997**, *36*, 141

22 Van Der Looy, J.F.A; Thys, G.J.H; Dieltiens, P.E.M.; De Schrijver, D.; Van Alsenoy, C.; Geise, H.J.; *Tetrahedron* **1997**, *53*, 15069

23 Saito, H.; Ukai, S.; Iwatsuki, S; Itoh, T.; Kubo, M.; *Macromolecules* **1995**, *28*, 8363

24 Soltzing, G.; Reynolds, J.R.; Steel, P.J.; *Chem. Mater.* **1996**, *8*, 882

25 Turbiez, M.; Frere, P.; Blanchard, P.; Roncali,J.; *Tett. Lett.* **2000**, *41*, 5521

26 March, J.; Smith, M. B.; *March's Advanced Organic Chemistry : Reactions, Mechanisms, and Structure* New York, NY, Wiley, **2001**.

27 Jones, C.L.; Higgins, S.J.; *J. Mat. Chem.* **1999**, *9*, 865

28 Xu, W.C.; Zhou, Q.; Ashendel, C.L.; Chang, C.; Chang, C.; *Bioorg. Med. Chem. Lett.* **1999**, *9*, 2279

29 Funaki, H.; Aramaki, K.; Hishira, H.; *Synthetic Metals* **1995**, *74*, 59

30 Miller, E.J.,; Landon, M.; Brill, T.B.; *Organometallics*, **1985**, *4*, 534

31 Frith, S.A.; Spencer, J.L.; *Inorg. Syn. Prep.* Vol. 28, 273

32 Gill, T.P.; Mann, K.R.; *Inorg. Chem.* **1980**, *19*, 3007

33 White, C.; Thompson; S.J.; Maitlis, P.M.; *J. Chem. Soc. Dalton* **1978**, 1654

34 Nguyen, P.; Gomez-Elipe, P.; Manners, I.; *Chem. Rev.* **1999**, *99,* 1515

35 White, C.; Yates, A.; Maitlis, P.M.; *Inorg. Syn. Prep.* Vol. 29, 228

36 (a) Gscheider, K.A.; Eyering, L.; *HandBook on the Physics and Chemistry of Rare Earths* Elsevier, **1998**, *25*, 101 (b) Jacobsen, S.M.; Tissue, B.M.; Yen, W.M.; *J. Phys. Chem.* **1992,** *96*, 1547

37 (a) Sinha, A.B.P; *Spectroscopy in Inorganic Chemistry, Vol II* New York, NY, Academic Press, **1971** (b) Dawson, W.R.; Kropp, J.L.; Windsor, M.W. *J. Chem. Phys.* **1966**, *45,* 2410

38 Dieke, G.H.; Hall, L.A.; *J. Chem. Phys.* **1957**, *27*, 465

39 (a) Bhaumik, M.L.; *J. Chem. Phys.* **1964**, *40*, 3711 (b) Werts, M.H.V.; Verhoeven, J.W.; Hofstraat, J.W.; *J. Chem. Soc. Perkin Trans. 2* **2000**, 433 (c) Iwarmuro, M.; Wada, Y.; Kitamura, T.; Nakashima, N.; Yanagida, S.; *Phys. Chem. Chem. Phys.* **2000**, *2*, 2291

40 Kido, J.; Okamoto,Y.; *Chem. Rev.* **2002,** *102*, 2357

41 (a) Zhao, D.; Wenlian, L.; Hong, Z.; Liang, C.; Zhao, D.; Peng, J; Liu, X.; *Jpn. J. Appl. Phys.* **1999**, *38*, L46 (b) McGhee, M.D.; Bergstedt, T.; Zhang, C.; Saab, A.P.; O'Regan, M.B.; Bazan, G.C.; Sradanov, V.I.; Heeger, A.J.; *Adv. Mat.* **1999**, *11*,

42 Joshi, K.C.; Pathak, V.N.; *J. Inorg. Nucl. Chem.* **1973**, *35*, 3161

43 Hebbink G. A.; Reinhoudt D. N.; van Veggel F. C. J. M.; *Eur. J. Org. Chem.* **2001**, *21*, 4101

44 Peng, Z.; Yu, L.; *J. Am. Chem. Soc.* **1996**, *118*, 3777

45 Sinha, S.P.; *Spectrochimica Acta* **1964**, *20*, 879

46 Bentley, R.K.; *J. Chem. Soc. (C)* **1970**, 2452

47 Bassler, R.M.; Bassler, G.C.; Morrill, T.C.; *Spectrometric Identification of Organic Compounds* New York, NY, Wiley, 1991

48 Shieh W.C.; Shekhar R.; Blacklock T.; Tedesco A.; *Synthetic Communications* **2002**, *32*, 1059

49 (a) Yang, J.P.; Jin, Y.D.; Heremans, P.L.; Hoefnagels, R.; Dieltins, P; Blockhuys, F.; Geise, H.J.; Van der Auweraer, M.; Borghs, G.; *Chem. Phys. Letts.* **2000**, *325*, 251 (b) Jin, Y.D. Yang, J.P.; F.; Rousseau, E.; Geise, H.J.; Van der Auweraer, M.; Borghs, G.; *Chem. Phys. Letts.* **2000**, *320*, 387 (c) Yang, J.P.; Heremans, P.L.; Tachelet, W.; Dieltiens, P.; Blockhuys, F.; Geise, H.J.; Borghs, G.; *Synthetic Metals* **2000**, *108*, 95 (d) Nguyen, T.; Molinie, P.; Destruel, P.; *Handbook of Advanced Electronic and Photonic Materials and Devices* Nalwa, H.S., Eds., San Diego, CA, Academic Press, **2001**, *10*, 1

50 Guillet, J. *Polymer Photophysics and Photochemistry* , Cambridge University Press: Cambridge, UK, 1985

51 Wong C.P.; Ventichler, R.F.; Horrocks, W.D.; *J. Am . Chem. Soc.* **1974**, *96*, 7149

52 Wong, C.P.; *Inorg. Syn.* **1979**, *10*, 156

53 Wong, W.K.; Zhang, L. Wong, W.T.; Xue, F.; Mak, T.C.W.; *J. Chem. Soc., Dalton Trans.* **1999**, 615

54 Harrison, B.S.; Foley, T.J.; Shim, J; Bouguettaya, M; Padmanaban, G; Boncella, J.M.; Holloway, P.H.; Ramakrishnan, S.; Reynolds, J.R.; Schanze, K.S.; *Applied Physics Letters* **2001,** *79*, 3770

55 Evans W. J.; Anwander, R.; Ansari, M. A.; Ziller, J.W. *Inorg. Chem.* **1995**, *34*, 5

56 (a) Bradley, D.C.; Ghotra, J.S.; Hart, F.A.; *J. Chem. Soc., Dalton Trans.* **1972**, 1021 (b) Ghotra, J.S; Hursthouse, M.B.; Welch, A.J.; *J. Chem. Soc., Chem. Comm.* **1973**, 669

57 Anwander, R.; Runte, O.; Eppinger, J.; Gerstberger, G.; Herdtweck, E.; Spiegler, M.; *J. Chem. Soc., Dalton Trans.* **1998**, 847

58 Minhas, R.K.; Ma, Y.; Song, J.; Gambarotta, S.; *Inorg. Chem.* **1996**, *35*, 1866

59 Wong, W.K.; Zhang,L.; Xue, F.; Mak, T.C.W.; *J. Chem. Soc., Dalton Trans.* **1999**, 3053

60 (a) Wong, W.K.; Zhang, L.; Xue, F.; Mak, T.C.W. *Polyhedron* **1997**, *16,* 345 (b) Wong, W.K.; Zhang, L.; Xue, F.; Mak, T.C.W.; *Polyhedron* **1997**, *16*, 2013

61 Wong, W.K.; Zhang, L. Wong, W.T.; Xue, F.; Mak, T.C.W.; *J. Chem. Soc., Dalton Trans.* **1999**, 615

62 (a) Deacon, G.B.; Koplick, A.J.; *Inorg. Nucl. Chem. Letters.* **1979**, *15*, 262 (b) Asprey, L.B.; Keenan, T.K.; Kruse, F.H.; *Inorg. Chem.* **1964**, *3*, 1137

63 (a) Wong, W.K.; Zhang L.L.; Xue, F.; Mak T.C.W. *Polyhedron* **1997**, *16*, 2013 (b) Evans,W.J.; Anwander, R; Ziller, J.W.; Khan, S.I. *Inorg. Chem.* **1995**, *34*, 5927 (c) Guan, J; Songchun, J; Shen, Q. *Organometallics*, **1992**, *11*, 248 (d) Campazzi, E; Solari, E; Scopelliti, R; Floriani, C; *Inorg.Chem.* **1999**, *38*, 6240

64 (a)Arnold, J.; Hoffman, C.G.; Dawson, D.Y.; Hollander, F.J. *Organometallics* **1993,** *12*, 3645 (b) Dawson, D.Y.; Brand, H.; Arnold, J. *J. Am. Chem. Soc* 1994, *116*, 9797 (c) Kane, K.M.; Lemke, F.R.; Petersen, J.L. *Inorg.Chem.* **1995**, *34*, 4085

65 Arnold, J; Hoffman,C.G. *J. Am. Chem. Soc.* **1990**, *112*, 8620

66 Sewchok, M.G.; Haushalter, R.C.; Merola, J.S *Inorg. Chim. Acta* **1988**, *144*, 47

67 (a) Traeger, J.C.; *Int. J. Mass. Spec.* **2000**, *200*, 387 (b) Paolucci,G.; Fischer, R.D.; Breitbach; H.; Pelli, B.; Tradli; *Organometallics* **1988**, *7*, 1918

68 Evans, W.J.; Johnston, M.A.; Fujimoto, C.H.; Greaves, J.; *Organometallics* **2000**, *19*, 4258

69 Trofimenko, S. *J. Am. Chem. Soc.* **1967**, *89*, 6288.

70 Klaui, W.; Dehnicke, K. *Chem. Ber.* **1978**, *111*, 451-468

71 Peng, J.X.; Li, K.F.; Zhang, L.L.; Wong, W.K.; Cheah, K.W.; *Chem. Phys. Lett.* **2000**, *332,* 313 (b) Wong, W.K.; Hou, A.; Guo, J.; He, H.; Zhang, L.; Wong, W.Y.; Li, K.F.; Cheah, K.W.; Xue, F.; Mak, T.C.W.; *J. Chem. Soc., Dalton Trans.* **2001**, 3092

72 Klaui, W.; Eberspach, W.; Schwarz, R.; *J. Org. Met. Chem.* **1983**, *252*, 347

73 Horrocks, W.D.W.; Wong, C.P.; *J. Am. Chem. Soc.* **1976,** *98,* 7157

74 (a) Luchinat, C.; *Coord. Chem. Rev.* **1996**, *150*, 185 (b) Bertini, I.; Coutsolelos, A.; Dikiy, A.; Spyroulias, G.A.; Troganis, A.; *Inorg. Chem.* **1996**, *35*, 6308 (c) Spyroulias, G.A.; Coutsolelos, A.G.; *Inorg. Chem.* **1996**, *35*, 1382

75 Drago, R.S.; *Physical Methods for Chemists*, Fort Worth, TX, Saunders College Publishing, **1992**

76 (a) Horrocks, W.D.W.; Wong, C.P.; *J. Am. Chem. Soc.* **1976**, *98*, 7157 (b) Horrocks, W.D.W.; Hove, E.G.; *J. Am. Chem. Soc.* **1978**, *100*, 4358

77 Babushkina, T.A.; Koreneva, L.G.; Zolin, V.F.; *Mag. Res. Chem.* **1986**, *24*, 1026

78 Arndt, S.; Okuda, J.; *Chem. Rev.* **2002**, *102*, 1953

79 Bassler, R.M.; Bassler, G.C.; Morrill, T.C.; *Spectrometric identification of organic compounds* New York, NY, Wiley, **1991**

80 Ghosh, A.; Ryeng, H.; *J. Am. Chem. Soc.* **2002**, *ASAP Article*

81 (a) Clarke, D.A.; Dolphin, D.; Grigg, R.; Johnson, A.W.; Pinnock, H.A.; *J. Chem. Soc. C* **1968**, 881 (b) Ogoshi, H.; Sugimoto, H.; Yoshida, Z.I.; Kobayashi, H.; Sakai, H.; Maeda, Y.;; *J. Organomet. Chem.* **1982**, *234*, 65 (c) Cocolios, P; Lagrange, G.; Guilard, R.; *J. Organomet. Chem.* **1983**, *253*, 65 (d) Hasegawa, Y.; Kimura, Y.; Murakoshi, K.; Wada, Y.; Kim, J.H.; Nakashima, N.; Yamanka, T.; Yanagida, S. *J. Phys. Chem.* **1996**, *100*, 10201

82 Savenijie, T.J.; Goossens, A. *Phys. Rev. B* **2001**, *64*, 115323

83 (a) Brinkmann, M.; Andre, J.J.; *J. Mater. Chem.* **1999**, *9*, 1511 (b) Linstead, R.P.; Lowe, A.R.; *J. Chem. Soc.* **1934**, 1022

84 (a) Jiang, J.; Liu, R.C.W.; Mak, T.C.W.; Chan, T.W.D.; Ng, D.K.P.; *Polyhedron* **1996**, *16*, 515 (b) Markovitsi, D.; Tran-Thi, T.H.; Even, R.; Simon, J.; *Chem.*

Phys. Lett. **1987**, *137*, 107 (c) Chang, A.T.; Marchon, J.C.; *Inorg. Chim. Acta* **1981**, *53*, L241 (d) Takahashi, K.; Tomita, Y.; Hada, Y.; Tsubota, K.; Kasuga, K.; Handa, M.; Sogabe, K.; Tokii, T.; *Chem. Lett.* **1992**, 759 (e) Jiang, J.; Arnold, D.P.; Yu, H.; *Polyhedron* **1999**, *18*, 2129

85 (a) Sugimoto, H.; Higashi, T.; Mori, M.; *Chem. Lett.* **1982**, 801 (b) Subbotin, N.B.; Tomilova, L.G.; Kostromina, N.A.; Luk'yanets, E.A.; *Russ. J. Inorg. Chem.* **1986**, 56, 345 (c) Iwase, A.; Tanaka, K.; *Electrochimica Acta* **1990**, *35*, 1707 (d) Sugimoto, H. Higashi, T. Maeda, A.; Hiral, Y. Teroka, J.; Mori, M.; Masuda, H.; Taga, T.; *J. Less Common Met.* ***1985****, 112,* 387 (e) Nemykin, V.N.; Chernii, V.Y.; Volkov, S.V.; *J. Chem. Soc., Dalton Trans.* **1998**, 2995

86 Frigerio, N.A.; *U.S. Patent # 3,027,391* **1962**

87 Barrett, P.A.; Frye, D.A.; Linstead, R.P.; *J. Chem. Soc.* **1938**, 1157

88 Bassler, R.M.; Bassler, G.C.; Morrill, T.C.; *Spectrometric Identification of Organic Compounds* New York, NY, Wiley, **1991**

89 Orti, E.; Bredas, J.L.; Clarisse, C.; *J. Chem. Phys.* **1990**, *92*, 1228

90 Huang, T.H.; Rieckeoff, K.E.; Voigt E.M.; *Chem. Phys.* **1979,** *36*, 423

91 Gordon, A. J.; Ford, R. A. *The Chemist's Companion*; New York, NY, Wiley, **1972**

92 (a) Deacon, G. B.; Koplick, A. J. *Inorg. Nucl. Chem. Letters* **1979**, *15*, 263 (b) Arnold, J.; Dawson, D.Y.; Hoffman, C.G. *J. Am. Chem. Soc* **1993,** *115*, 270

BIOGRAPHICAL SKETCH

Tim was born in St. Charles, Illinois. He grew up on a farm in rural Lena, Illinois. While finishing his High School Diploma at Lena Winslow High, he decided to attend Iowa State University and major in Chemistry. He began classes in the Fall of 1993. While doing research for Dr. Valerie Sheares in his senior year, he decided to pursue a graduate degree in chemistry. He enrolled at the University of Florida in the Fall of 1997 and he performed his research on various projects under the direction of Dr. James Boncella.

I certify that I have read this study and that in my opinion it conforms to acceptable standards of scholarly presentation and is fully adequate, in scope and quality, as a dissertation for the degree of Doctor of Philosophy.

James M. Boncella, Chair
Professor of Chemistry

I certify that I have read this study and that in my opinion it conforms to acceptable standards of scholarly presentation and is fully adequate, in scope and quality, as a dissertation for the degree of Doctor of Philosophy.

Lisa A. McElwee-White
Professor of Chemistry

I certify that I have read this study and that in my opinion it conforms to acceptable standards of scholarly presentation and is fully adequate, in scope and quality, as a dissertation for the degree of Doctor of Philosophy.

David E. Richardson
Professor of Chemistry

I certify that I have read this study and that in my opinion it conforms to acceptable standards of scholarly presentation and is fully adequate, in scope and quality, as a dissertation for the degree of Doctor of Philosophy.

Michael J. Scott
Assistant Professor of Chemistry

I certify that I have read this study and that in my opinion it conforms to acceptable standards of scholarly presentation and is fully adequate, in scope and quality, as a dissertation for the degree of Doctor of Philosophy.

Elliot P. Douglas
Assistant Professor of Materials Science and Engineering

This dissertation was submitted to the Department of Chemistry in the College of Liberal Arts and Sciences and to the Graduate School and was accepted as partial fulfillment of the requirements for the degree of Doctor of Philosophy.

August, 2002

_____

Dean, Graduate School